DEVELOPMENT OF TETRAVALENT CHROMIUM DOPED TUNABLE SOLID STATE LASER MATERIALS

by

DI YAO

A dissertation submitted to the Graduate Faculty in Engineering in partial fulfillment of the requirements for the degree of Doctor of Philosophy, The City University of New York

1999

This manuscript has been read and accepted for the Graduate Faculty in Engineering in satisfaction of the dissertation requirement for the degree of Doctor of Philosophy.

4/30/99 — Leslie Isaacs

Date — Professor Leslie L. Isaacs, Chair of Examining Committee and Co-mentor

9/13/1999 — Mumtaz K. Kassir

Date — Professor Mumtaz K. Kassir, Acting Executive Officer

Professor Vladimir Petricevic (Co-mentor)

Professor R. R. Alfano

Professor Alexander Couzis

Dr. A. B. Bykov

Supervisory Committee

THE CITY UNIVERSITY OF NEW YORK

ABSTRACT

DEVELOPMENT OF TETRAVALENT CHROMIUM DOPED TUNABLE SOLID STATE LASER MATERIALS

by

DI YAO

Advisors: Professor Leslie L. Isaacs and Professor Vladimir Petricevic

In this thesis, we describe the development of novel tunable solid state laser materials and the characterization of these materials. Tunable solid-state lasers based on tetravalent chromium ion (Cr^{4+}) are expected to cover the 1-2 μm range, which is an eye-safe range, and is of great importance for optical communications, remote sensing, lidar, scientific and various medical applications. First of all, chemical compounds with formula Cr^{4+}:$A^{+}_{4}(Si, Ge)O_4$, and $A^{+}_{2}M^{2+}(Si, Ge)O_4$, where A = Na, K, Li and M = Ca, Mg, Zn, Cd, were investigated in a search for potential crystalline hosts for Cr^{4+} doped tunable solid state lasers. Basic spectroscopic properties of the potential laser hosts were measured. Strong Cr^{4+} emission in near-infrared (1.1 to 1.6 μm) region has been observed in Cr-doped $Li_2M^{2+}X^{4+}O_4$ (X=Si, Ge) crystalline media. In Li_2CaSiO_4 and Li_2CaGeO_4, two phases were identified by DTA. The phase transition point is 960°C and 950°C for Li_2CaGeO_4 and Li_2CaSiO_4 respectively, and the melting point is 1150 °C and 1060 °C for Li_2CaGeO_4 and Li_2CaSiO_4 respectively. Pseudo-binary systems of Li_2CaSiO_4 - LiF and Li_2CaGeO_4 - LiF/LiCl were investigated, and the solubility curve of Li_2CaSiO_4 - LiF was obtained. High quality single crystals of Cr^{4+}:Ca_2GeO_4 and Cr^{4+}:Li_2CaSiO_4 (low temperature phase) have been successfully grown from the

Cr^{4+}:Ca_2GeO_4-CaF_2 and Cr^{4+}:Li_2CaSiO_4-LiF solution with the top seeding solution growth technique under nitrogen atmosphere and air atmosphere. The pulling rate used to grow good quality single crystals was between 0.1 to 0.5 mm/hr, and the rotation speed was 15 to 40 rpm. The growth direction was perpendicular to "c" axis for Cr^{4+}:Li_2CaSiO_4 and parallel to "b" axis for Cr^{4+}:Ca_2GeO_4. The crystals grown were confirmed to be that of the low temperature phase of Li_2CaSiO_4 by X-ray powder diffraction.

Absorption and emission spectra of the crystals Li_2CaSiO_4 and Ca_2GeO_4 were measured. Fluorescence spectra at room temperature and at liquid nitrogen temperature were also measured. In all the Cr^{4+} doped laser hosts, Cr^{4+} has been identified as the optically active center responsible for the near-informed emission in the 1100 to 1600 μm spectral range. The room-temperature lifetime of the Cr^{4+}- emission in Li_2MgGeO_4 is about 90 μs, the longest lifetime observed up to now for Cr^{4+}-doped laser systems.

Finally, the physical properties of the novel laser and the potential laser hosts were characterized. The DSC method was used to measure the heat capacity and TMA was used to investigate the thermal expansion coefficient. The samples for DSC and TMA include Ca_2GeO_4, Li_2CaSiO_4 and $LiScGeO_4$. The MDSC technique was used in studying the thermal conductivity of Ca_2GeO_4. The refractive indices were measured with the Brewster's angle method by using Cary500 spectrophotometer for Ca_2GeO_4 and Li_2CaSiO_4.

To my parents, Yumei and Junfan Yao

Acknowledgements

I am indebted to a number of people for help in the preparation of this thesis during the years of pursuing my doctorate degree in the City College of New York.

First, my most sincere thanks go to Professor Leslie Isaacs and Professor Vladimir Petricevic, whose knowledge, understanding, and professionalism provided me with the tools necessary to tackle such an endeavor. Each of them read the manuscript carefully and made numerous invaluable suggestions to improve it.

More debts are owed to Dr. Alexei Bykov. He generously supplied information and suggestions, which resulted in many improvements in my research and thesis.

I wish to express my appreciation to Mr. Zhen-rong Xu for his invaluable help and encouragement.

I also would like to acknowledge the support of the Chemical Engineering Department, the Institute for Ultrafast Spectroscopy and Lasers and New York State Center for Advanced Technology over the years. Faculty as well as staff members have contributed in many ways that are greatly appreciated.

I wish to gratefully acknowledge the support, encouragement, and assistance of my parent, especially when separated by such a large distance. Words can not be found to express my gratitude to them.

My most special thanks go to my wife Lan Yu, with her encouragement understanding and help.

This dissertation is a result of the contributions of so many wonderful people. It is not possible to name them all here, but I thank all of them; for I could never have done it without their support.

Table of Contents

List of Figures

List of Tables

Chapter One

Introduction

1.1 Background

In a solid-state laser the laser host is a crystal or glass and the lasing "dopant" has a sharp fluorescent spectral line. When excited by optical pumping it may behave as an oscillator or as an amplifier at the fluorescent wavelength. Solid-state laser hosts are transparent, heat resistant, and hard solids. The laser active ions are either transition metals or rare earth elements. Crystalline hosts are preferred for most applications due to their superior thermo-mechanical properties.

Wavelength tunable lasers are of considerable interest, given the widespread use of tunable coherent sources in many technical fields such as spectroscopy and photo-chemistry, and for the potentially important practical application in areas such as remote sensing and data transmission.

Tunability of the emission over a frequency range in solid-state lasers is due to the coupling of the stimulated emission of photons to the emission of vibration quanta (phonons) in the crystal lattice. In these "vibronic" lasers, the total energy of the lasing transition is fixed, but this energy can be partitioned between photons and phonons in a

continuous fashion. In other words, the existence of tunable solid-state lasers is a result of the subtle interplay between the Coulomb field of the lasing ion, and the crystal field of the host lattice with electron-phonon coupling permitting broad-band absorption and emission. Therefore, the gain in vibronic lasers depends on transitions between the coupled vibrational and electronic states, that is, a phonon is either emitted or absorbed with each electronic transition.

Chromium is a tunable-laser ion due to the special nature of its d electronic configuration. Particular advantages of Chromium over other transition metals are its chemical stability, existence of broad pump bands, large energy level splitting, and reduced excited state absorption. These advantages have led to at least a dozen crystals being demonstrated as laser hosts for Cr. Chromium as a laser has a tuning range of about 100 nm, with the center wavelength shifted by the particular crystal host. In conventional chromium-doped lasers, Cr^{3+} is the active ion and the tuning range rarely goes beyond 1μm. Compared with Cr^{3+}, the Cr^{4+} Oxidation State is rather unstable. Therefore, only few oxidic chromium (4+) compounds are known and fully characterized.

Cr: Mg_2SiO_4 was the first laser crystal in which the laser active center was identified as the tetravalent chromium. Since the first demonstration of Cr^{4+}: Mg_2SiO_4 laser operation (V. Petricevic, *et al*, 1988), the development of tunable solid-state lasers based the Cr^{4+} - ion was rapidly extended to other crystalline hosts.

During the past few years, a lot of effort has been expended on developing Cr^{4+} doped laser crystals, growing single crystals and investigating their spectroscopy, structure, and other relevant properties. Several materials of different crystal structures, which were believed to be suitable for the incorporation of the Cr^{4+} ion into their crystal lattice, were developed and investigated for potential application as lasers. All the materials that were developed clearly show the presence of tetrahedral Cr^{4+} in their absorption spectra. However, only few of these new materials show promise as viable lasers. The problems include very weak or nonexistent luminescence in many materials which could be grown readily as large single crystals, and the difficulty in growing large single crystals for those materials, like Cr^{4+}:$LiAlO_2$, Ca_2SiO_4 which have good fluorescence spectra.

1.2 Scope of thesis

Tunable solid state lasers based on tetravalent chromium ion (Cr^{4+}) are expected to cover the 1 to 2 μm wavelength range which is an eye safe range, and is of great importance for optical communications, remote sensing, lidar, scientific and various medical applications. In this research work presented, we have investigated a range of novel materials for their potential to be useful as tunable solid state lasers in the near infrared wavelength. Cr^{4+} doped Li_2CaSiO_4 and Li_2CaGeO_4 were found to be very promising. They have strong luminescence in the 1100 nm to 1600 nm wavelength range. Large singe crystal were grown and characterized.

The scope of the study is as follows:

1. We describe the search for potential crystalline hosts for Cr^{4+} doped tunable solid-state lasers. A group of materials with the chemical formula A_4MO_4 and A_2XMO_4 were investigated (where A stands for the alkali metals: Li, Na, K; X for the alkali earth metals: Ca, Mg, Cd, Zn; and M represent Si or Ge). Fluorescence spectra measurements indicated that only the Li_2XMO_4 group showed strong luminescence.

2. In order to establish the proper condition for the single crystal growth of $Li_2Ca(Si, Ge)O_4$, their thermodynamic and phase behavior were studied by differential thermal analysis(DTA), and the phase diagrams of potentially interesting materials were investigated.

3. The spontaneous flux growth technique was used to establish the growth conditions and provide seed crystals for later use (top-seeding solution growth).

4. Large singe crystals of Cr^{4+}:Li_2CaSiO_4 were obtained by the top seeded solution growth technique. X-ray diffraction analysis shows that the crystals grown were of the desired phase of Li_2CaSiO_4.

5. Optical properties were investigated by absorption and emission spectroscopy and the refractive indices were determined as a function of wavelength.

6. The properties relevant for the design of devices, i.e. the heat capacities, the thermal expansion coefficients and the thermal conductivities were measured.

Chapter Two

Literature Review

The impressive progress of research in tunable solid-state lasers and the steady improvement of existing solid-state laser materials have kept motivating the search for and the development of new laser materials.

The chromium ion has been successfully used as the optical activator in a large number of tunable crystalline laser materials. The discovery of the new near-infrared tunable solid state laser, chromium doped Forsterite, $Cr:Mg_2SiO_4$ (V. Petricevic *et al*, 1988), tunable in the 1.13 to 1.37 μm range, which employed a new laser active ion, tetravalent chromium(Cr^{4+}), generated growing interest in developing other new crystalline hosts that may accommodate the Cr^{4+} ion. In the time period of 1989 to 1996 additional chromium doped laser materials were developed and reported, culminating in the development of Cunyite, $Cr^{4+}:Ca_2GeO_4$ (V. Petricevic *et al*, 1996).

2.1 The characteristics of Cr^{4+} ion in laser host crystals.

2.1.1 Effect of the crystal field

Most of the existing tunable solid-state lasers use dielectric crystalline hosts containing small amounts of a transition-metal or rare-earth ion.

Optical transitions within the paramagnetic (3d) shell of transition-metal ions have wavelengths and oscillator strengths well suited for laser applications, particularly in applications where energy storage is desired. Optical spectra of 3d ions in crystalline solids exhibit broad bands associated with vibrational interactions. These broad emission bands provide an opportunity for making tunable lasers (A.B.P.Lever, 1968).

The strength of interaction with the lattice is critical to practical attainment of tunable laser action. The 3d shell of transition metal ions participates to some degree in lattice bonding. Thus, crystal field terms and interaction with the lattice are strong. This in turn makes the vibronic sidebands much stronger; the major fraction of the oscillator strength of a given transition often appears in the sidebands, rather than in the no-phonon line. This high relative strength of the vibronic sidebands makes tunable laser action possible.

Transition strengths are strongly influenced by certain symmetry properties. Electric dipole transitions within the 3d shell are strictly parity forbidden between pure 3d states, where magnetic dipole states are parity allowed. Nevertheless, except in cases where the crystal field point symmetry at the active ion site includes inversion, the 3d transitions are dominantly electric dipole transitions. This occurs because the crystal field mixes into the 3d states small contributions from shells with parities opposite to that of the 3d shell. This "configurational" mixing accounts for the electric dipole oscillator strength, but by no means offers a direct and simple way to derive the associated matrix elements or to fully understand the polarization properties of these hosts. This mixing, which is highly dependent on the specific ion and host, largely accounts for the great variance in

oscillator strength among the several transition metal ion - host combinations. Symmetry properties of the crystal field also have a major influence on transition strength and polarization properties. If the site of the active ion has inversion symmetry, electric dipole transitions are not allowed. As a result the oscillator strength will depend on the magnetic dipole interaction, which is usually weaker by at least an order of magnitude (P.F. Moulton, 1986).

2.1.2 Effect of the ligand field

When a transition-metal ion, such as Cr^{4+} or Cr^{3+} is incorporated into a host crystal during the crystal-growing process, its free-ion energy levels are split by the electric field (crystal field) of the surrounding ions (the "ligands"). The effect of ligand ions on the substituted ion depends on the number of ligand ions around the substituted ion and the symmetry of the site occupied by the substituted ion. Energy levels of transition-metal ions are particularly strongly influenced by the ligand crystal field (V. Petricevic, 1990).

The Cr^{4+} ion in tetrahedral coordination is interesting for the realization of tunable, room-temperature solid-state lasers in the near-infrared spectral range between 1.1 and 2 μm (Li Yang *et al*, 1994). The Cr^{4+} emission belongs to a transition between the $^3B_2$ ($^3T_2$) excited state into the $^3B_1$($^3A_2$) ground state, which is only magnetic-dipole allowed. $^3T_2$ and $^3A_2$ denote the energy levels in T_d symmetry (regular tetrahedron) and $^3B_2$ and $^3B_1$ denote the energy levels in D_{2d} symmetry (distorted tetrahedron). In Ca_2GeO_4, the Cr^{4+} in the ($3d^2$) configuration is in tetrahedral oxo coordination with a $^3A_2$ ground state, a $^3T_2$ emitting

state, and the higher excited spin triplet states $^3T_2(F)$ and $^3T_2(P)$. However, the tetrahedron is distorted and the true site symmetry is Cs. This leads to orbital splitting of the T state in T_d symmetry. A detailed assignment of the ground state absorption (GSA) spectrum of Cr^{4+} doped Ca_2GeO_4 was given by M. F. Hazenkamp (1996).

The Cr^{4+} ion exhibits broadband emission because of the coupling between the electronic levels of the 3d electrons with the lattice vibrations. Tanabe and Sugano (Tanabe 1970) presented a series of energy level diagrams for $3d^n$ ions in octahedral coordination showing energy levels of an ion as a function of crystal field parameter Dq and the Racah parameters B and C. Tanabe-Sugano diagrams can be used for tetrahedrally coordinated ions as well if we apply the rule (D.S. McClure, 1959);

$$d^n\,(tetr)=d^{10-n}\,(oct).$$

Where the symbol d^n (tetr) represents the energy level order for a d^n system in a tetrahedral field and d^{10-n} (oct) represents the energy level order for a d^{10-n} system in an octahedral field. Thus we can use the Tanabe-Sugano diagram, Figure 2.1, for $3d^8$ system in an octahedral environment to estimate the level split for the $3d^2$ ion in the tetrahedral environment.

Energy levels were calculated by diagonalizing the Tanabe-Sugano energy matrices using Dq and B as fitting parameters and assuming that the ratio C/B does not change from its value for the free ion. Elements of the energy matrices are shown in Table 2.1.

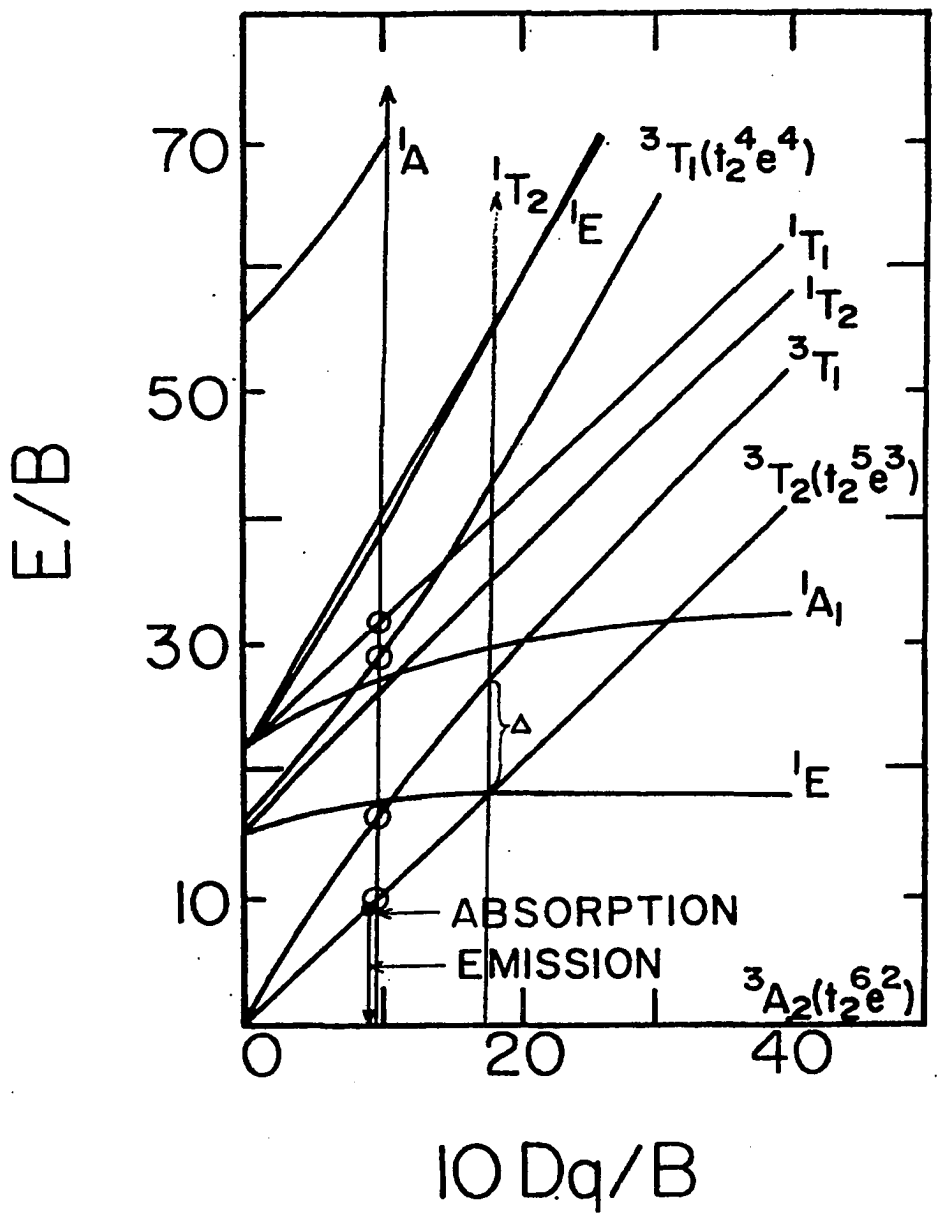

Fig 2.1 Tanable-Sugano diagram for Cr^{4+} in tetrahedral coordination.

Table 2.1: Energy Matrices for the configuration d^2 in a Cubic Field.

(D.S. McClure 1959)

$^1A_1$	T^2	10B + 5C - 10Dq	$\sqrt{6}$ (2B + C)
	e^2	$\sqrt{6}$ (2B + C)	8B + 4C + 10Dq
$^3A_2$	T^2	-8B + 10Dq	
^1E	t^2	B + 2C - 10Dq	-2 $\sqrt{3}$B
	e^2	-2 $\sqrt{3}$B	2C + 10Dq
$^1T_1$	et	4B + 2C	
$^3T_1$	t^2	-5B - 10Dq	6B
	et	6B	4B
$^1T_2$	t^2	B + 2C - 10Dq	2 $\sqrt{3}$B
	et	2 $\sqrt{3}$B	2C
$^3T_2$	et	-8B	

For the purpose of classifying materials, and relating the nature of the emission band to the ligand field, we introduce the parameter Δ that is shown in Figure 2.1 and represents the energy difference between the $^3T_2$ and ^1E states. From Table 2.2, it is clear that materials usable as tunable lasers must belong to the intermediate or low field ligand category.

Table 2.2: Classification of materials as emitters

High Field	$Dq/B > 18$	$\Delta > 0$	Sharpline emission (phosphorescence)
Intermediate Field	$Dq/B \sim 18$	$\Delta \sim 0$	Mixture of sharp and broad emission (fluorescence and phosphorescence)
Low Field	$Dq/B < 18$	$\Delta < 0$	Broadline emission (fluorescence)

In tetrahedral coordination, the transition-metal cation such as Cr^{4+} sits at the center of a tetrahedron surrounded by four anion ligands. Tetrahedral coordination produces lower crystal field splitting than octahedral coordination. For equal ligand ion charges and transition-metal impurity ion-ligand distances, the ratio of the tetrahedral to octahedral crystal field strength is given by (F.A. Cotton, 1990):

$$Dq(tetr) / Dq(oct) = -4/9$$

The most important consequence of this relation is that the absorption and the Stokes-shifted luminescence of ions residing in a tetrahedral environment is expected to shift significantly toward the infrared spectral region.

Cr^{4+} doped tunable laser operation is expected to cover the spectral range between 1 and 2 μm. This is best illustrated by the Tanabe-Sugano diagram for a $3d^2$ ion, such as Cr^{4+}, in tetrahedral coordination as shown in Figure 2.1. Assuming the crystal field splitting $10Dq \sim 10{,}000\ cm^{-1}$ and Racah parameter for Cr^{4+} $B \sim 1{,}000\ cm^{-1}$ it is obvious that the

emission should occur in the 1 to 2 μm spectral region. This is indeed the case for Cr^{4+} in Forsterite and YAG. This leads us to believe that Cr^{4+}, when incorporated in different dielectric crystal hosts, can exhibit laser action in different parts of infrared region due to different crystal fields acting on the Cr^{4+} ion.

Very important feature of $3d^2$ ions in tetrahedral sites, as seen from the Tanabe-Sugano diagram, is the existence of 3 spin-allowed absorption bands, indicated in the diagram, which is of great importance for efficient laser pumping, especially for flashlamp pumping. Due to lack of inversion symmetry, electric dipole transitions with high transition strengths are expected.

Another important aspect of Cr^{4+} substituting for a tetravalent cation, such as Si^{4+} in Forsterite, is that the tetrahedral site provides ideal environment for covalent bonding with surrounding ligand ions, such as divalent oxygen. The high covalence of the Cr(IV)-O(II) bond in Forsterite may account for its high chemical stability against disproportionation of the Cr^{4+} ion (V. Petricevic, 1990).

2.2 Crystal structures suitable for Cr^{4+} doping

The incorporation of Cr^{4+} as substitutional ions into tetrahedral sites requires that the following conditions are met (Li Yang, V. Petricevic, 1994):

1. Presence of a tetrahedral site containing a tetravalent cation;

2. The ionic size of the site be close to that of Cr^{4+};
3. No good sites are available for the competing Cr^{3+} ions.

Additional requirements for a good laser host crystal are:

1. The host must be transparent at the expected operating wavelengths;
2. The required crystal composition should melt congruently;
3. The host material has adequate thermo-mechanical properties.

Table 2.3: Selected Cation Ionic Radii in Oxides (R. D. Shanon, 1976)

	Radius in Å		
Ion	CN = 4	CN = 6	CN = 8
Cr^{4+}	0.41	0.55	
Si^{4+}	0.26	0.40	
Ge^{4+}	0.39	0.53	
Ti^{4+}	0.42	0.605	
Sc^{3+}		0.745	0.870
Cr^{3+}		0.615	
Cr^{2+}		0.73	
Zn^{2+}	0.60		
Mg^{2+}	0.57	0.72	0.89
Ca^{2+}		1.00	1.12
Na^{+}	0.99	1.02	1.18
Li^{+}	0.59	0.76	0.92
K^{+}	1.37	1.38	1.51

Table 2.3 displays selected ionic radii for various coordination numbers. Comparing the ionic radii of Cr^{4+} with Si^{4+} and Ge^{4+}, it is clear that tetrahedral Cr^{4+} is a closer match to Ge^{4+} than to Si^{4+}. Cr^{3+} and Cr^{2+} is a good match with Mg^{2+}. Stabilization of Cr^{2+} is particularly undesirable since it may cause weak absorption in the lasing wavelength region. On the other hand, it is obvious that Cr^{3+} and Cr^{2+} are incompatible with Ca^{2+} due to large size mismatch. Examples of Cr^{4+} substituting for Si^{4+} is Cr^{4+}:Mg_2SiO_4 (forsterite), and Cr^{4+} substituting for Ge^{4+} is Cr^{4+}:Ca_2GeO_4 (cunyite).

Cr^{4+} in tetrahedral sites forms covalent bonds with the surrounding oxygen ions, thus it will be chemically stable. By controlling the growing process Cr^{4+} can be incorporated in tetrahedral sites in a variety of other materials such as silicates, germanates and titanates. Germanates and titanates are particularly promising since there is better size match of the ionic radii, and a larger infrared shift is expected due to the bigger size of the Ge or Ti tetrahedra, and consequently smaller crystal fields at the Ge or Ti sites.

The type of crystal structure of the tetrahedral site (available for Cr^{4+} substitution) proved to be the most important factor. Cr^{4+} ions substitute for Si^{4+}, Ge^{4+} as well as Al^{3+}, P^{5+} ions in tetrahedral sites when there are no octahedral sites available for Cr^{3+} -substitution in the crystal structure. It should be pointed out that for crystalline materials without octahedral sites available for Cr^{3+} -substitution the incorporation for Cr^{4+} does not depend on the oxidizing properties of the synthesis atmosphere. For example, only Cr^{4+} incorporates into Ca_2GeO_4 in spite of the use of Cr_2O_3 as the doping impurity and nitrogen as the synthesis atmosphere for crystal growth of this material. On the other hand, for growing

single crystals of Cr^{4+} doped Forsterite or YAG garnets, the growth atmosphere has to contain a few percent of oxygen to stabilize Cr^{4+} in tetrahedral sites because there are numerous octahedral sites available for Cr^{3+} substitution in these structures.

Favorable incorporation of Cr^{4+} into the crystal structure is not a guarantee of providing the desired emission properties. Nonradiative relaxation may predominate over radiative transitions. Synthesis of numerous Cr^{4+} doped silicates, germanates, aluminates, phosphates and other complex materials having tetrahedral void sites in their structures, were already attempted, but only few compounds were found to exhibit strong Cr^{4+} emission. Among them, $LiSc(In)GeO_4$ and $Ca_2(Si, Ge)O_4$ with olivine type structure, $(Li, Na)AlO_2$ and $Li_2Mg(Si, Ge)O_4$ with pseudo-cubic wurtzite-like structure, and $Li_2Ca(Si, Ge)_4$ with tetragonal structure exhibit good emission properties and are very promising for tunable solid state laser application in the 1.1-1.6 μm region. Unfortunately, all compounds named above are difficult subjects for single crystal growth due to their incongruent melting behavior or unfavorable polymorphism.

Therefore, we propose the $Li_2M^{2+}(Si, Ge)O_4$ group of materials as the crystal hosts which will yield a new (important) class of tunable solid state lasers in the 1-2 μm wavelength region with unique properties. The wavelength range of these lasers are expected to cover is of great technological importance.

2.3 The history of developing Chromium doped lasers

2.3.1 Cr^{3+} doped lasers

The history of tunable solid-state lasers can be traced to the research performed at Bell Laboratories over forty years ago. In 1963, Bell-labs researchers reported the first vibronic laser, a nickel-doped magnesium fluoride (Ni^{2+}: MgF_2) device (L.F. Johnson *et al*, 1963). Soon after that, laser operation was obtained with a variety of Ni^{2+}, Co^{2+}, and V^{2+} doped materials. But, these flashlamp-pumped lasers had a serious drawback: they operated only at cryogenic temperatures (Walter Koechner, 1987).

In 1977, Alexandrite crystal (chromium doped $BeAl_2O_4$) was made to lase on a vibronic transition (Walling and Jenssen, 1979). It was the first room-temperature, broad wavelength-tunable laser, and marked the start of a family of room temperature tunable solid-state lasers. Shortly after the discovery of Alexandrite it became apparent that Cr^{3+}-doped tunable lasers can be constructed with hosts other than Alexandrite. For example, the emerald laser, Cr^{3+} in Be_3Al_2 $(SiO_3)_6$, had a higher gain cross-section than Alexandrite. Since then, the interest in Chromium doped tunable solid-state lasers has intensified, and the research has been aimed at looking for new host materials to be used with the chromium ion.

2.3.2 The development of Cr^{4+} doped lasers

In conventional chromium-doped lasers, Cr^{3+} is the active ion and their tuning range rarely goes beyond 1μm. Tunable solid-state lasers based on tetravalent chromium ion are expected to cover the 1-2 μm range. This range is of great importance, since it is eye-safe, for optical communications, remote sensing, lidar, scientific and various medical applications.

Compared with Cr^{3+} ion, the Cr^{4+} oxidation state is rather unstable. Therefore, only a few oxidic chromium (4+) compounds are known and fully characterized. Cr: Mg_2SiO_4 was the first laser crystal in which the laser active center was identified as the tetravalent chromium. Since the first demonstration of Cr^{4+}: Mg_2SiO_4 laser operation (V. Petricevic, Verdun, 1988), the development of tunable solid-state lasers based the Cr^{4+} -ion was rapidly extended to other crystalline hosts.

In the early of 1990's, a number of Cr^{4+} based crystals were grown and investigated for potential laser applications. Room temperature laser action was achieved in Cr^{4+} doped forsterite, in YAG (Shkadrevich, Zverev, 1989), in YSO (Koetke, S. Kuck, 1993) and in the $Y_3Sc_xAl_{5-x}O_{12}$ (S. Kuck 1994).

During the past few years, a lot of effort was expended on the Cr^{4+} doped crystal growth and investigation of their spectroscopy and structure. Several materials with different structures that were believed to be suitable for incorporation of the Cr^{4+} ion into their

crystal lattice were developed and investigated for potential laser applications. All the materials that were developed clearly show the presence of tetrahedral Cr^{4+} in their absorption spectra. However, only few of these efforts have produced new laser materials. The problems include very weak or nonexistent luminescence in many materials which could be grown readily, and the difficulty in crystal growth for those materials like Cr^{4+}:$LiAlO_2$, Ca_2SiO_4 which have good fluorescence spectra.

It was reported (D. Reinen, 1995) that Cr (IV) ions were successfully incorporated into the tetrahedral sites of various oxidic compounds with different structures, for example by isomorphic substitution of Ge(IV) and Si(IV) with a comparable ionic radii. However, they had difficulty in preparing pure Cr(IV) containing solids and to synthesize single crystals, due to the tendency of Cr^{4+} to disproportionate into Cr^{3+} and Cr^{5+}.

It was shown that Cr^{4+}:$LiAlO_2$, Cr^{4+}:$LiGaO_2$ (S. Kuck, B.H.T. Chai, 1996) and Cr^{4+}:Ca_2GeO_4 (Reinen 1995, Atanasov, and Kuck, 1996), have emissions between 1.1 μm and 1.7 μm. The room temperature lifetime of the Cr^{4+} emission in $LiAlO_2$ is 29 μs, the longest lifetime known up to 1994 for the Cr^{4+} systems. Cr^{4+}: Ca_2GeO_4, which has the olivine-like structure of Forsterite, is interesting because of the high distribution coefficient of the Cr^{4+} ion. M. F. Hazenkamp et al (1995) reported on near-infrared (NIR) absorption and luminescence experiments with Cr^{4+} doped Ca_2GeO_4 single crystals. The single crystals were grown by using the flux method and their size was quite small (about 0.5x 0.5x1.0mm). The flux used to grow Ca_2GeO_4 single crystals was $CaCl_2$. In

their studies, it was shown that Cr^{4+} ions could be incorporated into the crystal host of Ca_2GeO_4 with concentrations as large as 30 mol%. The luminescence of Cr^{4+}: Ca_2GeO_4 is much less quenched at room temperature than that of Cr^{4+} doped Forsterite.

2.3.3 The development of Cr^{4+}: Ca_2GeO_4

Since the identification of Cr^{4+} as the laser center in Forsterite, synthesis and spectroscopic studies of numerous Cr^{4+} doped olivine-like silicates and germanates have been carried out. It was shown (V.Petricevic, A.Seas, 1993) that Cr^{4+} doped Ca_2SiO_4, Mg_2GeO_4, $(Ca, Mg)_2GeO_4$, and Ca_2GeO_4 with the olivine type structure are among the few materials that exhibit strong emission in near infrared (IR) region and should be investigated as potential crystalline media for tunable laser applications. Unfortunately, all silicates and germanates belonging to olivine-type structure family (except Forsterite) are characterized by complicated polymorphism and/or incongruent melting behavior that creates many difficulties for the preparation of large single crystals. As a result, only Cr doped Forsterite was successfully grown and fully characterized as IR laser material. All other silicates and germanates of olivine structure were not considered as a potential laser materials due to the unfavorable crystal growth properties. However, the extremely strong luminescence of Cr^{4+} in above-mentioned olivine like materials (Li, Yang and Petricevic, 1993) was the incentive to consider alternate crystal growth methods for these materials. Therefore, attention was focused on single crystal preparation of Cr^{4+}:Ca_2GeO_4. Tunable laser emission of Cr^{4+}:Ca_2GeO_4 covers the important eye safe wavelength range of 1.4-1.6 μm.

According to the phase diagram of CaO-GeO (A. K. Shirvinskaya, 1966), calcium germanate(Ca_2GeO_4) has a congruent melting point at 1900°C and has two structural modifications (α and γ phases). The reversible phase transformation $\alpha \leftrightarrow \gamma$ occurs at 1453°C. Low-temperature γ-Ca_2GeO_4 is isomorphic with Forsterite (Mg_2SiO_4) and has the olivine type structure with the space group Pbmn. The chromium doped low-temperature phase of Ca_2GeO_4, which is isomorphic with Forsterite (Mg_2SiO_4), seemed to be very promising for infrared laser applications due to its unique spectral-luminescence properties. The lattice parameters of Ca_2GeO_4 are a = 5.240 Å, b = 11.400 Å, and c = 6.790Å. Obviously, the crystal growth process of the low temperature modification of Ca_2GeO_4 has to be carried out in a temperature range that is below the phase transformation temperature. Based on this reason, the flux growth technique was chosen for the preparation of Cr^{4+}:Ca_2GeO_4 single crystal.

The Cr-doped Ca_2GeO_4 crystals with the quality suitable for laser applications have been successfully grown in a radio-frequency (RF) heated crystal "pulling" equipment designed for the conventional Czochralski crystal growing method. In spite of the presence of additional chemical components in the system, such as CaF_2 used as the fluxing solvent, stable conditions for Cr^{4+}:Ca_2GeO_4 crystal growth were created without constitutional super-cooling. Large crystals of Cr-doped γ-Ca_2GeO_4, of the olivine structure with sizes up to 15 mm in diameter and 60 mm long were grown.

Only Cr^{4+}-substitution takes place in these Ca_2GeO_4 single crystals in spite of nitrogen atmosphere being used in this TSSG type growing process. High concentration of laser

active ions can be easily achieved in Cr^{4+}:Ca_2GeO_4 crystals using the above-described crystal growth method. Therefore, this crystal may represent a laser material suitable for diode pumping and fabrication of miniature laser devices such as microchip and waveguide lasers.

The emission spectra, shown in Figure2.3.1, of Cr:Ca_2GeO_4 were measured for 670-nm excitation at room temperature and at liquid nitrogen temperature. We attribute the single band with a maximum at 1290 nm in the room-temperature emission spectrum of Cr:Ca_2GeO_4 to Cr^{4+}, indicating that in the crystal structure of Ca_2GeO_4 only the Cr^{4+} substitution takes place. The low-temperature emission spectrum of Cr:Ca_2GeO_4 is characterized by a sharp zero-phonon line at 1200 nm followed by a vibrational sideband similar to the low-temperature spectrum of Cr doped Forsterite. The fluorescence lifetime of Cr^{4+} in Ca_2GeO_4 for 1064-nm excitation is about 5 μsecond at room temperature for a crystal with high concentration of Cr^{4+} ion and about 15 μsecond for a crystal with low Cr^{4+} doping.

Figure 2.3.2 shows the absorption spectra for a Cr:Ca_2GeO_4 crystal with polarization of the field parallel to the three crystal directions. The anisotropy of the electric dipole moment is clearly evident. The spectra are strikingly similar to those observed in the absorption spectra of chromium-doped forsterite and other olivines, the only difference being significant red shift. We attribute the absorption bands observed in the spectra exclusively to the transitions of the Cr^{4+} ion. In 1996, laser action of a Cr^{4+} doped Ca_2GeO_4 crystal was demonstrated (V.Petricevic, A. Bykov, 1996). 2 to 5 mm thick

slices cut from boules grown by the TSSG technique were used for the laser experiments. Pulsed laser action was observed upon pumping at 1064nm with a Q-switched Nd:YAG laser. The free-running laser output was centered at 1400nm. Tunability over the 1348 - 1482 nm spectral range with a maximum slope efficiency of 6.1% was demonstrated.

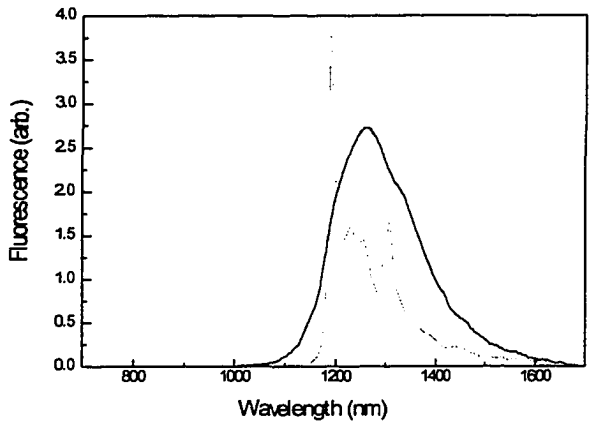

Figure 2.3.1 Emission spectra of Cr^{4+}: Ca_2GeO_4 crystals: thin spectrum at 77 K, thick spectrum at 300 K.

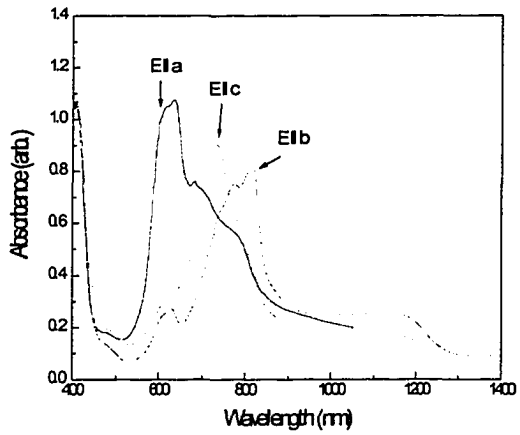

Figure2.3.2 Polarized absorption spectrum of $Cr:Ca_2GeO_4$ crystals

2.4 The methods of developing new laser materials

2.4.1 Introduction

Solid state electronic and optical devices are widely based on the use of high quality, defect free single crystals. Thus a variety of research and development studies aimed at understanding and improving the growth of single crystals have been undertaken which has led to many advances in crystal growing techniques. The basic methods were developed, modified, and refined to enhance their applicability for use with specific materials or groups of materials, as well as to obtain the desired quality of bulk crystalline solids.

A wealth of information exist in the specific areas of thermodynamics, phase equilibrium and stability, fluid dynamics, nucleation, growth kinetics, segregation, interface morphology and crystalline defects as related to the growing of single crystals. However, because of the complex nature of the processes involved in crystal growth and the large number of variables influencing the processes, there is still a large gap between theories and practical crystal growing.

The growing of any particular material requires careful selection of the proper technique based on the material's specific properties and the required quality. In addition, the scaling of the laboratory bench scale process to a commercially viable (profitable) process adds to the complexity of the tasks. Methods of crystal growing fall into three basic categories:

1. solution growth,
2. melt growth,
3. vapor phase growth.

And the solution growth method itself may be further divided into:

1. aqueous solution growth,
2. molten salt growth (flux),
3. metallic solution growth.

High-temperature crystallization from solution (so-called flux growth) has gained wide acceptance for growing single crystals of complex multi-component systems (D. Elwell et al, 1975). The "flux" is typically a molten salt or oxide used as a solvent. The use of the word "flux" is based on its more general usage as a substance that reduces the melting temperature, or dissolves oxides as in soldering process in joining pieces of similar or dissimilar materials.

The method of crystal growth from high-temperature solutions includes a number of related techniques that are often treated separately. The most widely used is flux growth, here the solvent is a molten salt or oxide, or a mixture such as $PbO + PbF_2$.

In the growing of crystals from high-temperature solutions (HTS) the constituents of the material to be crystallized are dissolved in a suitable solvent and crystallization proceeds as the solution becomes critically supersaturated. Supersaturation may be promoted by

evaporation of the solvent, by cooling of the solution or by a transport process in which the solute is made to transfer from a hotter to a cooler region.

The principal advantage of using a solvent is that crystal growth occurs at a lower temperature than that required for growth from the pure melt. A reduction in the temperature is desirable or even essential for many materials, in particular those in the following categories.

- Materials that melt incongruently, that is, decompose before melting so that crystallization from the melt results in the formation of some other phases.
- Materials that undergo a phase transition which results in severe strain or even fracture; crystals of such materials must be grown at temperatures below this transition temperature.
- Materials that have a very high vapor pressure at the melting point.
- Materials which have a very volatile constituent and whose chemical composition may therefore change on heating close to the melting point.
- High temperature refractory materials which require difficult or expensive techniques for crystallization from the melt.

Other advantages of growing crystal from solutions are based on the fact that the growing crystal is not exposed to steep temperature gradients and that the crystal can grow in an unconstrained fashion, thus the crystal can grow free from mechanical or thermal stresses in the solution and develop facets. This, in combination with the relatively low growth temperature compared with the melting point of the solute, often results in better crystal

quality with respect to point defects, dislocation densities and low-angle grain boundaries, compared to crystals grown directly from their own melt. The disadvantages of the method are substitution or interstitial incorporation of solvent molecules into the crystal, microscopic or macroscopic inclusions of solvent or other impurities, non-uniform doping, a slow growth rate and containment problems.

Crystals grown from fluxed melts are used both for research and by industry. One of the most important applications of flux growth is in the synthesis of new materials. Many examples can be found in the literature of new materials that were first made as small crystals by the flux growth method, either by accident or during the systematic studies of novel systems. This is especially true for transition metal or rare-earth compounds, particularly the complex oxides (for example, $Cr:Ca_2GeO_4$ and $Cr:LiScGeO_4$). In addition, materials obtained by powder reactions (sintering) have often been crystallized for the first time by the flux growth.

2.4.2 Choice of flux

In general, the choice of a flux is made empirically based on experience with related materials. Fluxes that have at least one ion in common with the desired crystal substitution impurity ions are preferred. The desirable properties of an ideal solvent are as follows (R.A. Laudise, 1970):

1. High solubility for the crystal constituents, dissolving at least 10 to 50 wt.% of the crystallizing substance.

2. The crystal phase required should be the only stable solid phase.
3. Appreciable change of solubility with temperature, to provide a temperature coefficient of solubility (slope of the liquidus curve) not less than 1 wt. % per 10°C;.
4. Viscosity in the range of 1 to 10 centipoise.
5. Low melting point.
6. Low volatility at the highest operating temperature (except when the solvent evaporation technique is used).
7. Low reactivity with the container materials.
8. Be inert in interaction with the crystallization atmosphere.
9. Absence of elements which could be incorporated into the crystal.
10. Ready availability in high purity at low cost.
11. Density that is appropriate for the mode of growth.
12. Ease of separation from the grown crystal by chemical or physical means.
13. Low tendency of the solvent to "creep" out of the crucible.
14. Low toxicity.

There is no solvent which fulfill all these ideal properties and a compromise is always necessary, depending on the crystal type, on the size requirement, and desired quality which makes some "ideal" properties particularly important. Both the physical and chemical properties of the flux are important. The earliest trends in selecting a flux tended to emphasize its physical properties. Low melting point, low viscosity and low volatility are particularly important for most applications. Examples of single crystal

growth using the flux method are the growing of $LiScSiO_4$ using lithium molybdovanadate (Jun Ito, 1977), $LiScGeO_4$ using $LiF\text{-}V_2O_5$ based flux, and Ca_2GeO_4 using $CaCl_2\text{-}CaF_2$ as flux (V. Petricevic, A. Bykov 1996).

2.4.3 Single crystal growth from solution

Spontaneous crystallization with slow cooling

Spontaneous crystallization is mainly used to prepare crystals used in research work. It is technically simple, but the sizes of the crystals are relatively small and quality of the crystals is generally rather low, because the crystallization conditions can not be controlled accurately. The required supersaturation of the solution is achieved either by reducing the temperature (slow cooling) or by evaporating the solvent. The former method is more popular, and serves as a basis in developing growth procedures for technically important crystals.

The most common slow cooling technique for producing supersaturation in flux growth is by using a linear cooling rate of 0.1°C/h to 10°C/h. The linear growth rate v (cm/hr) by slow cooling is related to the cooling rate (Laudise, 1963) by

$$v = \frac{V}{A\rho}\frac{dn_e}{dT}\frac{dT}{dt}$$

Where V is the volume of solution (cm^3), A the surface area of the growing crystal (cm^2) and ρ its density (gcm^{-3}), dn_e/dT the change in solubility per degree (gcm^{-3} $°C^{-1}$) and dT/dt the cooling rate in °C/hr.

Top seeding solution growth (TSSG) with pulling

The growing of large crystals is favored by the use of seed crystals. This is a common practice in crystal growth from aqueous solutions. However, technical reasons make the use of seeds very difficult in high-temperature solutions. The seeds cannot be observed in the (platinum) crucibles and in the usually opaque solutions. Therefore, the solubility curve has to be known very exactly and the conditions must be carefully adjusted in order to prevent dissolution of the seed crystals. Growth on a rotating seed immersed in the solution has been tried. In some reported attempts, seed crystals were attached near the base of an unstirred crucible but additional multi-nucleation was observed. This shows that the use of seed crystals is only of advantage when the solution is homogenized by forced convection or when the solution volume is small as is often the case in the traveling solvent technique and in liquid phase epitaxy (Elwell and Scheel, 1975).

The most popular means of nucleation control is by top-seeding. The position of the crystal-liquid interface is important with respect to inclusion formation, dislocation density and maximum attainable growth rate. With increasing depth of the growth face (in the solution) the temperature gradient at the interface becomes smaller and the supersaturation gradient increases. However, the stable growth rate decreases. The dislocation density in the crystal will decrease if inclusions are not trapped. The temperature gradient also determines the degree of facetting as discussed by Wilcox (1970). The technique of growth on rotating seed crystals at the top of a solution, with or without withdrawal, has been given a variety of names: Czochralski, Kyropoulos, pulling

from solution etc., but it seems that the term top seeding solution growth (TSSG) first introduced by Linz et al. (1965), and described in detail by Belruss et al. (1971), is most appropriate and is therefore adopted in the following discussion.

The crystal pulling technique is one of the most versatile and widely used of the variety of methods in use today. The method was introduced by Czochralski and is now one of the standard growth techniques used for laser rod production. The process is simple in principle. Material contained in a suitable crucible is heated until the charge is melted. The thermal environment is adjusted so that equilibrium between liquid and solid is approached on the surface of the melt in the crucible center. A seed crystal is placed into the "cold spot" and, by controlling the melt temperature, solidification may be started. If the seed is rotated and withdrawn (pulled) from the melt surface at a rate not exceeding the rate of solidification, a cylindrical crystal known as a "boule" or "ingot" is the result. The crystal diameter control is usually achieved by controlling the liquid temperature.

Although simple in principle, the pulling method is complex in detail and a wide variety of variables must be carefully controlled. The consideration of applicability starts with evaluation of the nature of material to be grown, because the method does not lend itself easily to growing materials 1) which melt incongruently, 2) exhibit high vapor pressure at the melt temperature, or 3) for materials which have a first order solid-solid phase transition.

If we consider the flux growth or high temperature solution growth methods, combined with the top-seeding and pulling technique, then we have the so-called "top seeding solution growth" (TSSG) method. Therefore, the disadvantages of pulling technique mentioned above could be overcome and large, high quality single crystals can be grown by using TSSG. However, there is a drawback for using pulling technique from solution. If crystal is grown from solution by the pulling technique, the excess solvent is rejected into the liquid at the growth interface. This diffusion transport step becomes the rate-limiting factor for the growth of crystal. If the rejected compounds build up to a critical level, the well-known phenomenon of constitutional supercooling occurs. Constitutional supercooling is the major reason for inclusions because of the unstable growth (cellular growth) which takes place in the crystal growing process by pulling from the flux technique. The critical growth rate at which the interface will break down due to constitutional supercooling is determined by the temperature gradient at the growth interface, the diffusion coefficient of solute in the liquid and the concentration of solution. The diffusion coefficient is a material property and not a controllable variable. By increasing the initial concentration of solution and the temperature gradient, it is possible to reach the maximum value of stable growth rate.

Chapter Three

Search for new laser hosts

3.1 Introduction

Growth of high quality laser materials is the key part of the research for the development of tunable solid-state laser materials. The evaluation of materials which may be useable as lasers includes the following steps:

1. Using resistively and/or inductively heated furnaces, initial preparation of ceramic type host materials and their doping by the laser active ion is accomplished;
2. X-ray diffraction and x-ray fluorescence techniques are used to determine the structural and chemical properties;
3. Determination of phase diagrams and investigations of phase transitions is performed using high-temperature differential thermal analysis. This is done to determine the necessary growth conditions and select materials suitable for the growth of optical and laser quality crystals;
4. Steady-state and time-resolved fluorescence measurement are performed to determine the emission properties of the tentative materials.

The incorporation of Cr^{4+} impurity ions into crystal lattice sites requires the following conditions to be met: presence of a tetrahedral site (containing a tetravalent cation, eg. Ge^{4+}, Si^{4+}); the ionic size of the site that is close to that of Cr^{4+}; no good sites to exist for the competing Cr^{3+} and Cr^{2+} ions.

The type of crystal structure and geometry of the tetrahedral sites(available for Cr^{4+} substitution) proved to be the most important factor. However, favorable, incorporation of Cr^{4+} into the crystal structure is not guaranteed of providing emission properties. Nonradiative relaxation may predominate over radiative transitions. Synthesis of numerous Cr^{4+} doped silicates, germanates, aluminates, phosphates and other complex having tetrahedral void sites in structure, were already carried out but only few compounds were found to exhibit strong Cr^{4+} emission.

We can plan the research work for the synthesis of new Cr^{4+} -doped materials as follows:

- Structure study (tetrahedral sites contained)
- Chemical composition
- Isomorphous substitutions
- Solid-state reactions
- New compounds(ceramics)
- Luminescence properties.

3.2 Preliminary studies

The oxidation state of Cr^{4+} is rather unstable compared with that of Cr^{3+}, therefore, only few chromium (4+) oxide compounds are known and fully characterized. Chromium (IV) oxide (CrO_2) is normally synthesized by hydrothermal reduction of CrO_3. It has the undistorted rutile structure (i.e., no metal to metal bonds as in MoO_2). It is ferromagnetic and has metallic conductance, presumably due to the delocalization of electrons into energy bands formed by overlap of the metal d and the oxygen pπ orbitals.

There were many Cr^{4+} doped materials synthesized over past few years, but only few compounds mainly with the olivine structure, such as Forsterite, were found to exhibit strong emission and have a sufficiently long lifetime to be useful. The study of incorporation of Cr^{4+} into tetrahedrally co-ordinated lattice sites, as the doping impurity began with the investigation of Cr^{4+}:Mg_2SiO_4(Forsterite), and the tetravalent chromium (Cr^{4+}) was identified as the active ion for potential laser action in the 1~2 μm range (V. Petricevic 1988).

The olivine structure type belongs to the orthorhombic space group: Pbnm. The chemical formula of olivine like structure materials is R_2MX_4 (where X = oxygen or halogen). The prototype is the Forsterite(Mg_2SiO_4) which was used for investigating the incorporation of Cr^{4+} as a dopant. It is believed that in crystals with olivine structure such as Forsterite, the extremely distorted oxygen tetrahedron, occupied by the Cr^{4+} ion, provides a low-

symmetry crystal field that may relax the electric dipole transition selection rules resulting in high quantum efficiencies. We can systematize the search for compounds available for Cr^{4+} substitution, by analogy with olivine-type compounds.

It was the intention of our research first to prepare a series of Cr^{4+} doped compounds related to the R_2MO_4 group (where M=Si, Ge), by the replacement of Mg and Si in forsterite with isomorphous elements. These compounds are usually crystallized as olivine, phosphate (Li_3PO_4), or vanadates types of structures. Within the R_2MO_4 (e.g. olivine-type) group, various isomorphous substitutions are possible:

- $2R^{2+} = 2A^{1+} + X^{2+}$

  Where A = Li, Na, K, X = Mg, Ca, Cd, Zn

- $2R^{2+} = A^{1+} + X^{3+}$

  Where A = Li, Na, K, X = Al, In, Sc

- $2R^{2+} = 4A^{1+}$

  Where A = Li, Na, K

Obviously, not all the compounds mentioned above are amenable to synthesis due to crystal-chemistry consideration, but the isomorphous substitutions may be considered for the evaluation of spectral (luminescence) properties.

3.3 Preparation of ceramic samples

Synthesis of the chemical compounds is carried out by solid state chemical reactions. e.g.:

$$2A_2CO_3 + MO_2 \Longrightarrow A_4MO_4 + CO_2 \uparrow$$

$$A_2CO_3 + XCO_3 + MO_2 \Longrightarrow A_2XMO_4 + 2CO_2 \uparrow$$

Where A = Li, Na, K; X = Ca, Mg, Cd, Zn; and M = Si, Ge.

At the first stage of the experiments, the R_2MO_4-type compounds are prepared by solid state reaction by mixing the reactants in appropriate molar amounts. The chemical compounds of A_2O and XO are obtained from the thermal decomposition of A_2CO_3 and XCO_3. All the A_2CO_3 and XCO_3 are subjected to thermogravimetric analysis, and the weights of A_2O and XO obtained form the thermal decomposition of A_2CO_3 and XCO_3 at about 350°C must agreed with the pre-calculated values. Cr_2O_3 is used as doping impurity (0.5 ~ 3wt.%). The process is carried out in a muffle furnace (Thermoline 48000) under ambient atmosphere. All processing parameters are chosen in accordance with the physico-chemical properties of initial reactants.

In the reaction, the reactants are slowly heated from 500 to 850 °C(see Fig. 3.1). This is to avoid the fast decomposition of CO_2 that will cause materials to "boil" out of the reaction crucible.

Finely ground mixtures of appropriate amounts of each starting material are heated in the muffle furnace. After the initial heating, the reaction product is thoroughly homogenized by crush-grinding in a mortar, then the second and third sintering procedures are applied under the conditions of fast heating from room temperature to about 900 °C, followed by isothermal "soaking" for 10 hours at 900 °C.

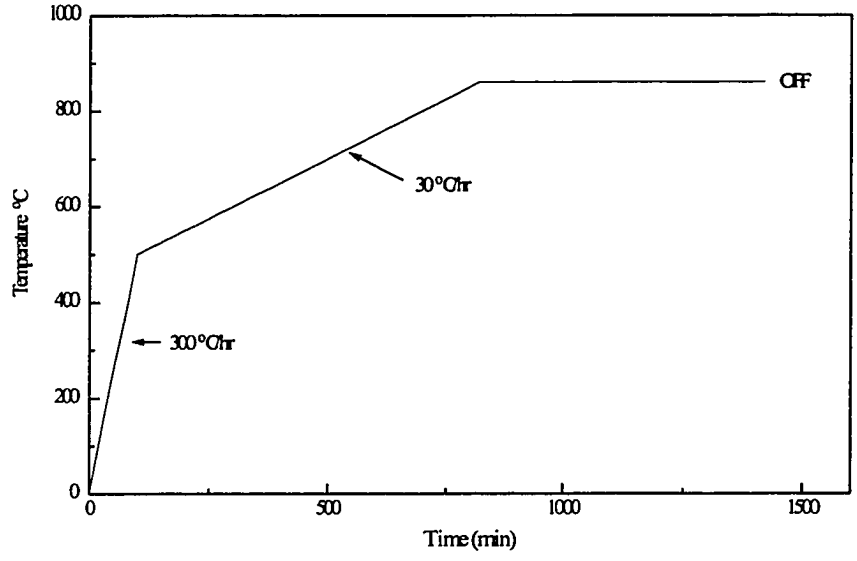

Figure 3.1 A typical thermal processing protocol for preparing the ceramics of A_4MO_4 and A_2XMO_4.

3.4 Luminescence spectroscopy measurement

The purpose of this step is to study systematically and identify which samples (compounds) possess the potential of being usable as a tunable solid-state laser. Therefore, we determine the luminescence of the synthesized compounds and the results are shown in Table 3.1. From Table 3.1, the groups of materials with the chemical formula A_4MO_4 have no Cr^{4+} luminescence. Only the group of materials with the chemical formula Cr^{4+}:$Li_2Ca(Mg,Cd,Zn)Ge(Si)O_4$ have the strong emission properties (Figure 3.2). All these Li contained materials are characterized by wide wavelength range of emission and by emission intensity stronger than that of Forsterite.

Comparing the emission spectra of Cr^{4+}:$Li_2CaGe(Si)O_4$ with forsterite(Cr:Mg_2SiO_4) (Fig.3.3), only Cr^{4+} -ions are incorporated into Cr^{4+}:$Li_2CaGe(Si)O_4$. But, in forsterite (Mg_2SiO_4), there are Cr^{3+} and Cr^{4+} both doped.

The next stage of the experiments is connected with single crystal growth of Cr^{4+}-doped materials. Table 3.2 shows us the phase transition information of the group of materials with chemical formula $Li_2(Mg, Zn)(Ge,Si)O_4$, and it is obvious that these materials are characterized by complicated phase diagrams. This makes the single crystal growth very difficulty.

Table 3.1 Experimental Results of Ceramic Synthesis with Cr_2O_3 Doping (1%wt)

Compounds	Heat Treatment °C	Luminescence	Other Characterization
Li_4GeO_4	900	No	Green
Na_4GeO_4	900	No	Yellow, Hygroscopic
K_4GeO_4	900	No	Yellow Green, Hygroscopic
Li_4SiO_4	900	No	Green
Na_4SiO_4	900	No	Yellow Green
K_4SiO_4	900	No	Yellow Green
Li_2MgSiO_4	**1000**	**Strong Cr^{4+}**	**Green**
Li_2MgGeO_4	**1000**	**Strong Cr^{4+}**	**Green**
Li_2CaSiO_4	**900**	**Strong Cr^{4+}**	**Dark Green**
Li_2CaGeO_4	**900**	**Strong Cr^{4+}**	**Green**
Li_2ZnSiO_4	**900**	**Strong Cr^{4+}**	**Green**
Li_2ZnGeO_4	**900**	**Strong Cr^{4+}**	**Green**
Li_2CdSiO_4	**900**	**Strong Cr^{4+}**	**Green**
Li_2MgGeO_4	**900**	**Strong Cr^{4+}**	**Green**
Na_2CaGeO_4	900	No	Yellow Green, Hygroscopic
Na_2CaSiO_4	900	No	Yellow Green
Na_2MgSiO_4	1000	Weak Cr^{3+}	Green
Na_2MgGeO_4	1000	Weak Cr^{3+}	Green
K_2CaSiO_4	900	No	Yellow
K_2CaGeO_4	900	No	Yellow Green
K_2MgSiO_4	1000	No	Yellow Green
K_2MgGeO_4	1000	No	Yellow Green

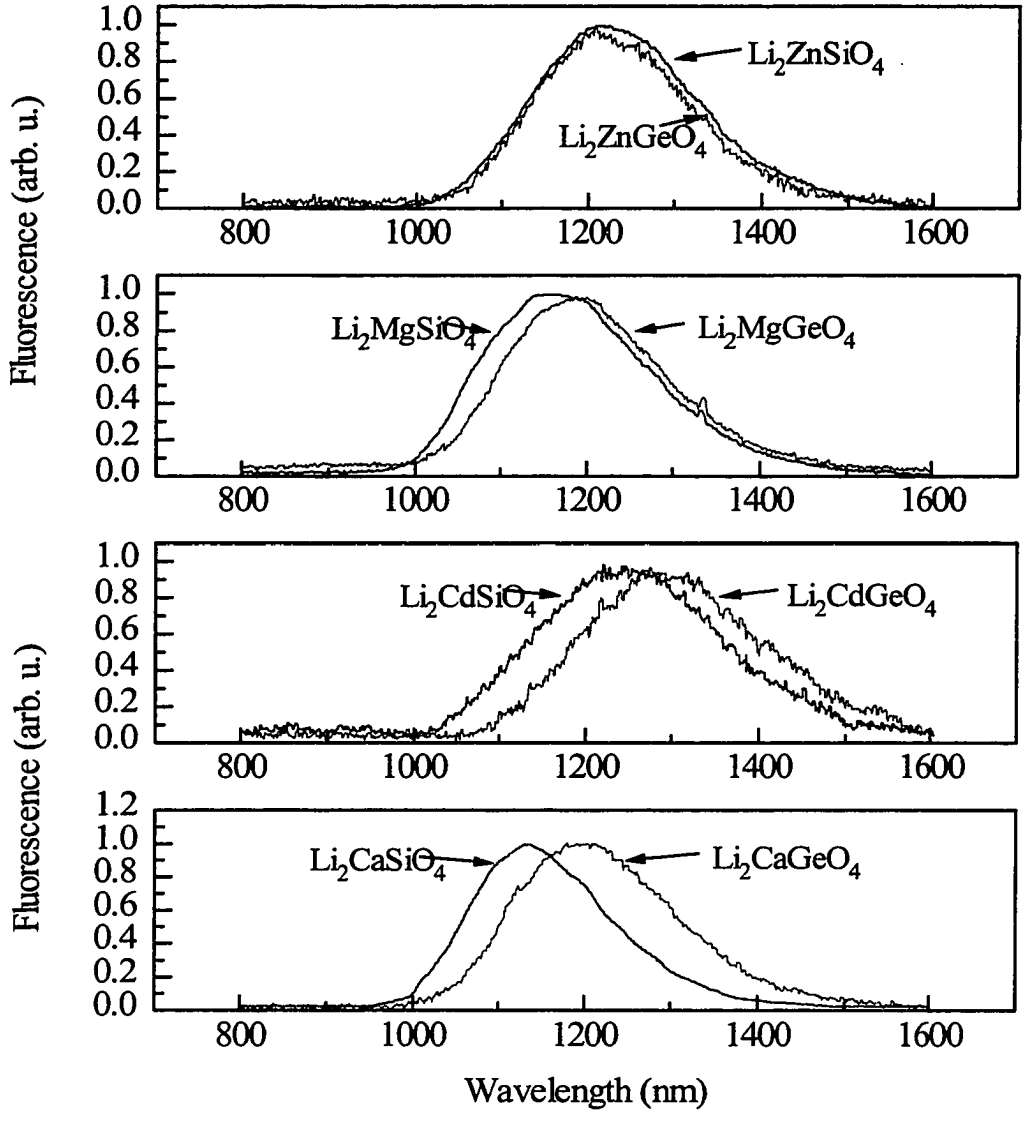

Figure 3.2 Typical luminescence spectra of the group of materials with the chemical formula Cr^{4+}:$Li_2Ca(Mg,Cd,Zn)Ge(Si)O_4$.

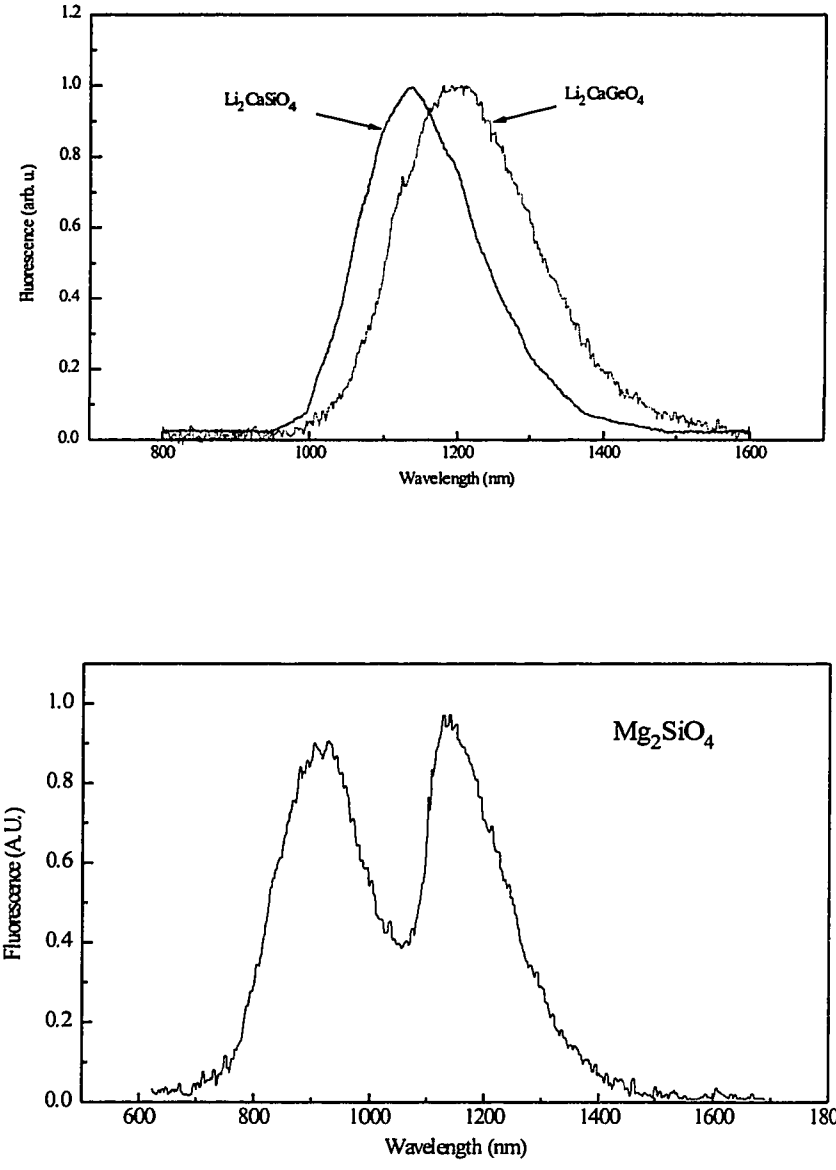

Fig. 3.3 The comparison of the emission properties of Cr^{4+}:$Li_2CaGe(Si)O_4$ with Cr:Mg_2SiO_4.

Table 3.2 The phase information of $Li_2(Mg, Zn)(Ge,Si)O_4$

Li_2MgGeO_4	β_{II}	β'_{II}	β_I	β'_I	γ_2	γ_0
Li_2MgSiO_4					γ_2	γ_0
Li_2ZnGeO_4	β_{II}	β'_{II}				
Li_2ZnSiO_4	β_{II}	β'_{II}			γ_2	γ_0

The β-phase or phases are stable at low temperature, and the γ-phase or phases are high temperature phases.

Preliminary research for the thesis started with the preparation of single crystal $Cr^{4+}:Ca_2GeO_4$. This work was used to develop the experimental methodology for the preparation and characterization of chromium 4+ doped single crystals. We have successfully grown single crystals of $Cr^{4+}:Ca_2GeO_4$ by using the spontaneous flux method with $CaCl_2$ + CaF_2 as the flux for the preparation of seed crystals. The use of the mixed salt flux system eliminated the problems caused by the high vapor pressure of $CaCl_2$ when used as the single solvent. CaF_2 was used as the flux with the Czochralski method for growing large single crystals from the melt. Small single crystals of $Cr^{4+}:Li_2CaGeO_4$ were grown with LiF/LiCl as the flux. Due to the excession evaporation of the solvent in the $Cr^{4+}:Li_2CaGeO_4$+ LiF/LiCl system, we will consider growing large $Cr^{4+}:Li_2CaGeO_4$ single crystal as future work. The method of single crystal growth of $Cr^{4+}:Li_2CaSiO_4$ is very similar to that of $Cr^{4+}:Ca_2GeO_4$. The difference is in the flux system. We choose LiF as the flux, and used the TSSG + Pulling technique to obtain

large single crystals. In this thesis, we are focusing on the crystal growth of Cr^{4+}:Li_2CaSiO_4.

A study to prepare some of these materials as nano-crystallites by the sol-gel technique sheds light on the chromium substitution chemistry. Figure 3.4 shows differential thermal analysis scan of the Cr^{4+}:Ca_2GeO_4 gel, as it is heated at a fixed rate. The important point deducible from the thermal analysis experiment is that the chromium substitution, which is endo-thermic, takes place in the 500 to 600°C range.

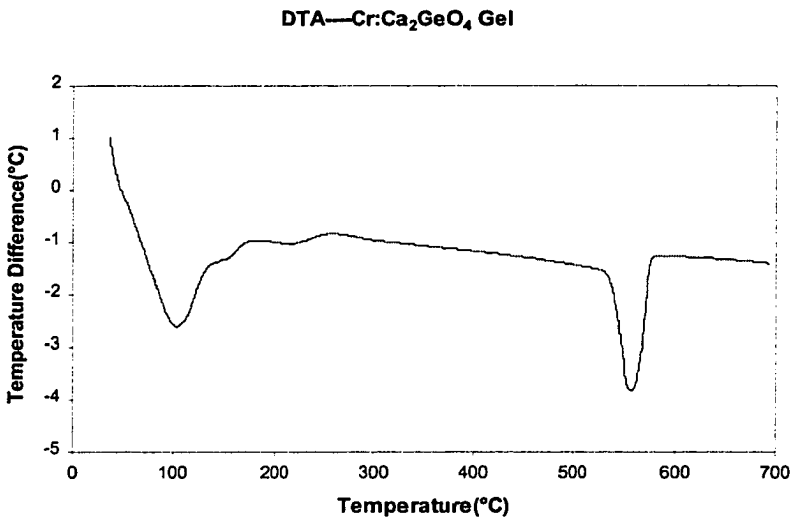

Figure 3.4 Differential thermal analysis scan of the Cr^{4+}:Ca_2GeO_4 gel.

3.5 The growth of Cr^{4+}:Ca_2GeO_4 single crystals

3.5.1 Spontaneous crystallization

The initial work for this thesis started with the synthesis of single crystal Cr:Ca_2GeO_4 using the flux method. The first attempt at growing a crystal was by using $CaCl_2$ as the flux and the conventional slow cooling procedure from 1200°C at 5°C per hour. After many tries only small single crystals of 3x2x2mm in size were obtained. The major problem was the high vapor pressure of $CaCl_2$ at high temperature (above 1000°C). The main advantage of this solvent is that it does not introduce additional unwanted cations into the system. The second attempt at growing Ca_2GeO_4 single crystals was done using a $CaCl_2$-CaF_2 eutectic mixture (0.2mol.% CaF_2 and 0.8mol% $CaCl_2$) as flux which was expected to have lower vapor pressure and allow Ca_2GeO_4 crystallization to proceed at a temperature lower than that using only $CaCl_2$ as the flux.

The phase equilibrium studies and the preparation of Ca_2GeO_4 crystals by the conventional slow cooling technique were done in a muffle furnace in ambient air atmosphere. A Pt crucible filled by the initial charge was placed into the furnace on an alumina pedestal providing a strong axial temperature gradient in the melt with an overheated crucible bottom. This kind of temperature distribution in a melt creates thermal conditions for the first crystallite (nucleation) formation being on the melt surface. Saturation temperature data were obtained by directly visual observation of the initial spontaneous crystallization on the melt surface through a hole in the top of the muffle furnace. By this method, solubility of Ca_2GeO_4 in the $CaCl_2$-CaF_2 eutectic

mixture was estimated to be 35wt. % Ca_2GeO_4 at 950°C and 40wt. % Ca_2GeO_4 at 1050°C. Ca_2GeO_4 shows congruent solubility, in the eutectic, over a wide temperature interval (1050-700°C). There were no additional phases found in this temperature range of crystallization.

Spontaneously formed, green, well shaped Cr:Ca_2GeO_4 crystals with dimensions as big as 5x5x10 mm were grown from the solution (35wt. % Ca_2GeO_4) by the slow cooling technique. The homogenization temperature for the solution was of about 1050°C, the cooling rates were between 0.5 and 2.0 ° C/hr, and the temperature range for crystallization was 950 to 700° C. The initial charges were mixtures of $CaCO_3$, GeO_2, CaF_2, and $CaCl_2$. Chromium (3+) oxide (Cr_2O_3) was added into the system as the doping impurity (0.5wt. % dopand relatively to Ca_2GeO_4). After grown, the crystals were separated from the melt by dissolving the flux medium in hot water. The habit of crystals (see Figure 3.5) was formed by a combination of the side pinacoid (010), first order prism (011) and rhombic di-pyramid (111). Anisotropy of the growth rate is strongly displayed at increased cooling rate, up of 5 to 10° C/hr. Occasionally elongated Ca_2GeO_4 crystals more than 2 cm long in the [100] direction were grown during short growing periods not exceeding two days. Traditional flux inclusions were often found in spontaneously grown crystals, as a consequence of unstable layered growth. The hydroscopic inclusions, attracting water from the ambient environment were the main cause of strong mechanical stress causing the crystals to crack. Crystallization from flux by conventional slow cooling technique is usually considered as a first step in the development of the top-seeding solution growth (TSSG) process. The Cr:Ca_2GeO_4 crystals prepared by

spontaneous crystallization were only used for preliminary absorption and luminescence experiments and as oriented seeds in TSSG method of growing single crystals.

Figure 3.5 The typical habit of Ca_2GeO_4 crystal grown by spontaneous crystallization from flux.

3.5.2 Top-seeding solution growth (pulling technique)

The development of pulling technique for $Cr:Ca_2GeO_4$ solution growth was based on using high temperature gradient growth conditions to speed up the stable growth rate of the crystals. A high temperature gradient normal to the growth interface would be expected to have a stabilizing influence and allow an increased growth rate without breakdown to cellular growth. RF-heated Czochralski growth apparatus produced by

Thermal Technology Inc. was used for the development of the pulling technique. Calcium chloride was excluded from the flux due to its high volatility at elevated temperatures, and only CaF_2 based flux was used for the growth experiments. Data on the temperature dependence of Ca_2GeO_4 solubility in CaF_2 was obtained experimentally and is presented in Figure 3.6. The saturation temperature, measured with a pyrometer, was taken as the temperature at the initial appearance of a crystallite. This solution as well as chlorine containing ones is characterized by congruent solubility of Ca_2GeO_4.

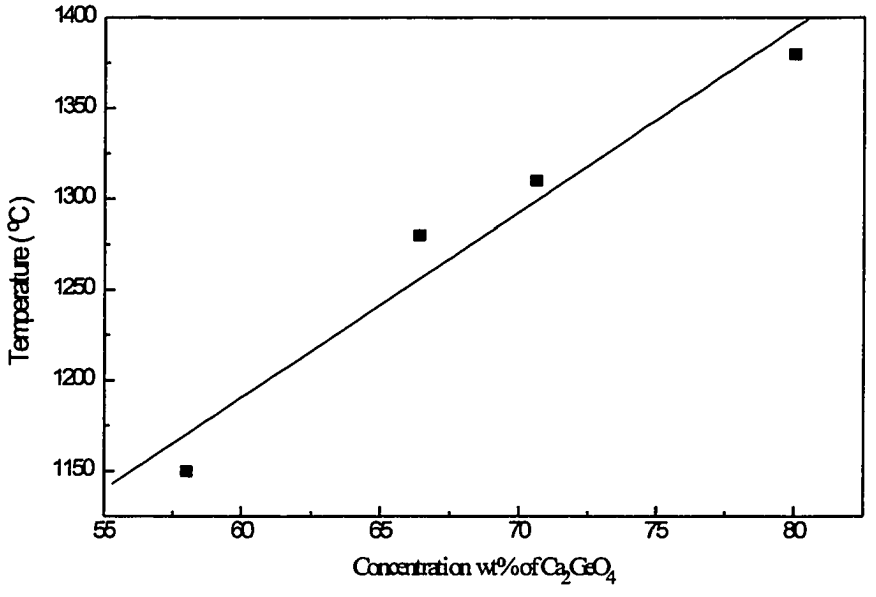

Figure 3.6 Temperature dependence of Ca_2GeO_4 solubility in CaF_2-based solution.

Since the crystallization temperature was expected to exceed 1300°C an iridium crucible, 5.08 cm diameter by 5.08 cm high, with 2.0 mm thick wall and bottom, and nitrogen atmosphere were chosen for the $Cr:Ca_2GeO_4$ growth procedure. A 15wt. % GeO_2-excess

relative to Ca_2GeO_4 stoichiometry led to the primary crystallization of the $Ca_3Ge_2O_7$ phase. The Cr-doped $Ca_3Ge_2O_7$, needle-like crystals, formed on the melt surface, after solidification of the GeO_2 enriched solution were characterized by a specific dark-blue color, different from the green color of $Cr:Ca_2GeO_4$ crystals.

To determine the optimal temperature-concentration range for crystallization of $Cr:Ca_2GeO_4$ by the pulling technique, numerous preliminary runs were carried out. The concentration of the trial solutions varied from 60 to 80 wt. % Ca_2GeO_4. It was shown that with CaF_2 based flux, Ca_2GeO_4 concentration of 70wt. %. with the corresponding saturation temperature of approximately 1350 °C, provided stable growth conditions for two week long growth run. Increasing the crystallization temperature was shown to lead to considerable losses of flux by evaporation and to unfavorable changes of flux composition. A white powder deposited on the walls of the chamber exhibited hydroscopic properties and attracted water from atmosphere after opening the chamber at the end of run. X-ray powder diffraction analysis of the compound deposited on the chamber walls showed presence of CaF_2 and unknown phases, one of which was probably $CaGeF_6 \times 2H_2O$ (after attracting water from the ambient air). Total losses of material by evaporation during two week long growth process at 1350-1300 °C temperature range are estimated to be of the order of 5wt. %.

A successful series of growth experiments by the pulling technique were carried out from CaF_2 based flux with Ca_2GeO_4 concentration of about 70wt. %. The Cr_2O_3 concentration (relative to Ca_2GeO_4) in the initial melt charge was varied from 0.05 wt. % to 0.5 wt. %.

The experimental parameters for crystallization were: growth direction [100], temperature range 1350 to 1300°C, pulling rate 0.2 to 0.1 mm/hr, seed rotation speed 60 to 20 rpm, growth atmosphere nitrogen.

Totally transparent, dark green $Cr:Ca_2GeO_4$ crystals, more than 15 mm in diameter and up to 60 mm long were grown under above mentioned growth conditions (Figure3.7a). After growth, slices 2-5 mm thick were cut and hand polished for spectroscopic and laser experiments (Figure3.7b).

There are no differences observed between the spectra of highly doped $Cr:Ca_2GeO_4$ prepared by the pulling technique and low-doped crystals grown by spontaneous crystallization except an approximately fivefold increase of absorption amplitude. The 4+ oxidation state for chromium ion in $Cr:Ca_2GeO_4$ crystals is very stable and does not depend on the growth atmosphere (nitrogen gas or air).

Figure3.7a. Cr^{4+}: Ca_2GeO_4 crystal grown by pulling technique from flux.

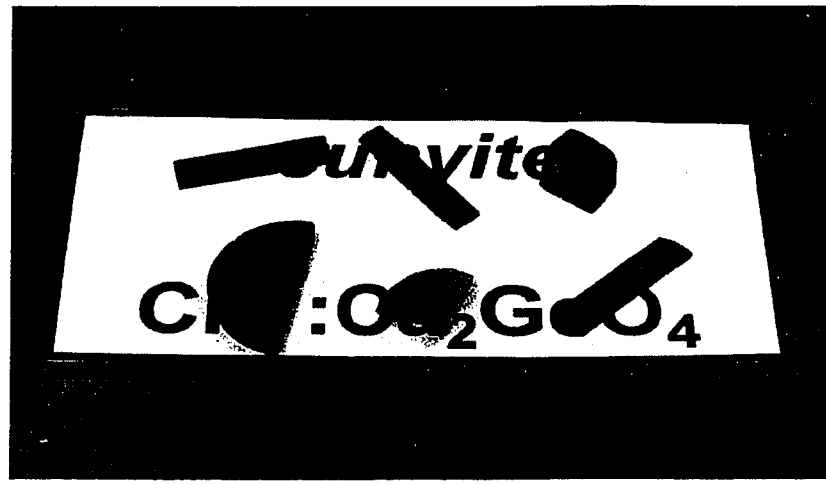

Figure3.7b Cut and hand polished Cr^{4+}: Ca_2GeO_4 single crystals.

Chapter Four

Preparation of single crystals

Detailed knowledge of the phase diagram of a material, e.g. melting and crystallization temperatures, delineation of phase fields, and transition temperatures, is necessary to determine the proper conditions for growing single crystals of the material. Experimentally, differential thermal analysis coupled with structure visualization (optical microscopy, electron microscopy, x-ray diffraction, etc.) is the fastest way to obtain the necessary information.

4.1 Differential thermal analysis

When using differential thermal analysis (DTA), the sample-reference couple is heated or cooled at some constant rate and the difference in temperatures, T_s - T_r (ΔT_{sr}) is monitored. The temperature difference is recorded either as a function of the sample temperature, or of the reference temperature, or of the furnace temperature or as a function of time. An inert material such as α–Al_2O_3 is usually chosen as a reference material. The temperature difference is caused by the specific heat difference between the sample and the reference material. The heat capacity of α-alumina (Al_2O_3) is a smoothly and almost linearly varying function of temperature between 300 and 1900°K. If the sample undergoes some kind of a transformation, either physical or chemical, at a

given temperature and the transformation is either endothermic or exothermic, then its heat capacity will change discontinuously at the transformation temperature. Thus ΔT_{rs} will also change discontinuously. Some phase transitions, reduction and dehydration reactions are endothermic, metastable state to stable state transitions, crystallization, oxidation and recombination reactions are exothermic. The *differential* technique makes it possible to accurately detect the difference between T_s and T_r and thus observe accurately the temperature where the event occurs. Figure 4.1 is a schematic representation of the DTA experiment.

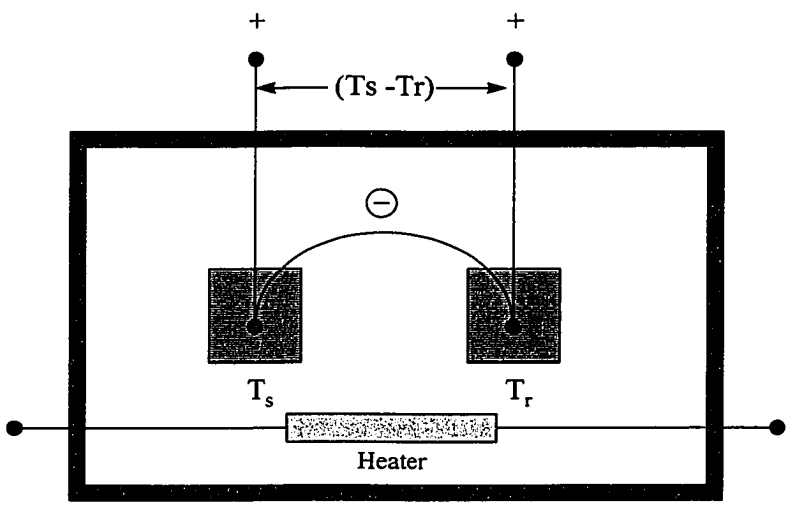

Figure 4.1 A schematic experimental setup of DTA.

4.1.1 Experimental DTA procedure

A characteristic feature of the TA Instruments high temperature system (DTA 1600) is that it has only a small working space, insulated by an alumina tube to decrease the perturbation of the ambient atmosphere during an experiment. The furnace can be purged with a gas flow or experiments can be performed in air. All the experiments for this work were done in air. Cylindrical platinum cups of 5 mm diameter, 5 mm height and 0.1 mm thickness, weighing about 370 mg each, were used as the containers for the sample and the reference materials. The instrument has three R-type (Pt/Pt-13% Rh) thermocouples: two of them are for measuring the temperatures of the sample and the reference while the third is set very close to the heater and is for thermal control of the system. The time, temperature of the sample and temperature difference between the sample and the reference are recorded every 0.6 second and stored in the data storage area of the TA 2100 Thermal Analysis system. The mathematical manipulations used in the analysis of the stored data, such as the derivative of the sample temperature and the derivative of the temperature difference, are performed by the TA 2100. 0.2 minutes are used as the averaging time for data reduction. Figure 4.2 shows typical experimental data from a DTA run. DTA data provides the necessary information for the design of the temperature profile used in the crystal growth experiment. From Figure 4.2 we can see that the phase transition of Ca_2GeO_4 happens at around 1450 °C that is well agreed with literature (Shirvinskaya 1966).

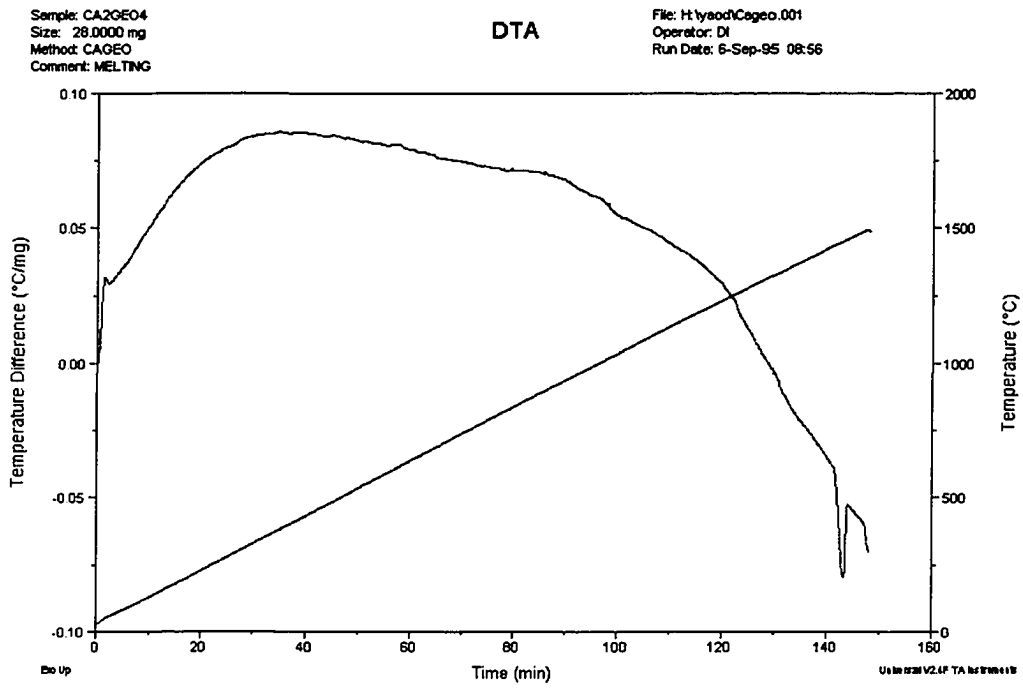

Figure 4.2 A typical experimental data from a DTA run (Ca_2GeO_4).

4.1.2 Differential thermal analysis of Cr^{4+}:$Li_2Ca(Si, Ge)O_4$

In order to obtain experimental support for the single crystal growth, the phase behavior of Cr^{4+}: Li_2Ca (Ge, Si) O_4 was studied by differential thermal analysis (DTA).

The samples were heated to 1200°C at the rate of 5°C/min, and were kept isothermal for 5 minutes at 1200°C, then, they were cooled down to room temperature in the same rate as the heating rate. Figure 4.3 and Figure4.4 shows the experimental DTA data from the Li_2CaSiO_4 and Li_2CaGeO_4 powders. The dotted line gives the heating cycle (5°C/min) to 1200°C. The solid line is the DTA response from the sample of Li_2Ca (Ge, Si) O_4.

From the DTA data, we find that the melting points of Cr^{4+}:Li_2CaSiO_4 and Cr^{4+}:Li_2CaGeO_4 are 1060°C and 1130°C respectively. During the heating part of the cycle, two endothermic peaks are seen for both samples. The first one is the 'phase transition' point below which the $Li_2Ca(Ge, Si)O_4$ forms the low temperature phase. The phase transition points of Cr^{4+}:Li_2CaSiO_4 and Cr^{4+}:Li_2CaGeO_4 are 950°C and 960°C respectively. The second peak corresponds to the melting point. Similarly, two peaks are observed during the cooling cycle. That means that the crystals which we are going to grow are polymorphism. It will be impossible to grow the crystals from the melt. Therefore, either the HTS (high temperature solution) or the flux method will have to be used for growing single crystals.

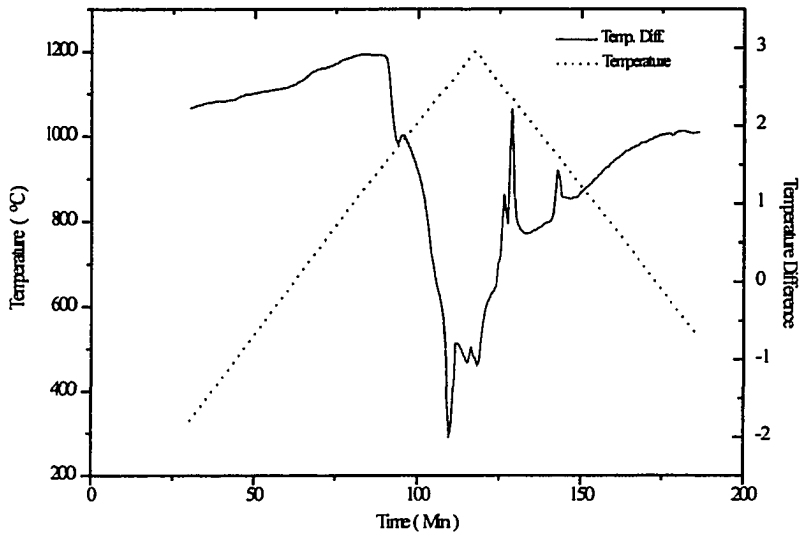

Figure 4.3 The original experimental DTA data of the Li_2CaGeO_4

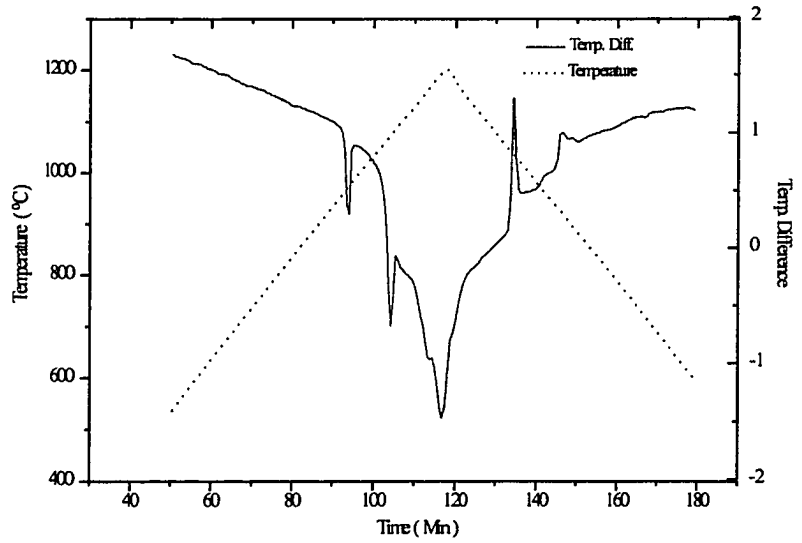

Figure 4.4 The original experimental DTA data of the Li_2CaSiO_4

4.2 Single crystal spontaneous flux growth

4.2.1 Choice of flux

Single crystals of Cr^{4+}:Li_2CaSiO_4 and Cr^{4+}:Li_2CaGeO_4 can be grown by the flux method. There are no fixed rules for choosing a flux. The most simple and easy approach is to attempt the growth of a given crystal with some representative fluxes.

Using the experience gained in growing Cr^{4+}:Ca_2GeO_4, as described before, we tried to use the flux systems of LiF, LiF/LiCl, and LiF/CaF_2 in growing crystals of Cr^{4+}:Li_2CaGeO_4 and Cr^{4+}:Li_2CaSiO_4. In order to choose a suitable flux, all these solvents were tested. It was found that LiF was good for Cr^{4+}:Li_2CaSiO_4, and LiF/LiCl was the best for Cr^{4+}:Li_2CaGeO_4.

4.2.2 Solvent system studies

In general, fluxes which have at least one ion in common with the crystal are preferred since they reduce the number of substitutional impurity ions. We choose LiF as the flux in order to minimize the introduction of impurities. That means we didn't introduce any extra cations into our crystal host. The solubility curve of Li_2CaSiO_4 in the LiF solvent was obtained so that the proper condition for crystallization could be chosen. The investigation of the Li_2CaSiO_4-LiF pseudo-binary system phase diagram was done with a muffle furnace in a platinum crucible. The reagents Li_2CO_3, SiO_2, $CaCO_3$ and LiF of

analytic purity were used as starting materials to prepare compositions corresponding to different points of the pseudo-binary phase diagram.

The crystallization point (liquidus curve) was determined by observing the surface of the solution and by using a platinum wire to probe into the solution. Under the microscope, we were able to observe the crystallization on the Pt wire when we took the Pt wire out of the solution. And the temperature of solution saturation was also determined by dissolution of a trial seed. (Fig. 4.5a, Fig. 4.5b)

From DTA experimental results, we know that both Li_2CaSiO_4 and Li_2CaGeO_4 are not congruent melting compounds. They have phase transitions at 950°C (Li_2CaSiO_4) and 960°C (Li_2CaGeO_4). By using the flux method, we could grow single crystal of the low temperature phase below the phase transition points. However, there will be problems with flux inclusion if too much flux is used. In order to decrease the amount of inclusion, as little solvent as possible should be used.

Based on DTA data for Li_2CaSiO_4 and Li_2CaGeO_4, we could choose the crystal growth temperature range from the liquidus of Li_2CaSiO_4-LiF pseudo-binary system (Figure 4.6). The crystal growth temperature range should be between 870 and 950°C, and the concentration of LiF flux should be between 25 and 45 mol.%.

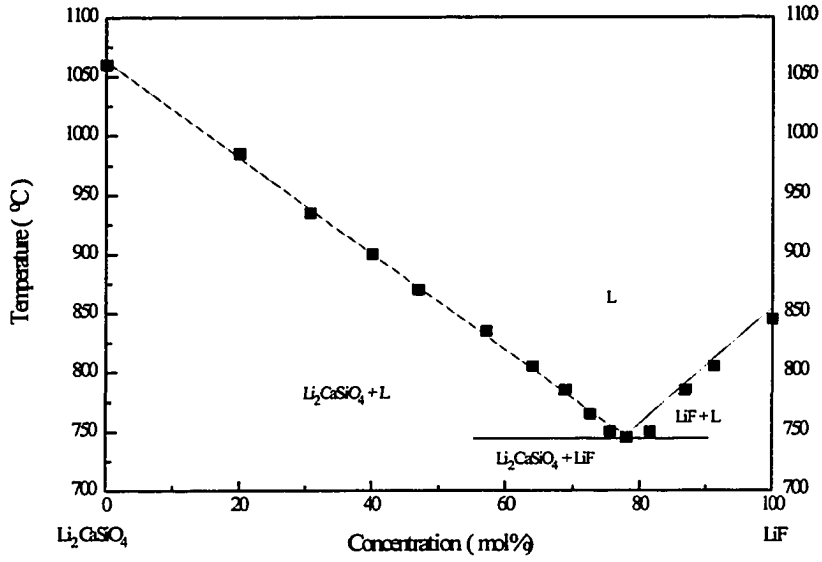

Figure 4.5a The liquidus of Li_2CaSiO_4-LiF pseudo-binary system.

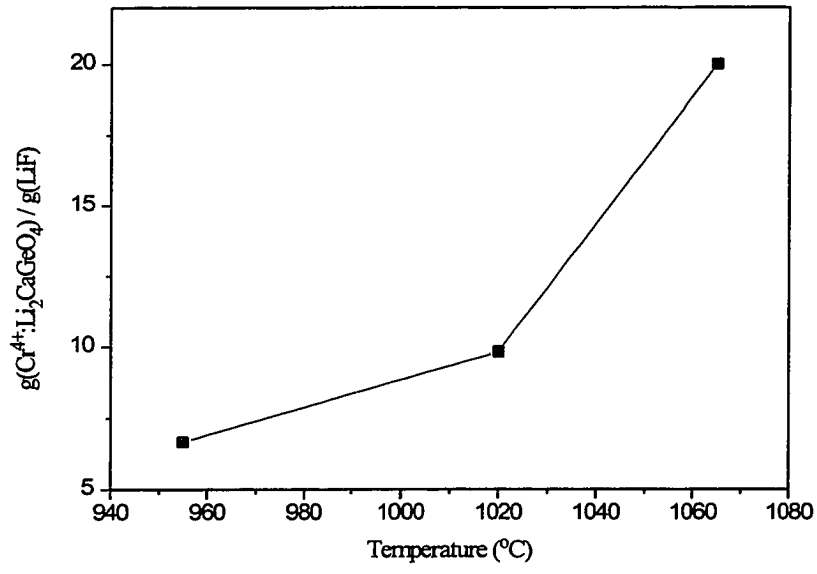

Figure 4.5b Solubility Curve of Li_2CaGeO_4 in LiF solvent

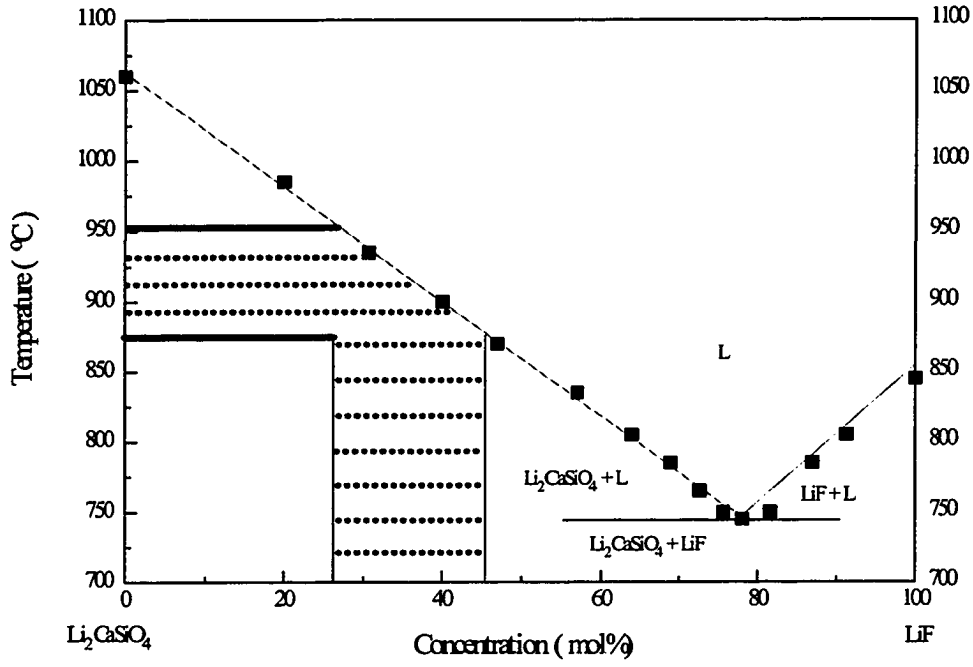

Figure 4.6 The crystal growth temperature range could be chosen from the DTA result and the liquidus of Li_2CaSiO_4-LiF pseudo-binary system.

4.2.3 Single crystal spontaneous flux growth

To initiate the growing of large single crystals one must prepare "seed" crystals. The starting materials for the seed crystallites must be of high quality. For the growing of seed crystals of Cr^{4+}:$Li_2Ca(Ge,Si)O_4$, using flux LiF for Cr^{4+}:Li_2CaSiO_4, and flux LiF/LiCl for Cr^{4+}:Li_2CaGeO_4, the following materials were used:

Li_2CO_3	99% (Metals Basis), Johnson Matthey
$CaCO_2$	ACS, 99+%(Assay), Johnson Matthey
SiO_2	99.995% (Metals Basis), Johnson Matthey
GeO_2	99.9% (Metals Basis), Johnson Matthey
LiF	99.9% (Metals Basis), Johnson Matthey
LiCl	99.9% (Metals Basis), Johnson Matthey
Cr_2O_3	99% (Metals Basis), Johnson Matthey

Seed crystal growth is by spontaneous nucleation from the LiF or LiF/LiCl flux. The LiF/LiCl mixture for Cr^{4+}:Li_2CaGeO_4 is not ideal due to its high vapor pressure at elevated temperatures. The starting materials are weighted, mixed thoroughly with a mortar and a pestle, and put into a platinum crucible ($50mm^2 \times 50mm$). The fully charged crucible is placed into the preheated muffle furnace (Thermaline, model 48000 with programmable ramp(2) and dwell(2) control), and the temperature program is started.

The saturation temperature of the solution was pre-determined from the phase diagram. If the temperature of a supersaturated solution is held constant for a long time, the small

crystallites will be dissolved and the size of the larger crystallites will increase. A reduction of the number of nuclei can be achieved by temperature cycling. According to Scheel and Elwell (1973), temperature cycling is only advantageous in the first stage of the process, when nucleation occurs. Figure 4.7 shows the temperature cycling technique.

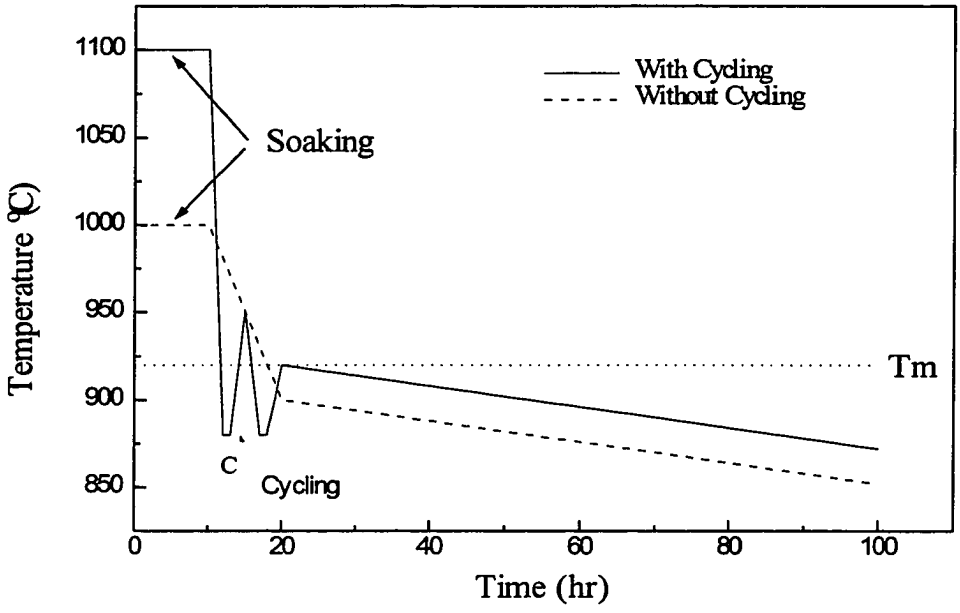

Figure 4.7 Temperature regimes for spontaneous flux crystal growth.

First, the mixture of solute and solvent is held at a temperature about 100°C above the liquidus temperature T_L, for about 10 hours (the soaking period) in order to ensure complete dissolution. Then the temperature is lowered to C, a temperature significantly

below Tm (the temperature of the limit of the metastable region). Most of the crystallites formed during this initial cooling are dissolved when the melt is heated to G. This procedure is repeated until a temperature below T_L is reached such that only a few crystallites have "survived". Then the temperature program is started for real crystal growth. Tables 4.2.1 and 4.2.2 summarize the conditions and results for spontaneous crystal growth of Cr^{4+}:Li_2CaSiO_4 and Cr^{4+}:Li_2CaGeO_4.

Table 4.2.1 Cr^{4+}:Li_2CaSiO_4 Crystal Growth by the Spontaneous Flux Method

No.	Starting Materials(wt.%)		Growth Range	Cooling	Crystal
	Cr^{4+}:Li_2CaSiO_4	LiF	(°C)	Rate(°C hr^{-1})	Maximum Size
1	83%	17%	1100 - 800 °C	1.2 °C/hr	2x1x1 mm^3
2	83%	17%	1100 - 900 °C	10 °C/hr	
			900 - 800 °C	0.6 °C/hr	3x2x2 mm^3
3	77%	23%	1000 - 900 °C	6 °C/hr	
			900 - 810 °C	0.6 °C/hr	8x7x6 mm^3

Table 4.2.2 Cr^{4+}:Li_2CaGeO_4 Crystal Growth by the Flux LiF/LiCl

Initial Composition(mol)						Growth Range (°C)	Cooling Rate (°C hr^{-1})	Crystal Maximum Size
Li_2CO_3	$CaCO_3$	GeO_2	LiF	LiCl	Cr_2O_3			
0.05	0.05	0.05	0.075	0.175	0.001	950~700°C	5°C / hr	3x2x2 mm^3

In order to make the "harvesting" of the crystals from the solution easier, the crystals should be separated from the residual flux before the growth solution solidifies. The decanting method (or hot pouring technique) is used for separating the grown crystals from the residual liquid, i.e., when the furnace temperature falls to a temperature well above the eutectic, the Pt crucible is removed from the furnace, the remaining flux is quickly decanted, then the crucible is put back into the furnace and cooled slowly (naturally) to room temperature. One of the chief disadvantages of the flux decanting method is that stresses are introduced into the crystals due to the "quench cooling" effect as the crucible is removed from the furnace.

By pouring off the flux at the end of the growth process, a large number of well-shaped single crystals were obtained. After cooling to room temperature, we get green transparent crystals with maximum dimensions of 8x7x6 mm. But mostly the crystals are 3×3×3mm in size and often form oriented aggregates (Figure 4.8) held together by flux.

A single crystal grown by the spontaneous flux method exhibits weaker luminescence properties than the polycrystalline powders of the same material. This seems to be due to the low chromium concentration in the single crystals. The color of Cr^{4+}:Li_2CaSiO_4 crystals is blue-green. The crystal structure of Li_2CaSiO_4 is body-centered tetragonal with space group I42m. The unit cell dimensions are a=5.047±0.005Å, c=6.486±0.006Å (Gard and West, 1973).

Figure 4.8 A picture of a single crystal aggregate from spontaneous flux growth

4.2.4 Single crystal top seeding solution growth (Czochralski technique)

Seeded growth in comparison with spontaneous nucleation allows control of orientation, growth rate, degree of crystal perfection, and adjustment of the doping level. Single crystals of $Cr^{4+}:Li_2CaSiO_4$ were grown, using the top seeding growth technique. The starting materials were a mixture of $Cr^{4+}:Li_2CaSiO_4$ and LiF powders. The $Cr^{4+}:Li_2CaSiO_4$ powder was prepared by sintering (see Chapter 3). Figure 4.9 is a schematic representation of the Czchosralski method of growing crystals from a melt, using an oriented seed.

The development of pulling technique for Cr: Li_2CaSiO_4 solution growth was based on the idea of using high temperature gradient growth conditions to speed up the stable

growth rate of crystals. High temperature gradient normal to the growth interface would be expected to have a stabilizing influence and allow an increased growth rate without breakdown to cellular growth. RF-heated Czochralski growth apparatus manufactured by Thermal Technology Inc. was employed for the development of the pulling technique. Calcium chloride was excluded as a flux due to its high volatility at elevated temperatures, and only LiF based fluxes were used for the growth experiments.

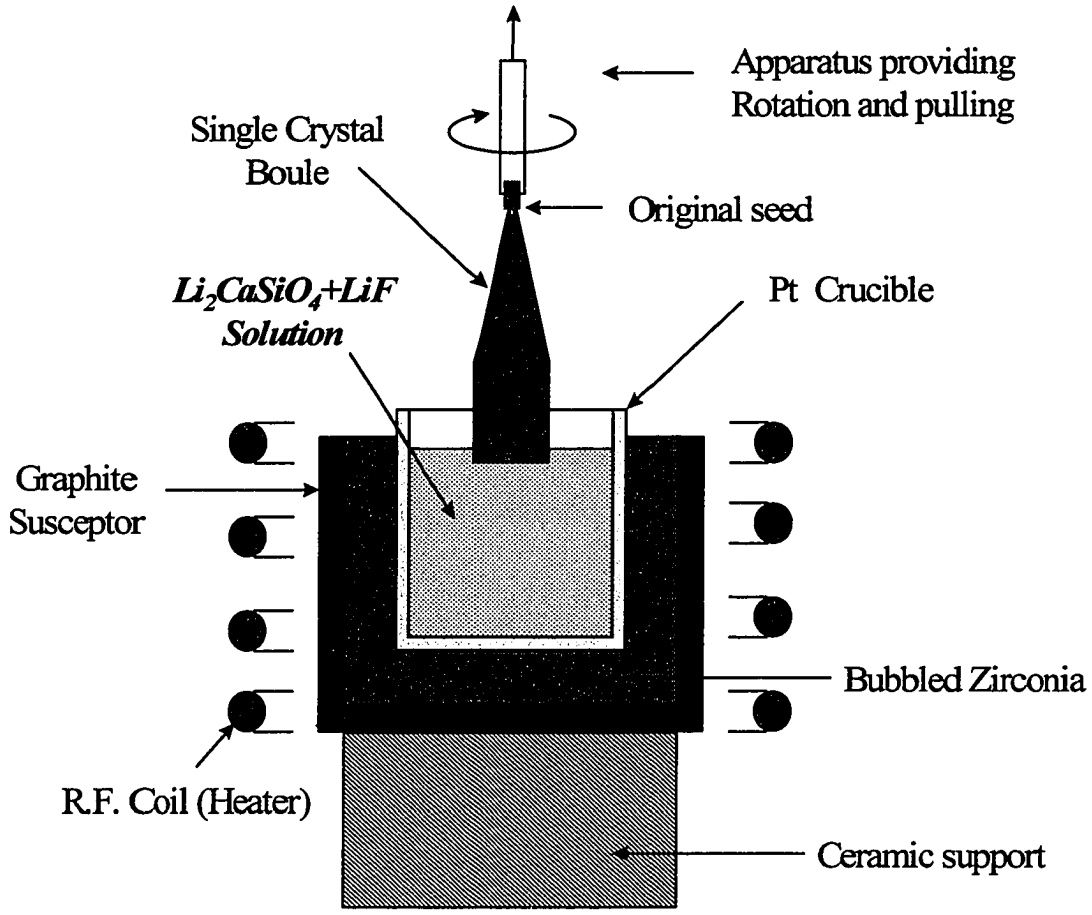

Figure 4.9 A schematic experimental setup of TSSG with Pulling Technique.

Description of the crystal growth equipment:

Furnace System:	Thermal Technology Inc. model #: 7004-CI crystal puller.
Crystal Puller:	Crystal Associates, Inc. model JP-1
Controller:	EUROTHERM CONTROLS 818P programmed set point with up to 8 ramp/dwell combinations.
RF Generator:	Lepel LSSIO
Power Supply:	LSS 10KW 200khz induction heating power supply.
Optical Pyrometer:	Thermalert Series 3 from Raytek.
Cooling System:	Water recirculator RWWEX-10 from Lepel.

Melts range from 150 to 200 gram, and fill the Pt crucible about 80% full. Because the solubility of Cr^{4+}:Li_2CaSiO_4 increases with temperature in the LiF solvent system, the growth rate of Cr^{4+}:Li_2CaSiO_4 from the solution is controlled by using the standard slow cooling approach. Crystal growing experiments described here were carried out with the seed oriented perpendicular to the c-axis. The basal plane is an easy cleavage plane for Cr^{4+}:Li_2CaSiO_4, and the seeds are found to be somewhat fragile and subject to thermal shock. Seeds are held rigidly using a platinum wire mounted on a ceramic seed rod, not cooled.

Typical experimental parameters used are shown in Table 4.2.3

Table 4.2.3 Typical Czochralski method parameters.

Crucible	Pt(50 mm diameter, 50 mm height)
Atmosphere	N_2
Pulling rate	0.1 - 0.3 mm / hr
Rotation Rate	10 - 20 rpm
Seed Crystal	Cr^{4+}:Li_2CaSiO_4
Growth Direction	normal to c - axis

To determine an optimal temperature-concentration range for crystallization of Cr: Li_2CaSiO_4 by the pulling technique, numerous runs were carried out. The composition of the melt was varied from 60 to 80 wt.% Li_2CaSiO_4. It was shown that LiF-based solution with approximate Li_2CaSiO_4 concentration of 80 wt.%. and with corresponding saturation temperature of ~1000 °C provided stable growth conditions for a two weeks long experimental run. Increasing the crystallization temperature was shown to lead to considerable flux loss by evaporation and to unfavorable changes in the flux composition. A white powder deposited on walls of the chamber exhibited hydroscopic properties and absorbed water from atmosphere when the chamber was opened at the end of run. X-ray powder diffraction analysis of compound deposited on chamber walls showed the presence of LiF. Total losses of material, by evaporation, during the two week long growing process in the 900 to1000 °C temperature range are estimated to be of around 5wt.%.

Using melts composed of 20wt.% LiF-based flux and 80wt.% Li_2CaSiO_4, the Cr_2O_3 concentration (relatively to Li_2CaSiO_4) in the initial charge was varied from 0.05 wt.% to 0.5 wt.%. When nitrogen gas was introduced into the pulling chamber, to keep the observation window clean, the crystal grown under this atmosphere showed higher chromium concentration than the crystal grown without Nitrogen.

Saturation of the melts and introduction of the seeds must be done carefully to avoid nucleating a polycrystal. Melts have to be saturated so that the coldest point in the system is just at the point of saturation, and the seeds have to be introduced at the coldest point. This is a trial and error procedure. The melts are then heated up a few degrees and the seeds are introduced. Heating is necessary to prevent the formation of spurious grains on the seed. Melts of approximately 80%wt Cr^{4+}:Li_2CaSiO_4 -20%wt LiF wet the seed and develop a positive meniscus on the seeds. The melts have to be heated sufficiently to raise the saturation isotherm above the meniscus level. When seeds are introduced carefully, crystal growth can be carried out in a rather straightforward manner. Seed rotation rates of 10 to 30 rpm are used, depending on the crystal dimensions. Care is taken to avoid altering the convective flow in the crucible due to an excessive rotation rate.

Crystals oriented perpendicular to the c-axis are grown by slowly pulling during growth. Pulling rate and cooling rate are determined empirically in order to maintain constant crystal cross-section. Overall, we start with cooling rates at 1 to 10°C/day. Typically, we

use 3 °C/day and a pulling rate of 2 to 5 mm/day with reasonably good results. After growth, the crystals are pulled free of the melt and the entire furnace is slowly cooled to room temperature at 10 to 50 °C/hr rate.

Growth is continued until the length of crystal is sufficient to be useful. Interfacial breakdown can be detected readily since, before its occurrence, the melt flow patterns can be seen clearly around the growing crystals, especially if seed rotation is halted for a few seconds to allow the radial star-shaped pattern to reappear. After the onset of interfacial breakdown, the melt convection is obscured.

In summary, Cr^{4+}:Li_2CaSiO_4 single crystals with good optical quality and up to 10 to 20 mm in diameter and 20 to 30 mm in length were grown from solution, with LiF as the solvent, by the top seeded technique with pulling. A typical crystal boule grown by this method is shown in Figure 4.10.

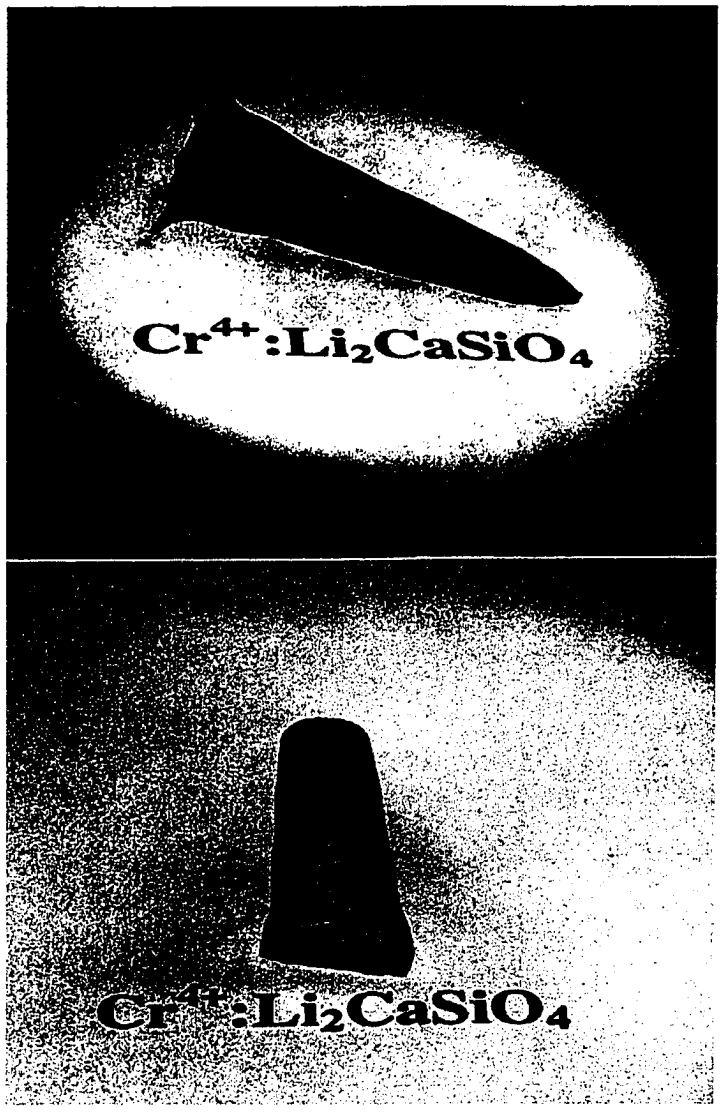

Figure 4.10 A typical crystal boule grown by TSSG technique.

4.3 Crystal quality

After growth, the crystal quality is assessed by optical microscopy using standard mounting and polishing methods. Most Li_2CaSiO_4 crystals grown contained internal defects. The predominant types of defect found were flux inclusions and voids. Discrete flux inclusion incorporation with typical dimensions being in the 50-100 nm range were formed in the core region and then extended to the perimeter of crystal. Incorporation of these inclusions was the first evidence of interface instability usually followed by breakdown to cellular growth. The main problem of Li_2CaSiO_4 solution growth by pulling technique was the tendency toward interface breakdown to a cellular structure beginning at the center of growth interface and spreading to the edges as growth proceeds (Figure 4.11). Cellular growth was often observed when uncontrolled changes of crystal diameter occurred. We were able to avoid unstable growth conditions by adjusting the axial temperature distribution and the pulling rate.

To avoid this type of inclusions, the higher axial temperature gradient was employed. Incorporation of bubbles or voids in crystals (Figure 4.12) proved to be very serious problem because of all crystals grown contained them. The void density was lower near the perimeter of crystal, where increased velocity of melt flow across the growth interface occur. The size of voids was around 5-20μm at the first stage of crystallization beneath the seed and increased up to 50-100 μm at the bottom part of crystal.

Figure 4.11 Unstable growth condition (inclusion incorporation followed by breakdown to cellular growth).

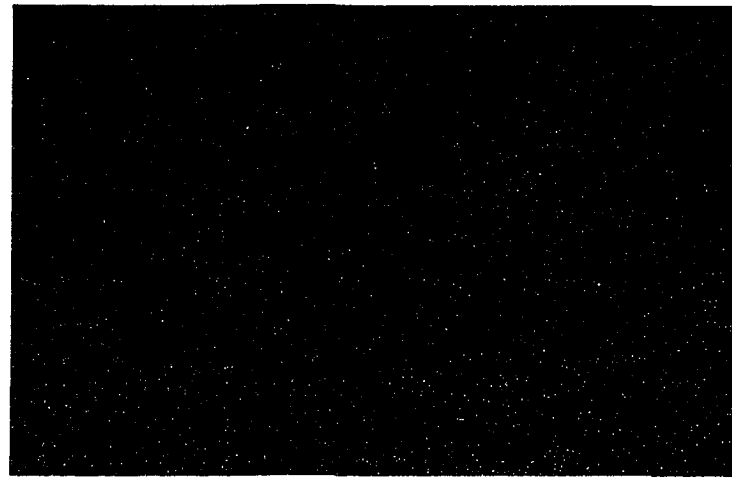

Figure 4.12 Voids in Li_2CaSiO_4 single crystals.

Typically, the larger the void dimension, the lower the void density. The mechanism of the void formation is not known with certainty. One possibility includes interface evolution of dissolved gas at growth interface followed by incorporation into crystal.

The quality of the crystals grown can be related to several of the process parameters.

1. Effects of the flux (LiF) concentration

The effects of LiF concentration upon crystal growth and quality were investigated in the composition range of 10 to 30 wt.% of LiF.

For the case of 10 wt% LiF flux, the crystal growth process could not be sustained because of the high LiF vapor pressure. From the phase diagram of the Li_2CaSiO_4 - LiF pseudo-binary system, the saturation (liquidus) point is around 950°C when the flux concentration is 10wt%. During crystal growth, a large amount of solvent is lost that makes the saturation shift to under saturation. The result is fast crystal growth and the crystal quality is very poor. Also the growth is unstable and the boule is polycrystalline.

When solvent (LiF) concentration is 30 wt%, the corresponding liquidus point is 880°C. At this temperature one has stable growth. The problem with high solvent concentration is inclusions that are trapped into the crystal boule. This leads to internal defects, such as inclusions and voids. (Fig. 4.13)

The crystal grown from 20 wt% LiF flux solution is fairly transparent and has high optical quality. It has almost no inclusions and the vapor pressure of LiF (solvent) is not high. Therefore, we consider that 20 wt% LiF flux concentration is most favorable for the growing of good quality crystals.

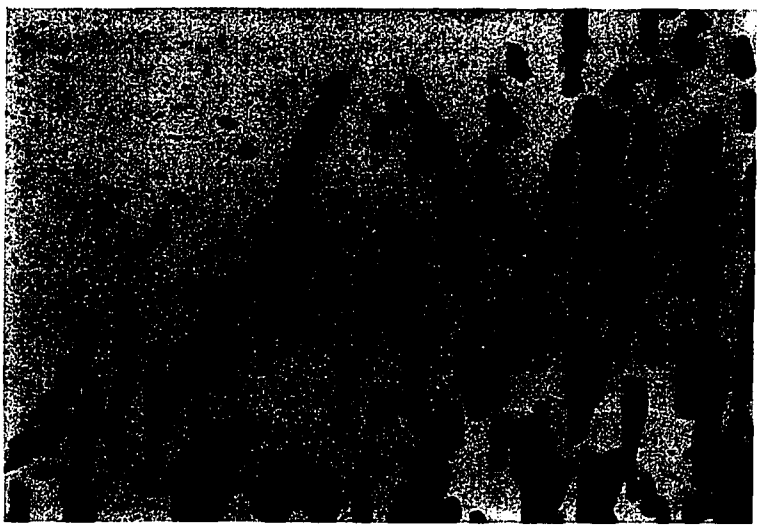

Figure 4.13 Inclusions in Li_2CaSiO_4 single crystals.

2. Effects of seeding on the crystal quality

The size of seeds used in HTS growth has to be a compromise between various requirements. Edge and spiral dislocations propagate from the seed in a direction approximately normal to the growing faces. The high-quality (nearly dislocation-free) regions between these dislocation bundles are obviously larger when small seeds are used.

Small seed crystals, on the other hand, have the disadvantage of being easily dissolved and also require an extremely low supersaturation if the maximum stable growth rate is not to be exceeded. Therefore one has to choose the optimum seed size in relation to the solution volume and the degree of control over the supersaturation. If large crystals are available for use as seeds, it is advantageous to use seed plates of that crystallographic orientation which is optimum with respect to low impurity incorporation, high stable growth rate and the intended application. As is well known, from crystal growing in aqueous solutions, it is desirable to etch the seeds (to dissolve the damaged surface layer and to remove adsorbed impurities) before growth is initiated in order to obtain high quality material. The first seeding step is very important if we want to obtain a high optical quality crystal. Improper seeding may cause " multi-blocking" or orientational changes which will result in the formation of many cracks in the crystal.

3. Effects of growth conditions on the shape and stability of the liquid-solid interface

The temperature control requirements necessary for stable and homogeneous growth are normally much more stringent than those necessary to prevent spontaneous nucleation. This implies that if spontaneous nucleation occurs during the growth of a crystal then its quality is often bad due to formation of inclusions and striations.

During crystal growth from melts and solutions, the shape of the liquid-solid interface is an important parameter determining crystal quality. The highest quality crystals are usually grown with a flat or slightly convex interface. We have studied the influence of

the growth conditions on the shape of the interface during Li_2CaSiO_4 growth from fluxed melts. With increasing rotation rates, forced convection gradually overcomes natural convection, eventually reversing the direction of radial fluid flow along the growth interface. This results in a lower supersaturation at the center of the growth interface and a change in the interface shape from convex to concave. It is also believed (D. Elwell and H.J Scheel, 1975) that a less convex interface occurs with increasing pull rates or with decreasing cooling rates.

A crystal was grown with a concave interface and subjected to unstable growth conditions by a sudden increase in the rotation rate. A high density of flux inclusions was the results. This must have occurred during the unstable growth period. Our experiments showed that suitable pulling rates and rotation rates are 2 to 5 mm/day and 10 to 30 rpm, respectively, in order to obtain a flat or slightly convex interface. If the pulling rate is too high, the growing crystal may be pulled out of the solution due to an imbalance between the amount of solute crystallizing from solution (controlled by the cooling rate) and the independently determined pulling rate.

One of the features of the Li_2CaSiO_4 growth by the pulling technique is that the surface of the boules never exhibited any facets usually associating with solution growth. Liquid-solid growth interface as well as external surface of crystal was smooth and without facets. The shape of the interface was always convex (Figure 4.14) under above mentioned growth conditions. The shape of growth interface is known to reflect the temperature isotherm, the character of convection and the mechanism of crystallization.

All these parameters are supposed to be close to those usually taking place for conventional pulling process from a melt.

The high temperature gradient at the growth interface is known to cause strong residual stresses and crystals readily crack when either pulled up from hot to cold zone or when cooling down to room temperature after completing growth procedure. Crack formation and its propogation was strongly dependent on the quality of Li_2CaSiO_4 crystals. Large crystals without cellular growth and other macroscopic defects seldom showed signs of cracking even when cooled down at 20 to 50°C/hr. If a polycrystalline region formed on a seed at the initial stage of crystallization or significant quantity of solution adhered to the bottom of the crystal, localized cracking would occasionally occur.

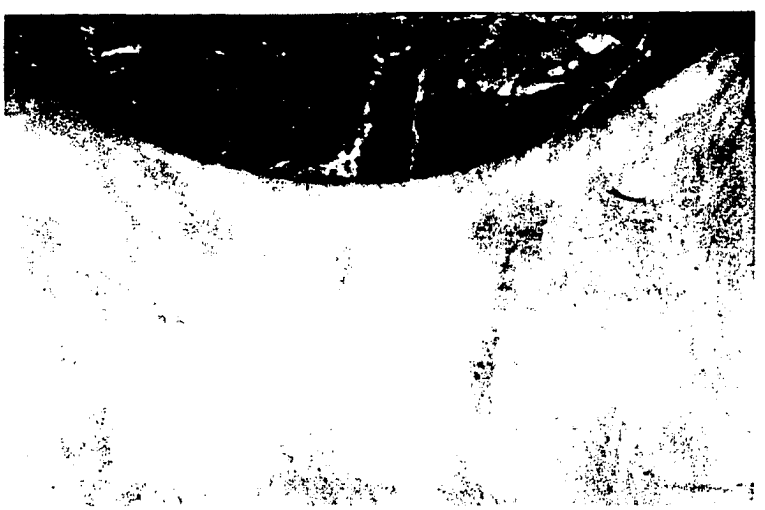

Fig. 4.14 Typical shape of growth interface.

4.4 Diffraction analysis

X-ray analysis of single crystals and powder samples of Cr^{4+}:Li_2CaSiO_4 confirmed the room temperature structure to be body-centered tetragonal, with lattice parameters: a = 5.042 Å, c = 6.484 Å. These are in good agreement with literature values (J. A. Gard and A. R. West 1973.), a = 5.047 ± 0.005 Å, c = 6.486 ± 0.006 Å. This confirms that the materials produced were the ones wanted.

In Tables 4.5.1 and 4.5.2 the X-ray data are presented. X-ray diffraction, confirmed that there are only two components coexisting in the solution of Cr^{4+}:Li_2CaSiO_4 and LiF.

During the growing process by the TSSG method, the vapor pressure of LiF is high. A large amount of white powder evaporated from the solution, and stuck onto the wall of the crystal-growing chamber. X-ray diffraction of the powder confirmed that the white powder was LiF. See Figures 4.15 and 4.16. Cr^{4+}:Li_2CaSiO_4 did not evaporated from the solution during the crystal growing process.

Table 4.5.1 Powder X-ray data for Cr^{4+}:Li_2CaSiO_4 grown by TTSG

No.	2-THETA	INT.	I / I0	WIDTH	d	hkl
1	24.950	2105	71	0.180	3.566	
2	26.630	74	3	0.165	3.345	
3	27.490	356	12	0.165	3.242	002
4	35.580	201	7	0.150	2.521	200
5	37.480	2950	100	0.165	2.398	
6	42.410	619	21	0.195	2.130	211
7	45.540	753	25	0.150	1.990	
8	51.190	791	27	0.165	1.783	
9	56.500	163	6	0.150	1.627	004
10	57.740	129	4	0.180	1.595	
11	59.100	225	8	0.195	1.562	
12	62.990	216	7	0.165	1.474	
13	65.130	795	27	0.180	1.431	
14	65.360	94	3	0.120	1.427	
15	68.840	549	19	0.180	1.363	
16	70.950	51	2	0.195	1.327	
17	75.290	69	2	0.225	1.261	400
18	79.700	73	2	0.150	1.202	
19	79.970	78	3	0.135	1.199	
20	80.760	87	3	0.150	1.189	
21	81.920	82	3	0.195	1.175	
22	85.340	191	6	0.210	1.137	
23	86.120	96	3	0.225	1.128	
24	86.570	47	2	0.135	1.123	
25	87.270	96	3	0.195	1.116	

Table 4.5.2 X-ray data for Cr^{4+}:Li_2CaSiO_4 by spontaneous flux growth

No.	2-THETA	INT.	I / I0	WIDTH	d	hkl
1	24.990	1449	58	0.210	2.560	
2	27.560	313	13	0.165	3.234	002
3	35.600	117	5	0.195	2.520	200
4	37.520	2481	100	0.165	2.395	
5	42.430	526	21	0.150	2.129	
6	45.590	555	22	0.210	1.988	
7	45.710	219	9	0.120	1.983	
8	51.220	420	17	0.180	1.782	
9	56.540	152	6	0.165	1.626	
10	57.800	94	4	0.180	1.594	
11	59.120	174	7	0.165	1.561	
12	63.030	250	10	0.150	1.474	
13	65.170	558	22	0.165	1.430	
14	68.890	295	12	0.165	1.362	
15	75.350	63	3	0.195	1.260	
16	80.020	54	2	0.135	1.198	
17	80.790	83	3	0.150	1.189	
18	81.980	77	3	0.150	1.174	
19	85.370	150	6	0.180	1.136	
20	86.190	68	3	0.210	1.127	
21	87.320	51	2	0.225	1.116	

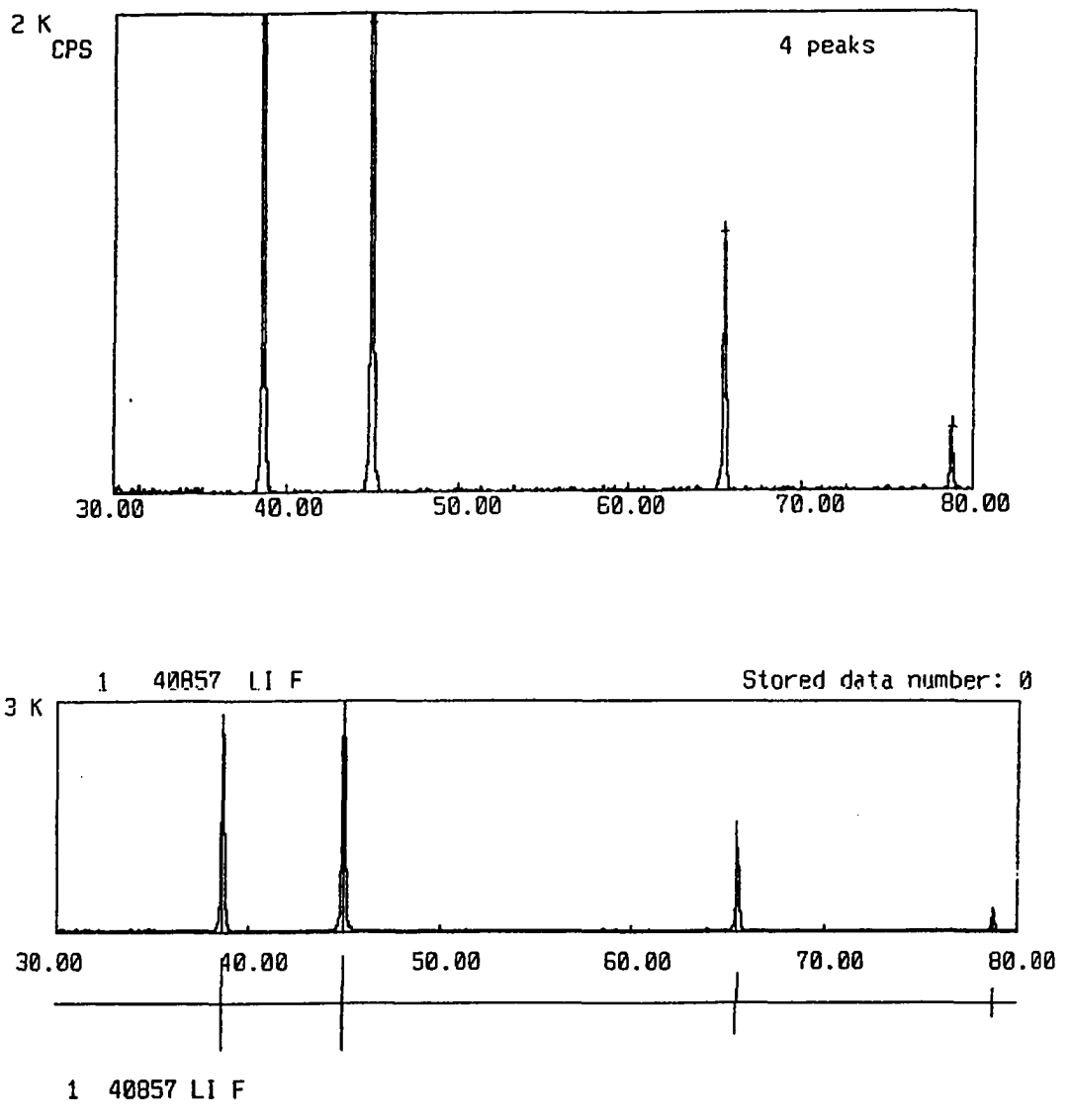

Figure 4.15 X-ray powder diffraction data from the powder produced by evaporation from the solution during TSSG crystal growth.

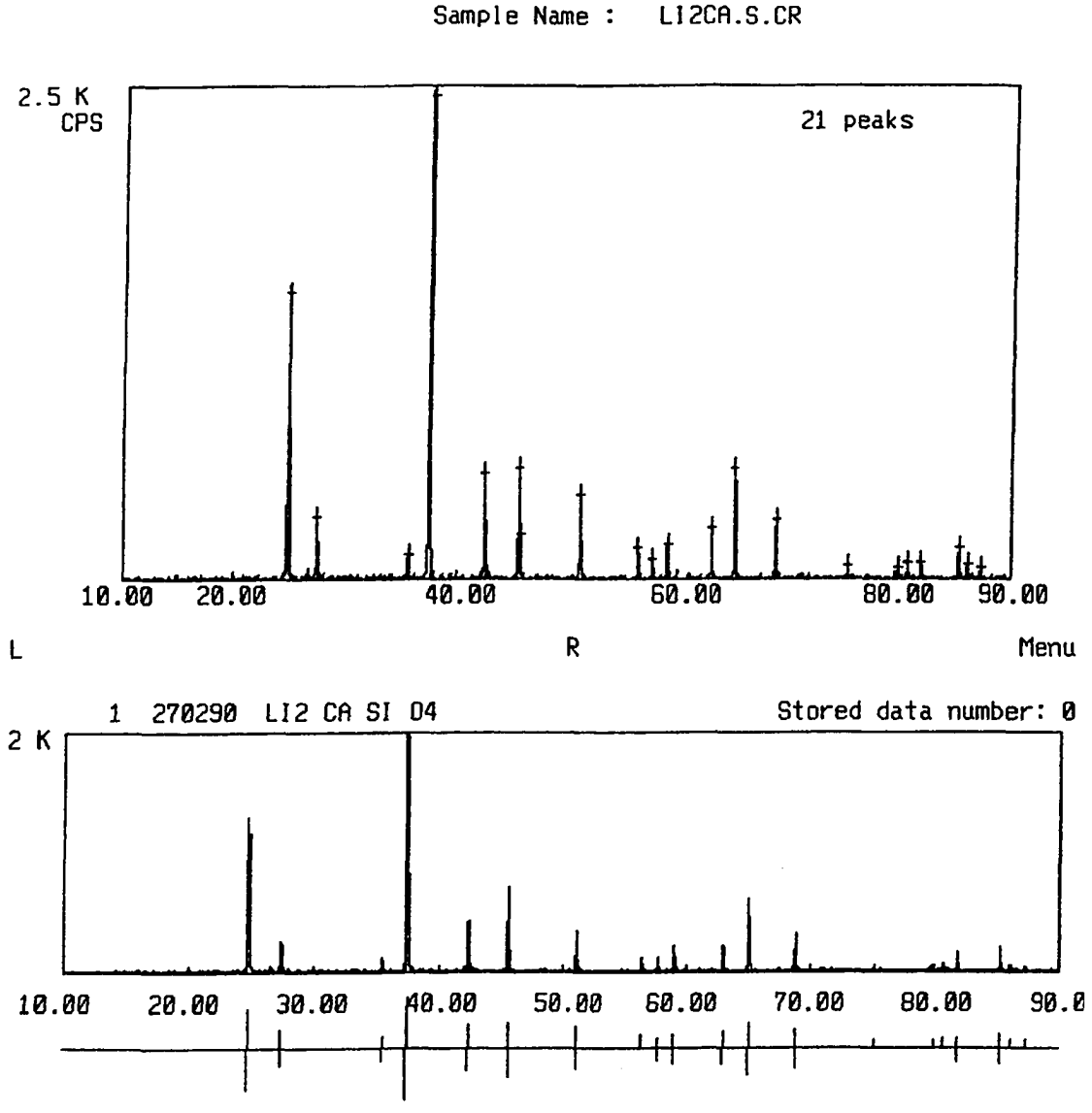

Figure 4.16 X-ray powder diffraction patterns of the single crystals grown by TSSG technique.

Chapter Five

Optical Property Studies

5.1 Fluorescence Spectroscopy

The fluorescence spectrum is determined from the measurement of the fluorescence intensities, at a selected excitation wavelength. The fluorescence wavelength is always red shifted as compared to the absorption wavelength and it is unique (characteristic) for each molecule and is largely independent of the excitation wavelength. Thus, fluorescence spectrum could be used to determine molecular structure as well as to determine which molecule is responsible for the particular fluorescence spectrum.

In the work presented here, the fluorescence spectra were excited by modulated 670-nm excitation from an Ar^{+} ion laser. Fluorescence was detected by a Hamamatsu P394A PbS detector (not- cooled) and a PAR Model HR-8 lock-in amplifier. The PbS detector was placed at the exit slit of a SPEX Minimate 0.25-m mono-chromator equipped with a 1000-nm blazed grating. To resolve features at shorter wavelength, the PbS detector was supplemented by a photomultiplier tube (PMT) with S-20 response, see Figure 5.1.

The emission spectra of Cr^{4+}:$Li_2M^{2+}X^{4+}O_4$ poly-crystalline materials were measured for the 670-nm excitation at room temperature. The spectra are shown in Figures 5.2 to 5.5.

The room temperature emission spectra of $Li_2M^{2+}X^{4+}O_4$ materials screened for viability as laser hosts for the Cr(4+) ion each show only a single broad band with a maximum between 1150 and 1300 nm, as listed in Table 5.1. The only one band result is attributed to the Cr^{4+} ion, which indicates that only the Cr^{4+} substitution takes place in the crystal structure of Cr^{4+}:$Li_2M^{2+}X^{4+}O_4$. Comparing the spectra of germanates with silicates for the same M^{2+}, it is seen that the spectral bands of the germanates are red shifted. Emission spectra did not exhibit significant concentration quenching for chromium concentration levels ranging between 0.5 and 3.0 wt. % Cr_2O_3.

Low temperature fluorescence of Cr^{4+}: Li_2CaSiO_4 was measured (see Figure 5.6). In the near infrared region, very strong fluorescence was detected from Cr^{4+}: Li_2CaSiO_4. The low temperature fluorescent spectrum consists of five peaks at 1045nm, 1070nm, 1085nm, 1105nm, and 1130nm. We assign this spectrum to the $^3A_1(^3T_2) \rightarrow {}^3A_2$ transition of Cr^{4+} ions, which replace Si^{4+} ions in tetrahedral sites. The lifetime of this emission is 30 μs at room temperature. With increasing temperature, the spectrum broadens, merging with the phonon side band (Figure 5.6).

5.2 Absorption Spectroscopy Experiments

The absorption spectrum of an atom or molecule depends on its energy level structure, and absorption spectra are useful for the identification of compounds. A Lambda 9 spectrometer was used to obtain the absorption spectra for different orientations of a Cr^{4+}: Li_2CaSiO_4 single crystal. The spectrum is shown in Figure 5.7, with a peak at approximately 600nm for light polarization perpendicular to the growth axis and at 750nm for light polarization parallel to the growth axis. The absorption spectra show features that are strictly similar to those observed in the absorption spectra of chromium (4+) doped Ca_2GeO_4. We attribute the absorption bands observed in the spectra exclusively to the transitions of the Cr^{4+} ion.

Because of the large Stokes shift and the thermal broadening of the absorption and emission band at room temperature, there is a rather small spectral overlap between absorption and luminescence. Therefore re-absorption will be small or nonexistent. Re-absorption would be expected to have a detrimental effect on laser performance on the short wavelength side of the emission.

5.3 Fluorescence lifetime

The fluorescence lifetime of a substance usually represents the average amount of time the molecule remains in the excited state prior to its return to the ground state. Lifetime

measurements are frequently necessary in fluorescence spectroscopy. These data can reveal the frequency of collision encounters with quenching agents, the rate of energy transfer, and the rate of excited state reactions.

Room-temperature fluorescence lifetimes of Cr^{4+}:$Li_2M^{2+}X^{4+}O_4$ group materials for 1064nm excitation were measured. The results are summarized in Table 5.1. Cr^{4+}:Li_2MgGeO_4 looks particularly interesting because of its unusually long lifetime of about 90 μs. It might be worthwhile to prepare single crystals of this material for device applications.

Table 5.1 Fluorescence life times

Crystal	Peak Emission Wavelength (nm)	Room-Temperature Fluorescence Lifetime (μs)	Status
Cr^{4+}:Li_2CaGeO_4	1200	15	Small Single Crystals
Cr^{4+}:Li_2CaSiO_4	1150	30	Large Single Crystals
Cr^{4+}:Li_2CdGeO_4	1300	25	Powder
Cr^{4+}:Li_2CdSiO_4	1250	30	Powder
Cr^{4+}:Li_2MgGeO_4	1180	90 - 100	Powder
Cr^{4+}:Li_2MgSiO_4	1150	90 - 100	Powder
Cr^{4+}:Li_2ZnGeO_4	1210	40	Powder
Cr^{4+}:Li_2ZnSiO_4	1200	45	Powder

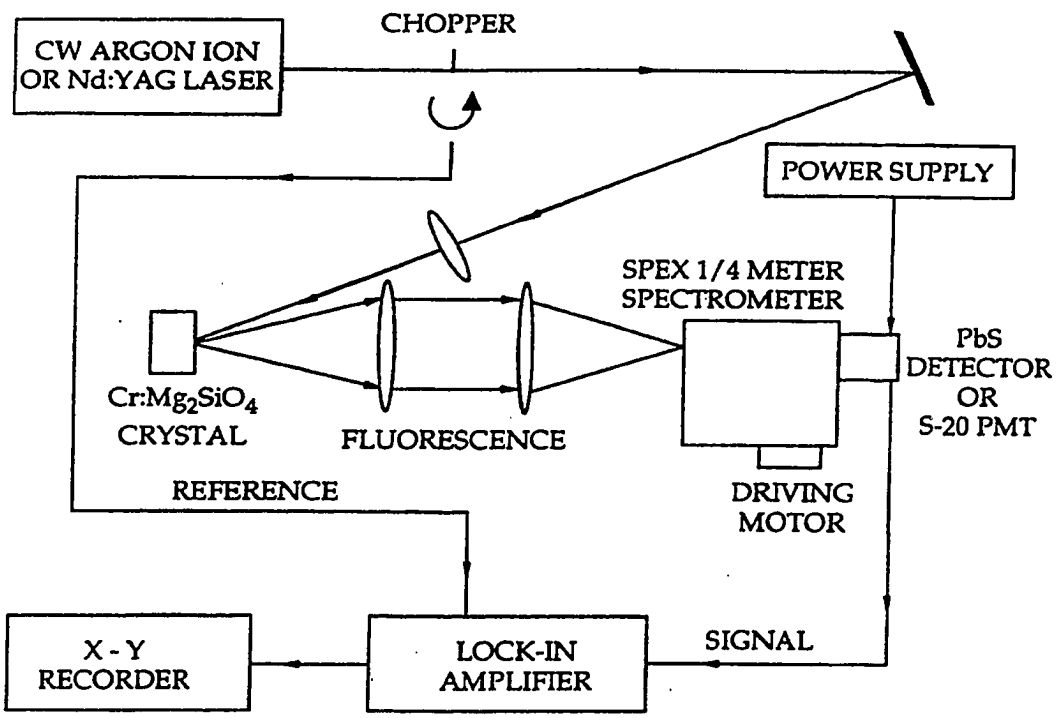

Figure 5.1 Experimental setup for measurement of the fluorescence spectra.

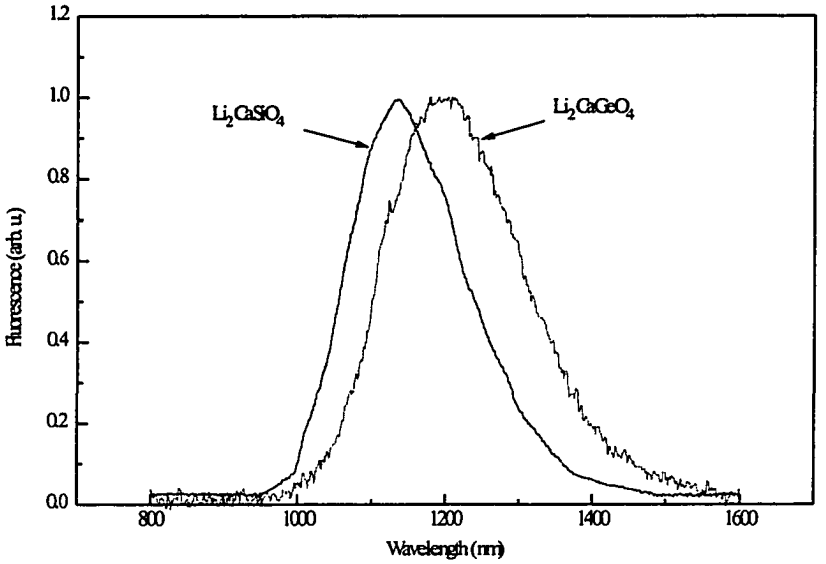

Figure 5.2 Room temperature fluorescence spectra of Li_2CaGeO_4 and Li_2CaSiO_4.

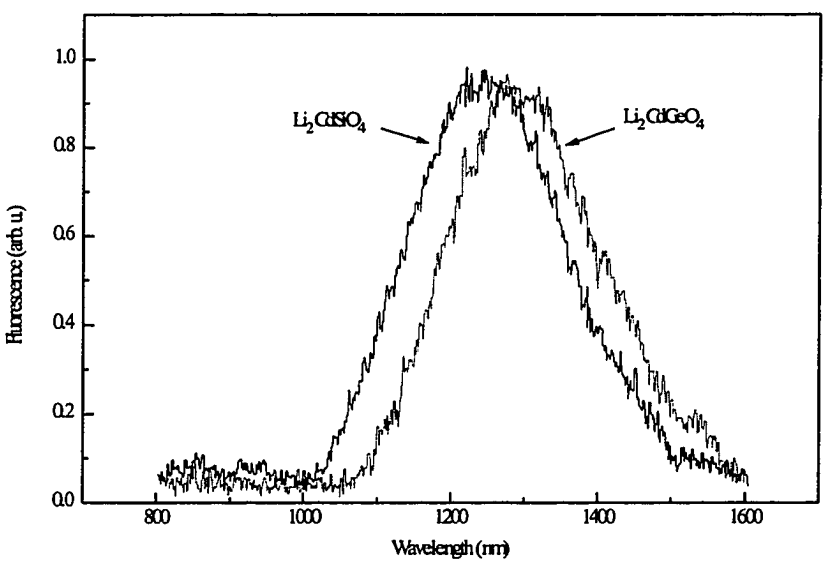

Figure 5.3 Room temperature fluorescence spectra of Li_2CdGeO_4 and Li_2CdSiO_4.

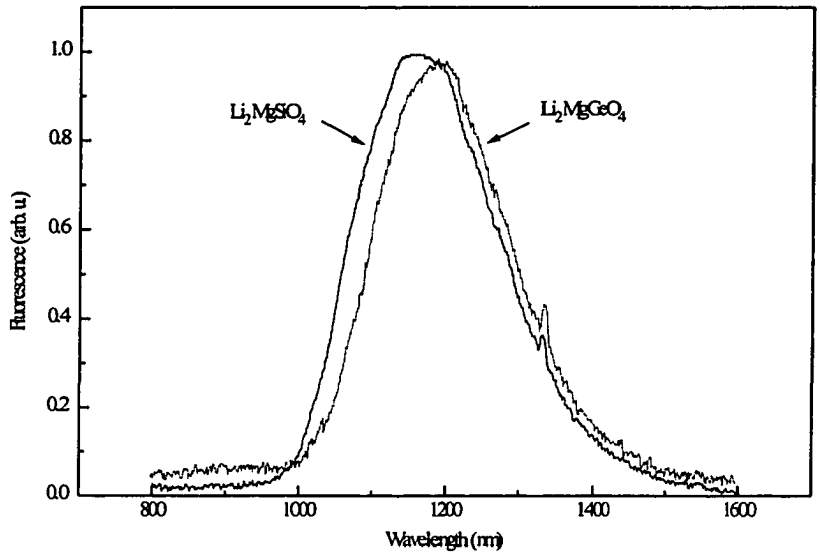

Figure 5.4 Room temperature fluorescence spectra of Li_2MgGeO_4 and Li_2MgSiO_4.

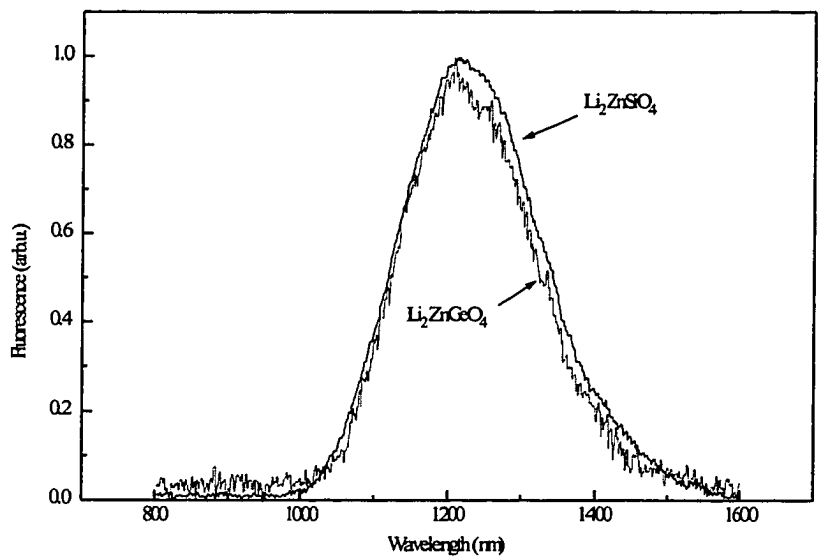

Figure 5.5 Room temperature fluorescence spectra of Li_2ZnGeO_4 and Li_2ZnSiO_4.

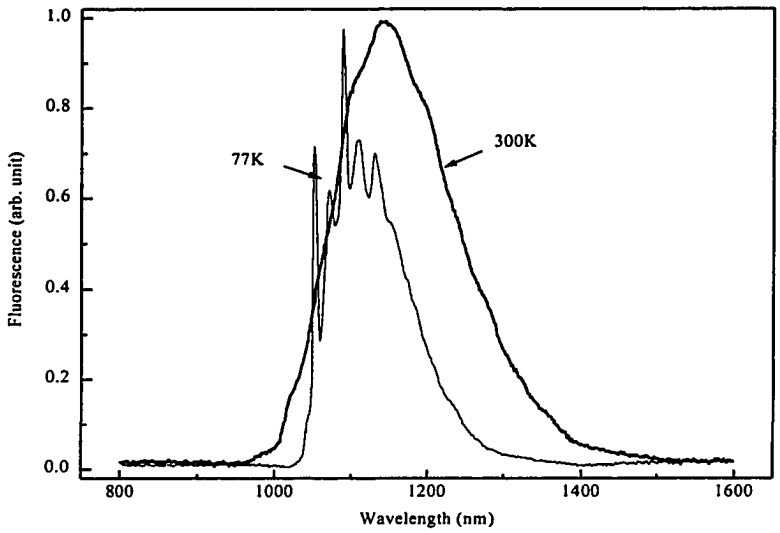

Figure 5.6 Fluorescence spectra of Cr^{4+}:Li_2CaSiO_4 single crystal at 77 K and 300 K.

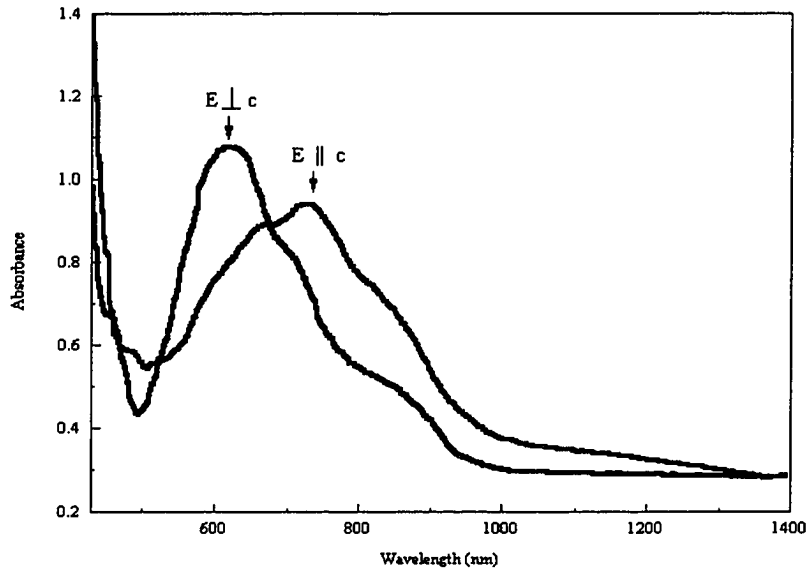

Figure 5.7 Polarized absorption spectra of Cr^{4+}:Li_2CaSiO_4 for two different crystal orientations.

5.4 Refractive Index

5.4.1 Introduction

The behavior of light entering a crystal is fundamentally controlled by the crystal structure. Perhaps the most important property to understand is the refractive index. The velocity of light is dependent on the medium through which it is traveling. In silicate glass for example the speed of light is only about 2 x 10^8 m/s. A convenient way of characterizing a material is to quote its refractive index.. For a transparent materials, the refractive index, n, is defined as the ratio of the velocity, c, of electromagnetic radiation in vacuum to the phase velocity, v, of the same radiation in the material, i.e.,

$$n = c/v.$$

Based on the above definition, the larger the refractive index, the slower light travels in that medium. Most crystals have refractive indices between 1.32 and 2.40. Since the index of refraction of air is only about 1.0003, n is conventionally measured with respect to air instead of vacuum and no correction needs to be made. The refractive index is also a function of the frequency of the light, normally decreasing as the wavelength increases. This change with wavelength is known as dispersion of the refractive index.

The refractive index of a single-crystal may be anisotropic, reflecting the crystal's symmetry. The internal symmetry restricts the distribution and position of the atoms in the unit cell of the material. Two basic types of behavior are possible:

1. Isotropic; the refractive index is the same regardless of the orientation of the crystal with respect to the light direction. Optically isotropic materials include glasses (e.g., volcanic glass) and all isometric (cubic symmetry) crystals.
2. Anistropic; different refractive index in different crystallographic directions. Optically anisotropic crystals divide into two types:
   - Uniaxial, these have two refractive indices (tetragonal and hexagonal system crystals); Li_2CaSiO_4 belongs to this type.
   - Biaxial, these are characterized by three refractive indices (triclinic, monoclinic and orthorhombic system crystals); Ca_2GeO_4 belongs to this type.

5.4.2 Experimental determination of the refractive index

There are many methods to determine the refractive index. One is the application of reflectivity measurements made at the Brewster's angle. This can be done by measuring the amount of reflected *p*-polarized light as a function of the angle of incidence. At Brewster's angle we may not find exactly zero intensity reflection because of "stray" light effects. Taking the angle at the minimum reflection as the Brewster's angle will yield the refractive index n if we use

$$\tan\theta_B = n.$$

It is well known that the reflection coefficient, the ratio of the amplitude of the incident wave to the amplitude of the reflected wave, is a function of the grazing angle. Considering Figure 5.8, light (unpolarized) is incident on the surface of a material of

refractive index n_2 at a grazing angle θ_B. A portion of this light is reflected. This reflecting light is plane polarized. The Fresnel equations

$$r_s = \frac{E_{sreflected}}{E_{sincident}} = r_{E\perp} = \frac{\cos\theta - (\frac{n_2}{n_1})\sqrt{1-[(\frac{n_1}{n_2})\sin\theta]^2}}{\cos\theta + (\frac{n_2}{n_1})\sqrt{1-[(\frac{n_1}{n_2})\sin\theta]^2}} \qquad (5.4.1)$$

$$t_s = \frac{E_{stransmitted}}{E_{sincident}} = t_{E\perp} = \frac{2\cos\theta}{\cos\theta + (\frac{n_2}{n_1})\sqrt{1-[(\frac{n_1}{n_2})\sin\theta]^2}} \qquad (5.4.2)$$

$$r_p = \frac{E_{preflected}}{E_{pincident}} = r_{E\parallel} = \frac{-(\frac{n_2}{n_1})\cos\theta + \sqrt{1-[(\frac{n_1}{n_2})\sin\theta]^2}}{(\frac{n_2}{n_1})\cos\theta + \sqrt{1-[(\frac{n_1}{n_2})\sin\theta]^2}} \qquad (5.4.3)$$

$$t_p = \frac{E_{ptransmitted}}{E_{pincident}} = t_{E\parallel} = \frac{2\cos\theta}{(\frac{n_2}{n_1})\cos\theta + \sqrt{1-[(\frac{n_1}{n_2})\sin\theta]^2}} \qquad (5.4.4)$$

allow the calculation of the reflection and transmission coefficients as a function of the grazing angle and of the indices of refraction. When $n_2 > n_1$, at Brewster's angle, the reflected polarization parallel to the incident plane is zero and produces a highly polarized reflected light beam perpendicular to the incident plane, that is, only light having a component of its electric field vector perpendicular to the plane of incidence is reflected, so $(r_s)^2$ is not equal to 0, and $(r_p)^2$ is equal to 0. To find Brewster's angle θ_B, we set $r_p = 0$ in Fresnel's equation (no reflected light in the parallel direction), and we have:

$$(n_2/n_1)\cos\theta_B + (1-((n_2/n_1)\sin\theta_B)^2)^{1/2} = 0 \qquad (5.4.5)$$

$$\text{or } \tan\theta_B = n_2/n_1 \qquad (5.4.6)$$

We immediately see that θ_B is larger than 45°, since it was assumed that $n_2 > n_1$. At the Brewster's angle, θ_B, the reflection coefficient is a minimum, i.e. the least amount of energy is transmitted as a reflected wave. The reflection coefficient for vertically polarized waves are much more dependent on grazing angle than the reflection coefficient of horizontally polarized waves. Increasing or decreasing the grazing angle from the Brewster's angle causes an increase in reflection coefficient and hence a corresponding increase in the energy transmitted as a reflected wave. Figure 5.9 shows the amplitude of the reflected beam as a function of the grazing angle, for a given n.

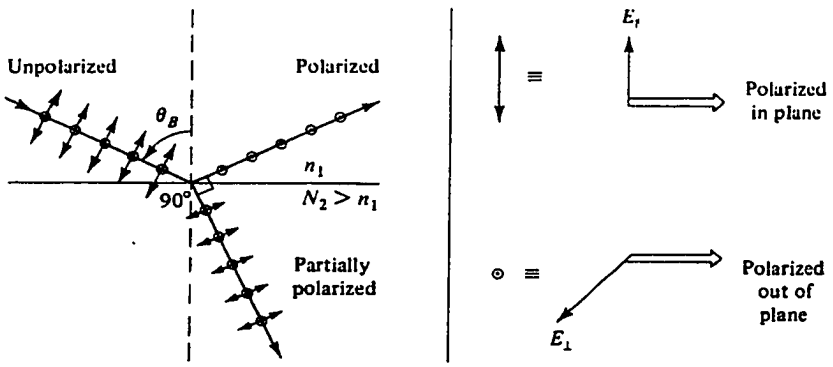

Figure 5.8 Illustration of polarization by reflection at Brewster's angle.

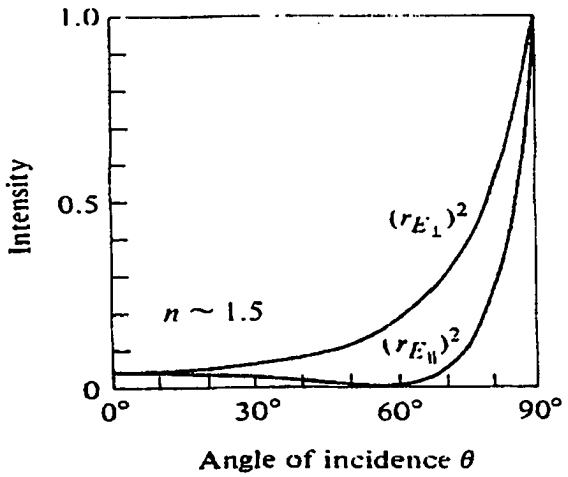

Figure 5.9 Intensity of reflected light at a dielectric interface where $n_2 > n_1$.

Experimental setup:

The instrument used to determine the refractive index is a Variable Angle Specular Reflectance Accessory (VASRA) mounted in a Cary Scan 500 Spectrophotometer. The VASRA allows you to measure the specular (mirror-like) reflectance of a sample surface. It is installed in the sample compartment of the Cary 500 spectrophotometer. The accessory has several unique features:

- The sample mounting platform moves as the angle is changed. This ensures that the center of the image is always in the same position.
- The accessory is supplied with several different aperture masks. These allow you to change the height of the image to suit your sample size.

- The sample is mounted at the slit image position. You can change the width of the image to suit your sample by simply selecting the appropriate spectral bandwidth (SBW).
- Angles can be set in 0.5° increments.
- The accessory is motor driven and is completely computer controlled (Cary WinUV software).

VASRA specifications

Wavelength range: 175–3300nm

Maximum horizontal beam divergence: ±2.5° (5nm SBW)

Maximum vertical ray divergence: ±2.2°

Aperture masks supplied: 20, 10 and 2 mm. Also a mask for 2.5 cm diameter circular samples.

Optical design:

The VASRA features a five-mirror design with two cylindrical, two torodials and one flat mirror. See Figure 5.4.3. Motor driven mirrors are used to ensure that correct imaging is maintained in both the vertical and horizontal planes. The design is symmetrical, taking advantage of the already symmetrical beam profile throughout the sample compartment. The slit image is positioned at the sample mounting position. This achieves a very small beam size at that point, allowing small samples to be measured.

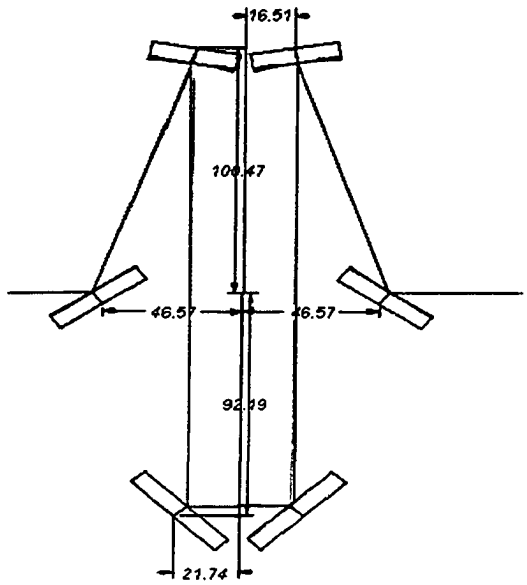

Fig. 5.10 The optical design of the Variable Angle Specular Reflectance accessory.

5.4.3 Results and Discussion

The information of the refractive index of a material is very important for the designer of optical systems. Because wide band light sources with accurate continuous wavelength calibration, either in absorption or emission, are not available, the refractive index is usually measured only at discrete wavelengths. To obtain the wavelength dependence of the refractive index one must use the Sellmeier formula (Dmitriev, V. G. 1991)

$$n^2 = 1 + \sum_j A_j \lambda^2/(\lambda^2-\lambda_j^2) \qquad (5.4.7)$$

where n = refractive index, λ = wavelength (in microns), and A_j, and λ_j are unknown constants to be determined mathematically so as to minimize the sum of square residuals

to fit the experimental data to obtain a refractive index dispersion curve. The Sellmeier formula is based on theoretical considerations that facilitate a more compact expression for the fitting equation than would generally be expected from a completely empirical formulation. Also, this formula often provides at least a rough guide to the values of certain other physical parameters of the optical material, in addition to the fitting of the refractive indices.

Wavelength dependence

The refractive indices of Ca_2GeO_4 and Li_2CaGeO_4 were determined in the region of 500 to 1700nm by the Brewster's angle method. Figures. 5.11 to .5.14 show the typical experimental results obtained.

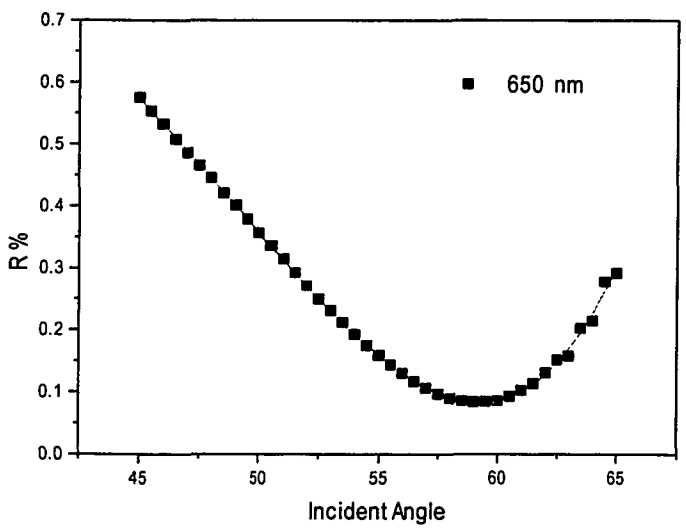

Fig. 5.11 The reflectance vs. incident angle for CUNYITE at 650nm

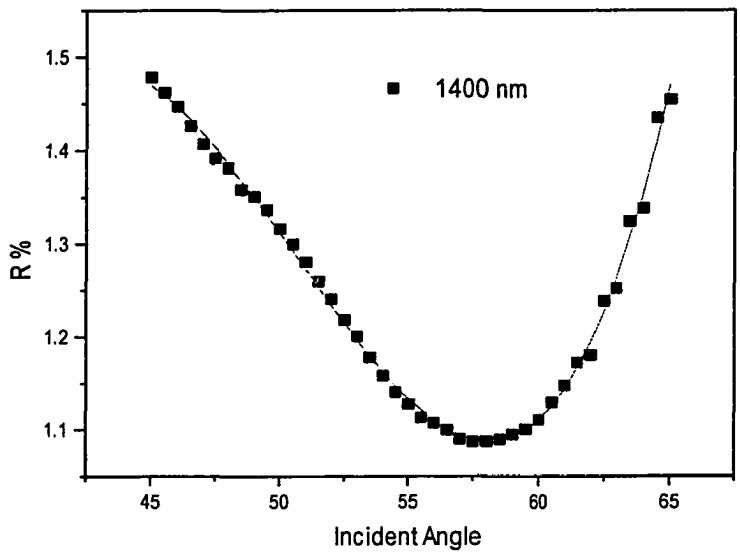

Fig. 5.12 The reflectance vs. incident angle for CUNYITE at 1400nm

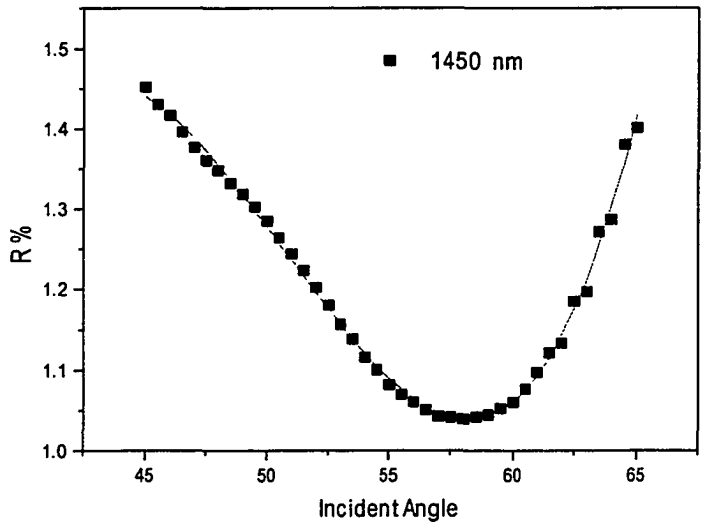

Fig. 5.13 The reflectance vs. incident angle for CUNYITE at 1450nm

The experimental data were fitted with least squares polynomial equations. Then the minimum value of the reflectivity was calculated from the polynomial equation and the index of refraction, n, was calculated at each wavelength, for each material. The discrete points shown in Figures 5.14 and 5.15 were obtained in this manner.

Here we fitted a two-term Sellmeier formula to data consisting of values of the refractive index measured at given wavelengths. The fitting equation was of the form:

$$n^2 - 1 = \frac{A_1\lambda^2}{\lambda^2 - \lambda_1^2} + \frac{A_2\lambda^2}{\lambda^2 - \lambda_2^2} \qquad (5.4.8)$$

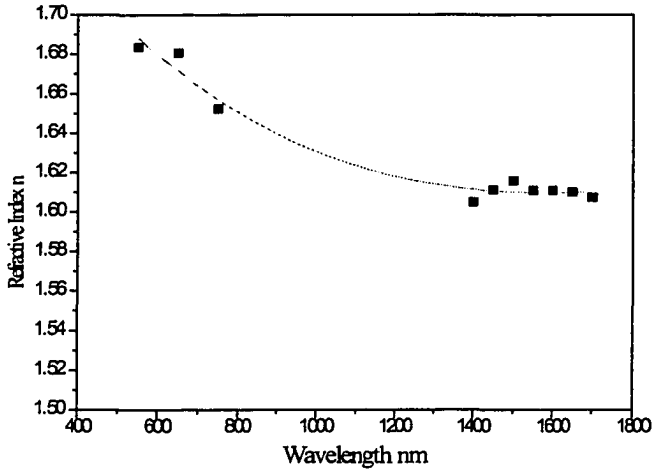

Fig. 5.14 Dispersion curve of CUNYITE along the growth direction, or crystallography direction: b. The solid square is the experimental data, and the thin solid line is the fitting curve with the least square method.

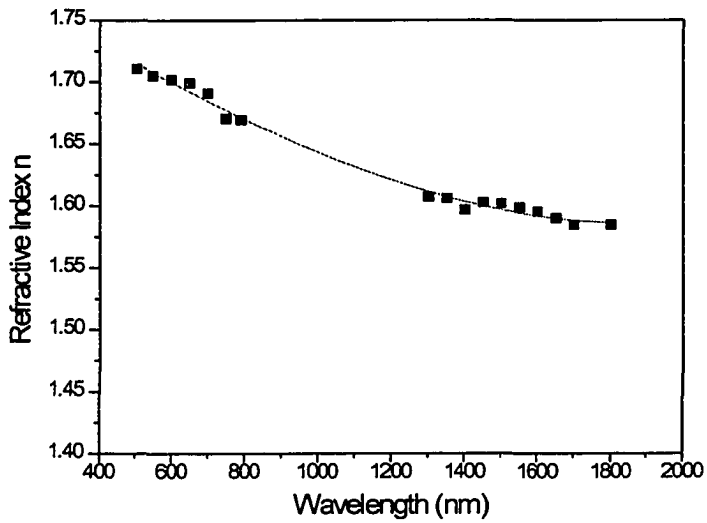

Fig. 5.15 Dispersion curve of Li_2CaSiO_4, perpendicular to the growth direction, or crystallography direction: c. The solid square is the experimental data, and the thin solid line is the fitting curve with the least square method.

By convention, λ_1 is used to denote the singularity of Eq.(5.4.8) on the low wavelength, ultraviolet, side of the data range , while λ_2 denotes the singularity on the, infrared, high side of the data range.

Tables 5.4.1 and 5.4.2 show the experimental results of dispersion of the refractive index for CUNYITE and Li_2CaSiO_4. All the data were collected at the room temperature.

Table 5.4.1 Dispersion of refractive indices of $Cr(4+):Ca_2GeO_4$, T = 300 K.

λ [μm]	n_a	n_b	n_c
0.55	1.735945	1.683827	1.750581
0.65	1.735348	1.680856	1.745972
0.75	1.72328	1.652561	1.72418
1.40	1.663131	1.615952	1.65328
1.45	1.66423	1.611424	1.653949
1.50	1.662246	1.605124	1.652549

Table 5.4.2 Dispersion of refractive indices of $Cr^{4+}:Li_2CaSiO_4$, T = 300 K.

λ [μm]	n_a	n_c
0.55	1.64939	1.70515
0.65	1.64035	1.69928
0.75	1.63472	1.67055
1.40	1.56923	1.60378
1.45	1.56521	1.60297
1.50	1.55902	1.60183

Chapter Six

Thermo-Physical Property Studies

As has been already stated in previous chapters, a good tunable solid state laser host should have good thermal properties, small refractive index variation with the temperature, and good mechanical integrity. Differential thermal analytic techniques were used to determine the heat capacity, thermal conductivity and the thermal expansion coefficients of the materials. Differential thermal analysis (DTA) was used to obtain thermodynamic and phase diagram information. The DTA results were discussed in chapter three.

6.1 The Experimental Techniques

6.1.1 Theory of differential thermal analysis

The theory of differential thermal analysis and differential scanning calorimetry (DSC) can be treated with the same mathematical model. They are analytical techniques in which the difference in heat flow between a sample and an inert reference is measured as a function of time and temperature. During the measurement the sample-reference system is in a controlled environment with regard to atmosphere, pressure, temperature and time. The temperature of the system is ramped in a linear manner

$$T(t) = T_o + \beta t$$

where T_o is the starting temperature and β is a linear heating rate (°/time). The system response is monitored either as the evolution of the temperature difference between sample and reference (DTA), or as the evolution of the heat flow, dq/dt, between sample and reference (DSC).

Linear temperature ramping imposes severe limitations on the type of experiments one can perform using DSC. In a new technique, modulated DSC (MDSC) (TA Instruments Publication), the same experimental sample-reference set up is used, but the applied heating profile has a modulation component:

$$T(t) = T_o + \beta t + A_T(\sin\omega t)$$

where A_T is the amplitude of temperature modulation($\pm$°), and ω is the modulation frequency(t^{-1})

This yields two additional experimental variables.

The theoretical interpretation of differential analytical curves was the subject of numerous theories. Gray (1968) developed a general theory describing DSC and DTA curves, which were later improved by Baxter (1969). One can apply heat balances and Newton`s law

$$dq/dt = A\Delta T$$

to the analysis of the situation. This relation simply states that the rate of heat flow (dq/dt) between to points is driven a temperature difference (ΔT) and A is the heat transfer coefficient. Newton`s law is the thermal equivalent of Ohm`s law for an electrical circuit,

if we replace dq/dt by di/dt, the current flow rate, and ΔT by V, the potential drop between two points. Then A is the conductance (R^{-1}).

The essential components of a thermal analysis cell are shown schematically in Figure 6.1.1. They consist of a sample at temperature T_s, its container at temperature T_{sh} a temperature programmed source at temperature T_b. Heat will flow between sample and reference sites at a constant rate of di/dt depending on the temperatures involved and the thermal resistances connecting these positions. The sample and its container have a heat capacity C_s. Similar descriptions can be developed for the reference side.

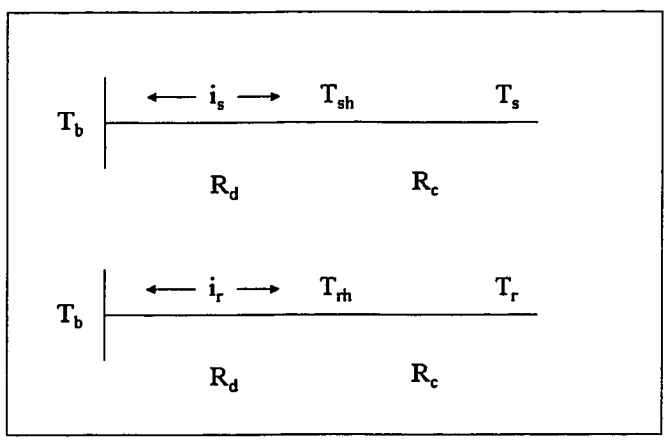

Figure 6.1.1 A schematic of thermal Ohm's law equivalent of DSC.

Assume that the thermal cell is symmetrical, that the thermal resistances are identical on the reference and sample sides at any given temperature, that the temperatures of the sample and reference and their containers are uniform, and that the heat flow between the

sample and the reference can be neglected. The thermal resistance (R_d and R_c) is the inverse of the heat transfer coefficient (A_d and A_c). Assuming that the sample is generating heat at a rate dH/dt (exothermic transition) then the equations for heat flow on the sample and reference sides are:

$$\frac{di_s}{dt} = \frac{T_{sh} - T_b}{R_d} = \frac{T_s - T_b}{R_c + R_d} \tag{6.1}$$

$$\frac{di_r}{dt} = \frac{T_{rh} - T_b}{R_d} = \frac{T_r - T_b}{R_c + R_d} \tag{6.2}$$

Heat evolved by the sample can either increase the sample temperature or be lost to the surroundings. Since energy must be conserved, the sum of these two effects must be equal to dH/dt. Thus

$$\frac{dH}{dt} = C_s \frac{dT_s}{dt} + \frac{di_s}{dt} \tag{6.3}$$

$$0 = C_r \frac{dT_r}{dt} + \frac{di_r}{dt} \tag{6.4}$$

Combination of equations (6.1) and (6.3), and (6.2) and (6.4) yields:

$$\frac{dH}{dt} = C_s \frac{dT_s}{dt} + \frac{T_s - T_b}{R_c + R_d} \tag{6.5}$$

$$0 = C_r \frac{dTr}{dt} + \frac{T_r - T_b}{R_c + R_d} \tag{6.6}$$

Subtracting the equation for the reference (6. 6) from that of the sample side, equation 6.5, gives:

$$\frac{dH}{dt} = C_s \frac{dT_s}{dt} - C_r \frac{dT_r}{dt} + \frac{T_s - T_r}{R_c + R_d} \tag{6.7}$$

$$\frac{dT_s}{dt} - \frac{dT_r}{dt} = \frac{d(T_s - T_r)}{dt} \tag{6.8}$$

Substituting equation (6.8) into (6.7) yields:

$$\frac{dH}{dt} = \frac{T_s - T_r}{R_c + R_d} + (C_s - C_r)\frac{dT_r}{dt} + C_s \frac{d(T_s - T_r)}{dt} \tag{6.9}$$

Equation 6.9 represents a typical DTA curve since dH/dt is proportional to the difference between the sample and reference temperatures.

The quantity measured is the difference in temperature between the sample and reference holders, not the sample and the reference temperatures themselves. Using equation (6.1) and (6.2), the following relationship is obtained:

$$\Delta T = T_{sh} - T_{rh} = \frac{R_d}{R_c + R_d}(T_s - T_r) \tag{6.10}$$

The final expression is obtained by combining equation (6.9) and (6.10)

$$\frac{dH}{dt} = \frac{T_{sh} - T_{rh}}{R_d} + (C_s - C_r)\frac{dT_r}{dt} + C_s \frac{R_d + R_c}{R_d}\frac{d(T_{sh} - T_{rh})}{dt} \tag{6.11}$$

From equation (6.11), at any time, the rate of heat evolution can be consider the sum of three terms (see Figure. 6.1.2):

1. The instrument response divided by a constant, $(T_{sh} - T_{rh})/R_d$ which is proportional to the difference between the sample and reference sides.
2. A term, $(C_s - C_r)dT/dt$, depending on the heat capacity of the sample and on the heating rate, which is the displacement from the zero level.
3. A term, $[(R_d + R_c) /R_d]\times C_c \times d (T_{sh}-T_{rh}) / dt$ involving the time constant, $[(R_d+R_c)/R_d]\times C_s$, and the rate of change of the recorded quantity.

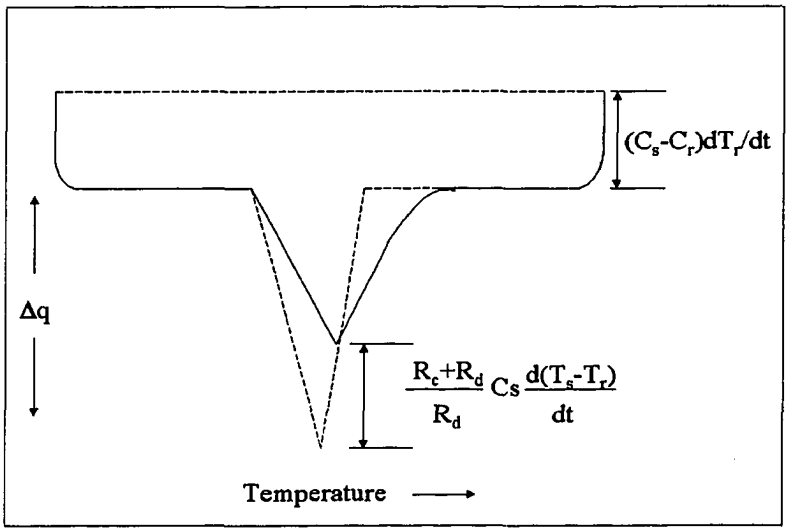

Fig. 6.1.2 The subdivision of the DSC response curve.

For DSC the measured quantity is the difference in heat flow into or out of the sample and reference.

$$\Delta q = \frac{di_s}{dt} - \frac{di_r}{dt} \tag{6.12}$$

Substituting the temperature values from equation (6.1) and (6.2) for the individual heat flow yields:

$$\Delta q = \frac{T_{sh} - T_{rh}}{R_d} = \frac{\Delta T}{R_d} \tag{6.13}$$

Where the temperature difference sensed by the detectors is directly proportional to the heat flow into or out of the sample and reference. Substituting `equation (6.13) into equation (6.11) yields

$$\frac{dH}{dt} = \frac{dq}{dt} + (C_s - C_r)\frac{dT_r}{dt} + C_s(R_d + R_c)\frac{d^2q}{dt^2} \tag{6.14}$$

This relationship models the differential scanning calorimeter.

Equation (6.14) may be recast into the form

$$dq/dt = C_s(\beta) + f(t, T) \tag{6.15}$$

where f(t, T) is the kinetic component and $C_s\beta$ is the heat capacity component of the heat flow. The use of the MDSC technique allows an analysis of the kinetic component and will be discussed later.

6.1.2 Differential scanning calorimetry

By definition heat capacity (specific heat) is the amount of energy that must be absorbed by a material in order to raise its temperature by one degree. In the past, heat capacity measurements have been accomplished using tedious and complex procedures. With the introduction of the differential scanning calorimetry (DSC) technique, many of the problems which made these measurements difficult have been eliminated.

In a generic sense DSC is a technique in which the difference in energy inputs into a substance and a reference material is measured as a function of temperature or time while the substance and the reference material are subjected to a controlled temperature program. All DSC instruments feature similar characteristics:

1. In all cases the recorded output is the heat flow derived from the temperature difference between the sample and the reference taken using temperature sensors as the primary transducers.
2. The temperature sensors are located external to the sample in order to make calorimetric measurements
3. All DSC devices display the heat flow as their primary output.

An example of the differential temperature type DSC is the DuPont (TA Inst.) 910 DSC System. A cross sectional diagram of the module is shown in Figure 6.1.3. Small containers (pans) containing the sample and the reference materials are placed on raised portions of a constantan disk which serves as the primary heat source and as one element of the temperature measuring

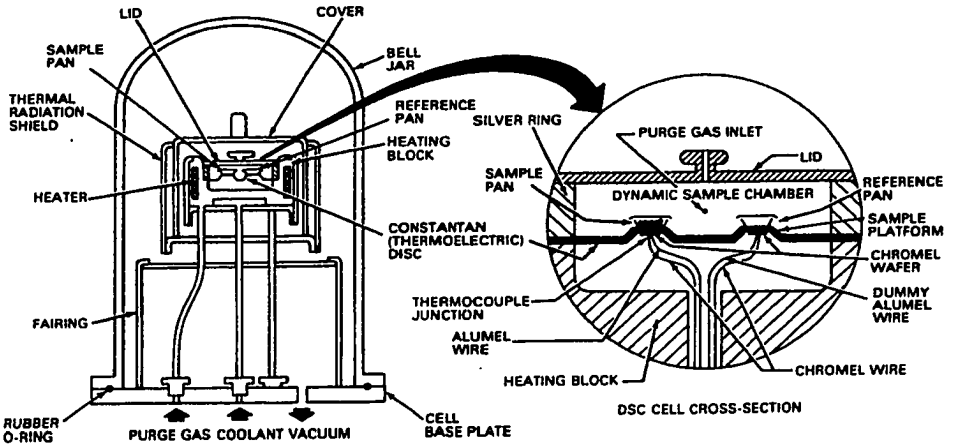

Fig. 6.1.3 The DuPont 910 DSC instrument for measuring Heat Capacity.

thermoelectric junctions. The chromel wafers attached to the underside of the constantan platform form a chromel-constantan differential thermocouple system which allows the differential temperature, ΔT, to be monitored. The actual temperature of the sample is determined by a chromel-alumel thermocouple formed by chromel and alumel wires connected underneath the chromel disks. The temperature output is fed to a variable gain amplifier which amplifies and electronically scales the signal to be displayed in heat flow units. This differential power output can be plotted either versus sample temperature or versus time.

For example, at a constant heating rate, the heat capacity of a sample through its melting point theoretically increases to infinity while the sample temperature becomes invariant; thus, a ΔT develops between the sample and the constantly rising reference temperature. The ΔT signal is proportional to the heat flowing into the sample.

The basic method for heat capacity measurements using the DSC technique was originally described by O'Neil (1964) and modified by Cassel (1974). Samples for heat capacity measurements are generally encapsulated in sample pans. Different versions of these pans are available and the physical and chemical characteristics of the samples determine the type of pan to be used. Once the sample pan has been selected, it should be weighed, then filled with the sample and weighed again. The mass of the sample can be determined from the difference between these weightings. Using an empty pan with lid in the reference side, the first run involves a scan with an empty pan and lid on the sample side. The empty pan should be similar to the one that will contain the sample. The second run, also with an empty pan on the reference side, is a scan of a sample pan containing a material whose heat capacity is well known, such as sapphire. From this run a calibration factor, F, can be determined using the equation:

$$F = \text{Cp(sapphire,lit.)}/\ \text{Cp (sapphire, obs.)} \qquad (6.16)$$

This factor, F, is actually the individual calibration constant of the calorimeter at each temperature, Cp is the heat capacity.

Subsequent runs are for the samples themselves, each of which should be encapsulated in pans similar to the one used on the reference side. The heat capacity of the sample, Cp, is determined by using the heat flow values obtained together with the equation:

$$C_p = F \times Y/m \qquad (6.17)$$

where Y is the difference in heat output between sample and empty pans curves at each temperature of interest, and m is the mass of the sample.

Measurements of phase transitions can usually be treated with the method for the heat capacity described above. The main concern is to assign the correct temperature in regions where the heat capacity is varying rapidly. Second order transitions, such as glass transition, are determined by observing that the slope of the DSC signal changes when the transition occurs at a temperature which is characteristic of the material. In general, other transitions, such as melting, are reflected as a peak on the DSC curve. The area under this peak is direct measurement of the enthalpy involved in the transition

Limitations of conventional DSC

- The heating rate is the only experimental variable available.
- Sensitivity and resolution vary in the opposite way with heating rate.
- Heat capacity cannot be measured isothermally or during a reaction.
- Often several thermal events take place simultaneously and cannot be resolved.

6.1.3 Modulated differential scanning calorimetry

Thermal conductivity is a basic material property, and is a measurement of the case with which heat is transmitted through a material. Determination of a material's thermal conductivity is important in evaluating its utility for specific applications. For novel materials such as the solid-state tunable laser materials we are developing, we have to measure the thermal conductivity in order to supply this important information for their applications.

Thermal conductivity can be measured using several different instrumental techniques. One of these is based on DSC. As we have seen earlier heat flow, in this approach is measured using the thermal equivalent of Ohm's Law where $dq/dt = \Delta T/R$. Here R is the thermal resistance of thermoelectric disk. A number of research groups (Chiu, 1979; Sircar, 1982; Keating, 1990; and Duswalt, 1993) have modified heat flux DSC instruments to measure the thermal conductivity of insulating materials (thermal conductivity in the range from 0.1 to 2 W/° C m). In this approach a test specimen is placed in the DSC cell in contact with the sample platform. The temperature of the test specimen is monitored on the side opposite to the contact side. From the recorded heat flow and the temperature difference across the sample the thermal conductivity can be calculated using the equation:

$$dq/dt = -KA\ dT/dx \qquad (6.18)$$

where:

q = Heat (J)

t = Time (sec)

K = Thermal conductivity (W/°Cm)

T = Temperature (°C)

x = Height of test specimen (m)

A = Cross Sectional Area of Test Specimen (m^2)

This DSC measurement of thermal conductivity works well but requires modification of the commercially available DSC cell as well as very careful attention to experimental

details. A recent extension of traditional DSC technique, MDSC, minimizes those limitations.

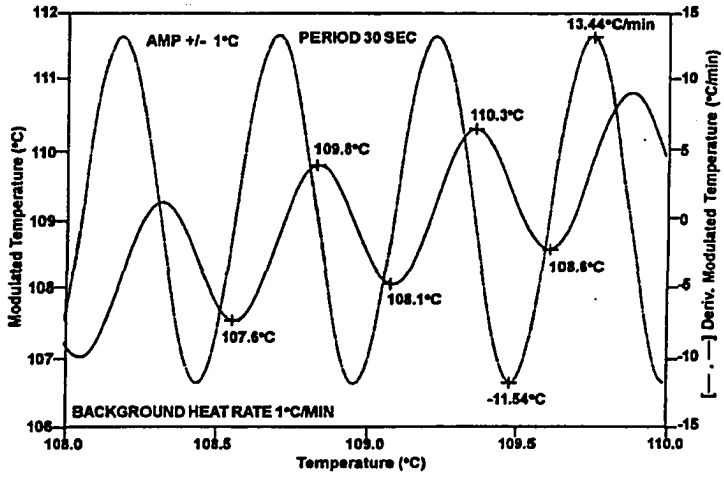

Figure. 6.1.4 MDSC Heating Profile. The dashed line is at the traditional linear heating.

In MDSC, the same heat flux DSC cell arrangement used as in conventional DSC (Figure 6.1.3), but the heating profile applied to the sample and reference by the furnace has a sinusoidal modulation (oscillation) overlaid on the traditional linear heating ramp to yield a heating profile (solid line in Fig. 6.1.4) in which the sample temperature still continuously increases with time but not in a linear fashion. The net effect of imposing this more complex heating profile on the sample is the same as if two experiments were run simultaneously on the material: one experiment at the traditional linear heating rate [dashed line in Fig. 6.1.4] and one at a more rapid sinusoidal heating rate [dot-dash line in Fig. 6.1.4].

The exact nature of these two simultaneous experiments is dependent on three operator-selected variables:

1. Underlying heating rate
2. Period of modulation
3. Temperature amplitude of modulation

In contrast to the steady state heat flow approach of Chiu and others mentioned previously, the modulated heat flow of MDSC establishes a dynamic equilibrium in the test specimen permitting the measurement of thermal conductivity by applying a cyclic temperature program to only one side of the test specimen.

The one dimensional heat flow model described in equation (6.18) can be expanded using the modulated heat flow generated by MDSC, to yield equation (6.19) (S.M. Marcus and R. L. Blaine):

$$(\frac{dQ}{dt})^2 = 2(ZT_0KA)^2 \frac{(1-2e^{2ZL}\cos(2ZL)+e^{4ZL})}{(1+2e^{2ZL}\cos(2ZL)+e^{4ZL})} \qquad (6.19)$$

where:

dQ/dt = Heat flow amplitude (J/sec), K = Thermal conductivity (W/°Cm)

ω = Angular frequency (2π/sec) , A = Sample Cross Sectional Area (cm^2)

L = Sample length (cm) , M = Sample mass (g)

ρ = Sample Density ($g/(cm)^3$), C_p = Sample Specific Heat (J/°Cg)

$Z^2 = \omega\rho\, C_p/(2K)$, C = Apparent Heat Capacity (J/°C)

T_o = Temperature Modulation Amplitude (°C)

There are additional assumptions implicit for this method:

- The specimen must be a right circular cylinder with cross sectional area (A) and height (L). The end-faces must be parallel to each other.
- The face of the specimen at the heat source (sample platform) follows the applied temperature modulation.
- The heat flow through the opposing face is zero.
- There is no heat flow through the side of the specimen.

For materials with low thermal conductivity, the e^{4ZL} term is large and dominates the term in brackets on the right of the equation (6.19) driving it to unity. Rearranging equation (6.19), noting that $C = (dQ/dt) / (\omega T_o)$ and $\omega = 2\pi / P$ (period), and solving for K yields:

$$K = (2\pi C^2) / (C_p \rho A^2 P) \qquad (6.20)$$

For a right circular cylinder, $\rho = M / AL$ and $A = \pi d^2/4$. Equation (6.3) becomes:

$$K = (8LC^2) / (C_p M d^2 P) \qquad (6.21)$$

Sample length (L), diameter (d) and mass (M) are easily measured physical parameters. The specimen's specific heat (C_p) may be measured using the MDSC under the optimum conditions. The period (P) is an experimental parameter. And the apparent heat capacity (C) is the measured parameter from the thermal conductivity optimized experimental conditions. Thus, MDSC provides all of the experimental information needed to calculate thermal conductivity.

6.1.4 Theory of thermo-mechanical analysis

Although the most widely used thermal analysis techniques are the DSC and DTA methods, there are a number of other thermal techniques that are employed to supplement or complement the principal techniques in solving technological and engineering problems. Thermo-mechanical methods constitute the broad area of thermal analysis that involve measurement of changes in volume, or shape, or length while a sample is subjected to an applied stress, and the same time, to a temperature ramp program. Three common techniques are; dilatometry, thermo mechanical analysis (TMA), and dynamic mechanical analysis (DMA).

When compared to other techniques, the TMA instrumentation is quite simple. For the DuPont model 943 TMA module (see Figure 6.1.5), linear displacements of the sample probe are sensed by a linear variable displacement transformer(LVDT). A thermocouple, used to measure the sample temperature, is in direct contact or in close proximity to the sample which is surrounded by a controlled cylindrical heater and Dewar assembly. The final output is a plot of the sample dimensional change, and/or its derivative, versus temperature or time. Various types of probes allow the TMA apparatus to be used for measuring; expansion, compression, penetration, tension, and stress relaxation coefficients as a function of temperature and applied loading. In our studies, TMA was used to determine the thermal expansion coefficient of single crystals.

For TMA, a non-oscillatory stress is applied to the sample as it is heated at a constant rate and the deformation under the load is measured as a function of temperature. The measured linear and volumetric changes are directly related to crystal structure changes, and changes in the physical and/or chemical state of the sample under investigation.A change in the sample length can be expressed as the following equation:

$$L = L_0 (1+\alpha T) \qquad (6.22)$$

where L is the sample length at temperature T, L_0 is the sample length at 0 °C, and α is the linear coefficient of thermal expansion. In the TMA method, L is recorded as a function of temperature. Differentiation of equation (6.22) assuming that α is constant gives:

$$dL/dt = L_0\alpha\ (dT/dt) \qquad (6.23)$$

where dT/dt is the constant heating rate.

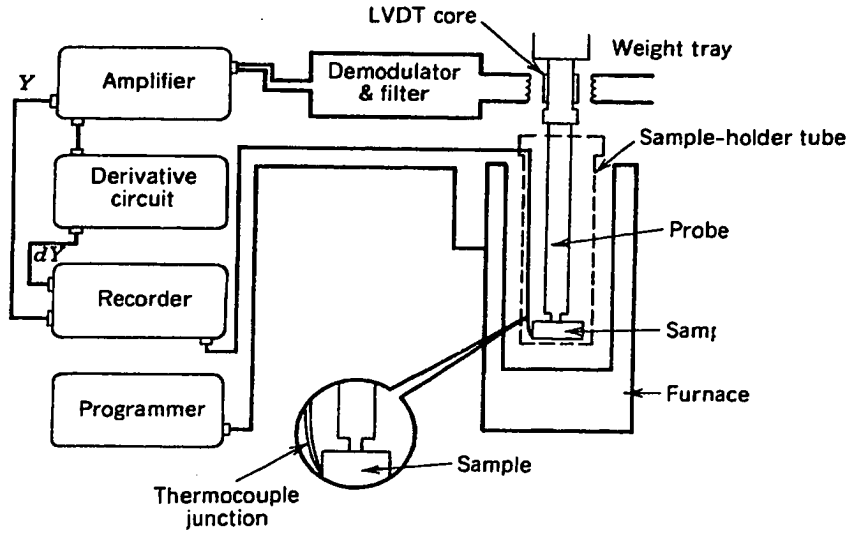

Fig. 6.1.5 Du Pont Model 943 TMA module

6.2 Measurement of heat capacities

Drop calorimetry determinations of the isobaric heat capacity (Cp) of Olivine type materials; Mg_2SiO_4, Ca_2GeO_4, and $CaMgGeO_4$ were reported (Guillaume Fiquet *et al*). The upper limit of the measurements is 1700 K. The samples they used were synthesized by solid state chemical reaction. The products they obtained had a grain size of about 10 μm. However, below 600 K drop calorimetry is inaccurate. For the application of most solid-state laser materials, the heating temperature range will be below 500K in most cases.

In this work, we measured the heat capacity of both large size single crystals and polycrystalline samples by using DSC. The samples include Ca_2GeO_4, Li_2CaSiO_4, and $LiScGeO_4$.

6.2.1 Experimental set up

The instrument for measuring heat capacity is the Du Pont 910 DSC controlled by the TA2100 thermal analyzer system.

The samples used to measure the heat capacity were single crystals grown by the TSSG method, and polycrystalline powders synthesized by solid-state chemical reactions from stoichiometric mixtures of reagent grade components.

Samples for DSC are sealed into aluminum sample pan using a sample encapsulating press. The DSC 910 was calibrated using standard reference materials (Indium, Zinc). The experimental protocol includes the determination of the calibration factor F, given by equation (6.16), using a sapphire disc for each experimental run.

Subsequent runs are for the samples themselves, each of which should be encapsulated in pans similar to the one used on the reference side, and the thermal programs are run under the same conditions as that of standard material. The heat capacity of the sample, C_p, is determined by using the heat flow values obtained, and the calibration factor. All experiments are run at the nominal heating rate of 10 °C/min. Experiments are run between 300 and 1000 K.

6.2.2 Calculation of the specific heat

To find the heat capacity of a material we use the expression

$$C_{p(\text{material})} = F \times (\text{heat flow} - \text{base line}) / (dT/dt) \qquad (6.24)$$

The temperature dependence may be shown graphically, as illustrated in Figures. 6.2.1 through 6.2.3, where C_p is plotted vs. temperature for Cr-doped Ca_2GeO_4, Li_2CaSiO_4 and $LiScGeO_4$.

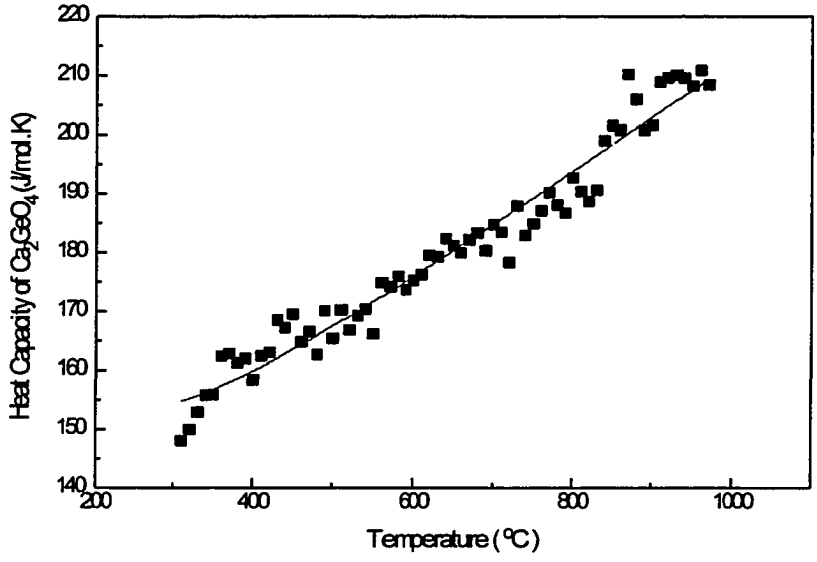

Fig.6.2.1 Heat capacity of Ca_2GeO_4 vs temperature.

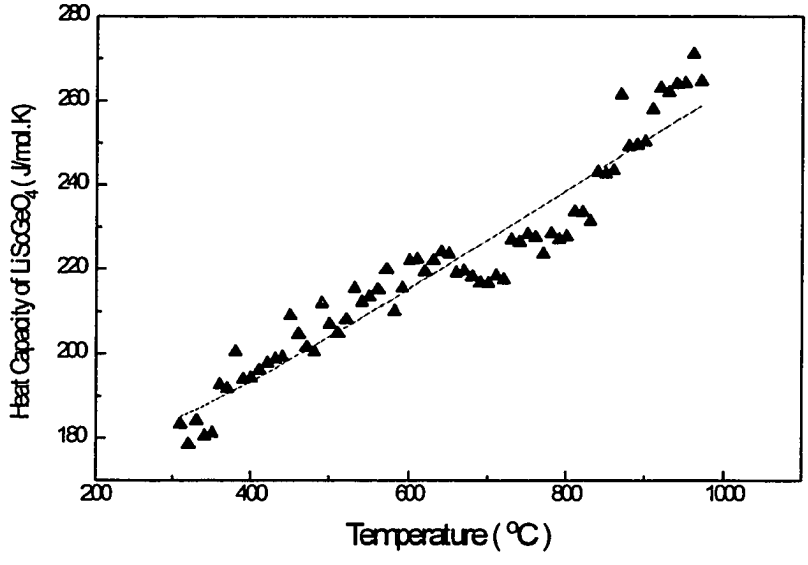

Fig.6.2.2 Heat capacity of $LiScGeO_4$ vs temperature.

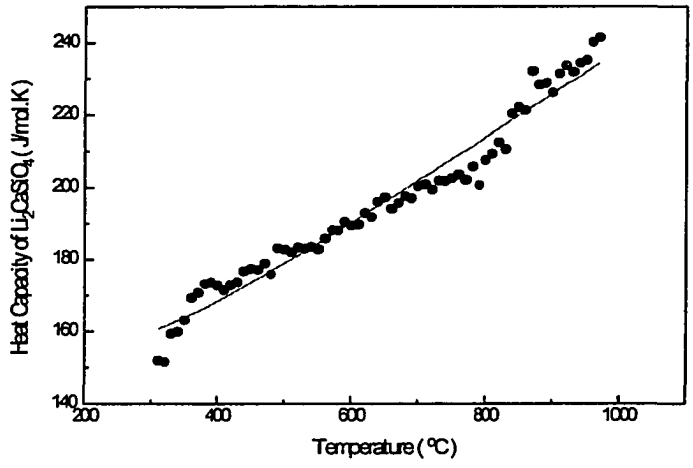

Fig.6.2.3 Heat capacity of Li_2CaSiO_4 vs temperature.

Commonly, the temperature dependence is fitted by the equation(Smith and van Ness,1987):

$$C_p = A + BT + DT^{-2} \qquad (6.25)$$

The constants of A, B, and D were obtained through least-squares fits made to the experimental data (see Table 6.2.1).

Table 6.2.1 Constants for the equation $C_p = A + BT + DT^{-2}$, T(K) from 300K to 1000K:

Chemical species	A	B	D
$Cr:Ca_2GeO_4$	117.38102	0.09397	793949.30144
$Cr:LiScGeO_4$	141.51544	0.12027	612378.06694
$Cr:Li_2CaSiO_4$	114.42938	0.12275	792499.44863

The effects of temperature on Cp are mostly determined by experiments. Fig.6.2.4 shows the Heat Capacity vs. Temperature from the fitted equations. It is obvious that the Heat Capacity of the single crystals Ca_2GeO_4, Li_2CaSiO_4, and $LiScGeO_4$ has the similar property with that of sapphire. The behavior of the heat capacity as a function of temperature is real and reproducible. It has been observed that the heat capacity of the measured materials increases as the temperature increases. In the measurement temperature range, there was no phase transition observed. This is agreed with the phase information from the literature and our DTA measurement.

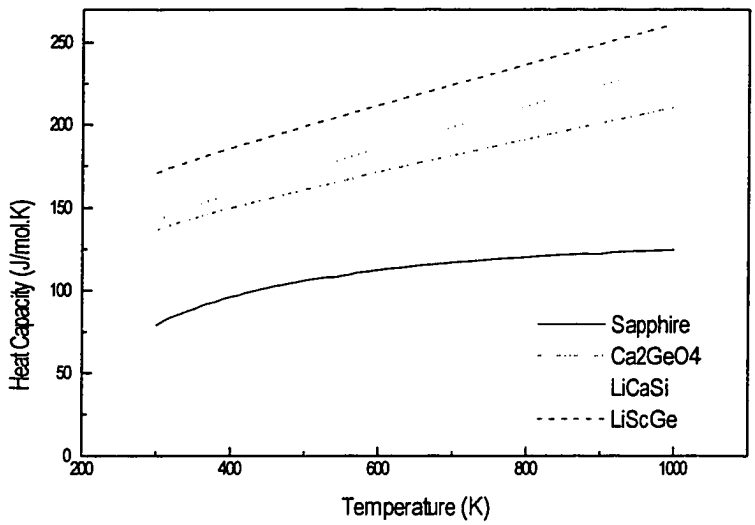

Fig. 6.2.4 Heat capacity from the fitted equations.

Table 6.2.2 Typical heat capacity (J/mol.K) of Ca_2GeO_4, Li_2CaSiO_4 and $LiScGeO_4$

Temperature(K)	Ca_2GeO_4	Li_2CaSiO_4	$LiScGeO_4$
300	136.7504	142.4488	170.7922
320	139.698	145.9701	174.0216
340	142.4627	149.3088	177.1099
360	145.0841	152.5044	180.0875
380	147.5914	155.5862	182.9772
400	150.0068	158.5763	185.7961
420	152.3476	161.4918	188.5573
440	154.6268	164.3459	191.2711
460	156.8551	167.1491	193.9456
480	159.0407	169.9097	196.5871
500	161.1902	172.6344	199.2009
520	163.3092	175.3285	201.7911
540	165.4021	177.9966	204.3612
560	167.4725	180.6423	206.9139
580	169.5235	183.2686	209.4517
600	171.5576	185.878	211.9764
650	176.5824	192.3411	218.2415
700	181.5397	198.737	224.4547
750	186.4471	205.083	230.6293
800	191.3165	211.3911	236.7746
850	196.1566	217.67	242.8974
900	200.9738	223.926	249.0024
950	205.7728	230.1638	255.0934
1000	210.5571	236.3869	261.1731

6.3 Measurement of the Thermal Conductivity

Thermal conductivities of solids must be measured experimentally because they depend on many factors that are difficult to predict. In this work, we measured the thermal conductivity by using MDSC.

6.3.1 Sample information

In this work, we only measured the thermal conductivity of the CUNYITE ($Cr:Ca_2GeO_4$). The samples were prepared from a single crystal grown from TSSG method. The shape of the samples was cylindrical with two parallel end faces. One was thin with thickness of 0.4 mm, and the other was thick with thickness of 6.40 mm. A key requirement for any high precision measurement is the preparation of a test specimen of uniform and known geometry. The test specimens were prepared by first grinding a single crystal boule into the shape of a right, circular cylinder of 6.40 mm diameter. The rod was the sectioned into slabs using a diamond saw, and the faces were polished. Other shapes may be used but the cylinder is convenient to machine or extrude and simplifies the measurements.

6.3.2 Experimental measurements

The general experimental procedure for determining thermal conductivity values at a specific temperature are described here:

1. Normal calibration of the MDSC is performed using indium metal and sapphire standard reference materials.
2. Thermal conductivity calibration is performed using a reference material of low and known conductivity. Polystyrene specimens 0.4 and 3.4 mm in thickness and the same diameter as the unknowns were used for the instrument calibration.
3. Specific heat capacity (Cp) of the unknown material is obtained using standard MDSC procedures and a thin (<0.5 mm) specimen.
4. The apparent heat capacity (C) of the unknown material using a thick (>3.0 mm) test specimen is determined. The specimen mass, length and diameter are also measured. (Note: The measurements in (4) and (5) are improved by putting a thin aluminum foil disk (wetted on both sides with silicone oil) between the test specimen and the DSC measurement platform. This disk acts to provide a more uniform heat transfer path. An equivalent foil disk with silicone oil is used on the reference position of the cell to balance the thermal effects of the aluminum.)
5. Due to the loss of thermal energy through the sides of the test specimen, there exists the discrepancy between the thermal conductivities measured and literature values. To correct this effect, a thermal conductivity calibration (D) is used(S.M. Marcus and R.L. Blaine). The value for D is obtained using a calibration material of known thermal conductivity, and equation(6.26):

$$D = (K_o * K_r)^{0.5} - K_r \qquad (6.26)$$

where: D = Thermal conductivity calibration constant

K_o = Observed reference material thermal conductivity (W/°Cm)

K_r = True reference material thermal conductivity (W/°Cm)

6. Using the specific heat (Cp) and apparent heat capacity thus determined, calculate the observed thermal conductivity (K_o). Substituting this value, along with the thermal conductivity calibration constant (D) into equation (6.26) (S.M. Marcus and R.L. Blaine) to yield the thermal conductivity (K) of the unknown.

$$K = [K_o - 2D + (K_o^2 - 4DK_o)^{0.5}]/2 \quad (6.27)$$

Where: D = Thermal conductivity calibration constant

K_o = the observed thermal conductivity of the unknown specimen.

The actual experimental work was done at the Applications Laboratory of TA Instruments. We thank them for their help.

The experimental work consisted of the number of MDSC scans necessary to generate thermal conductivity data. The "thin" disks were used to determine the specific heat capacity of the samples. The "thick" disks were used to determine the apparent heat capacity of the samples. After calculating a calibration constant using Pyrex 7740, the calculation was done to determine thermal conductivity.

Two sets of experiments were performed: one set using an amplitude of ±0.5°C and a period of 100 seconds, and a second set using the same amplitude and a period of 80 seconds. The following thermal method, making measurements at two temperatures, was used for each experiment:

1. data storage: off

2. equilibrate at 100°C
3. modulate +/- 0.50°C every 100 seconds (80 for 80 second period)
4. data storage: on
5. isothermal for 15 minutes
6. data storage: off
7. equilibrate at 200°C
8. modulate +/- 0.50°C every 100 seconds (80 for 80 second period)
9. data storage: on
10. isothermal for 15 minutes.

Figures 6.3.1 through 6.3.6 show the specific and apparent heat capacity data collected for the samples using an amplitude of ±0.5°C and a period of 100 seconds. Figures 6.3.7 through 6.3.12 shows that same data for amplitude of ±0.5°C and a period of 80 seconds.

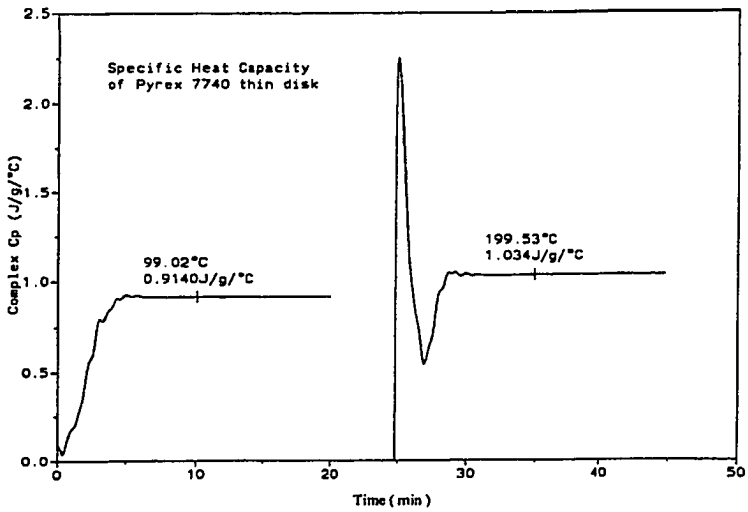

Fig. 6.3.1 Specific heat capacity of Pyrex 7740 thin disk. Modulation at 100 seconds.

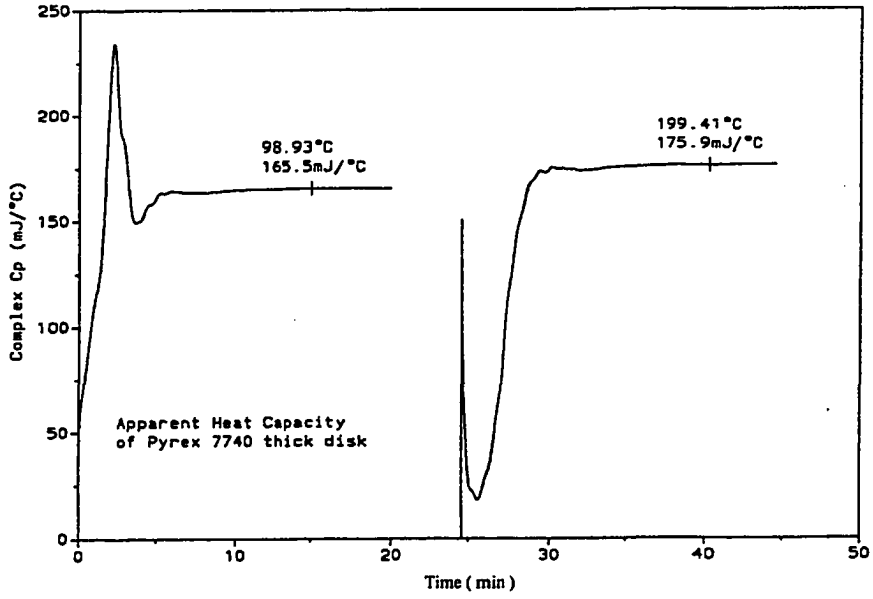

Fig. 6.3.2 Apparent heat capacity of Pyrex 7740 thick disk. Modulation at 100 seconds.

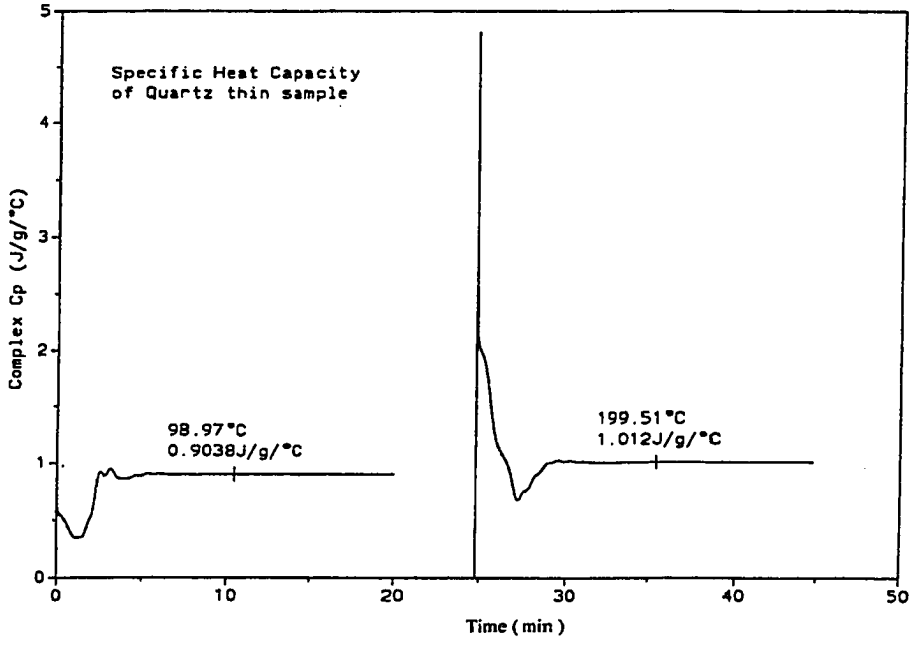

Fig. 6.3.3 Specific heat capacity of Quartz thin disk. Modulation at 100 seconds.

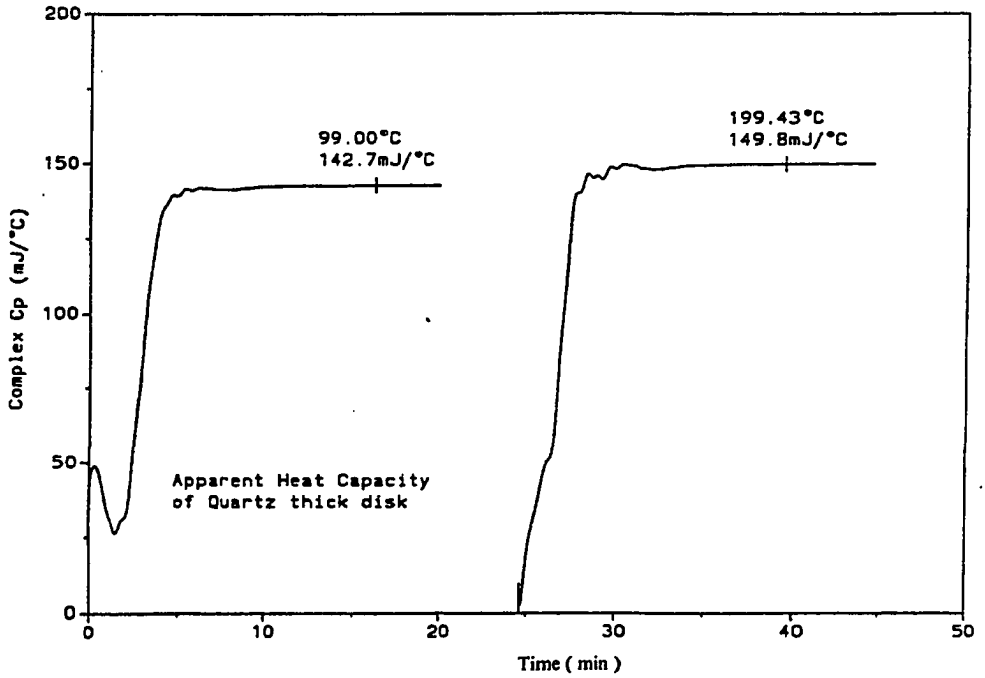

Fig. 6.3.4 Apparent heat capacity of Quartz thick disk. Modulation at 100 seconds.

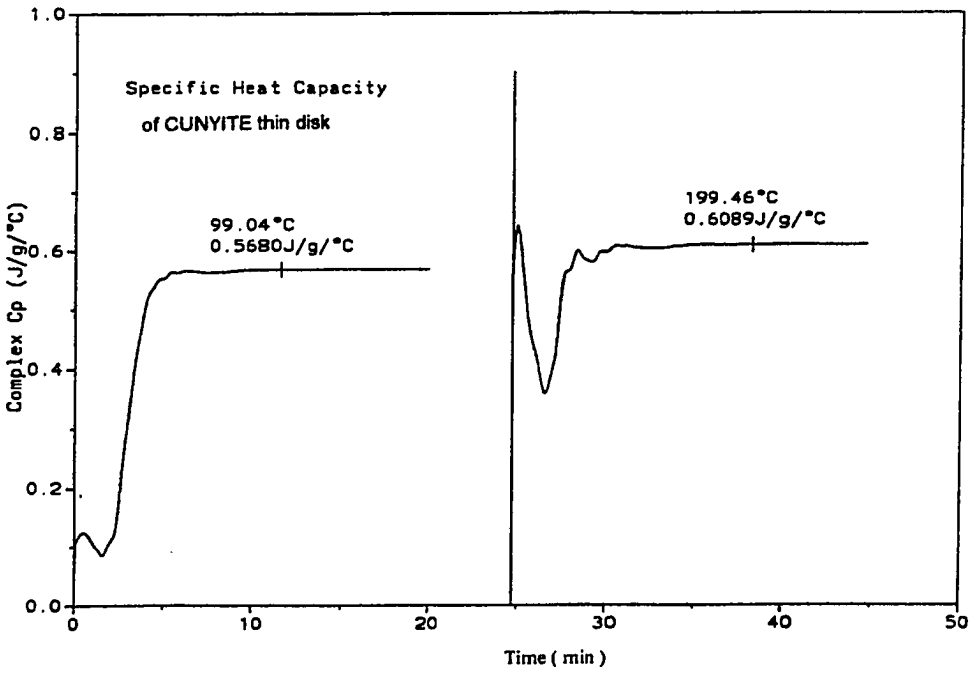

Fig. 6.3.5 Specific heat capacity of CUNYITE thin disk. Modulation at 100 seconds.

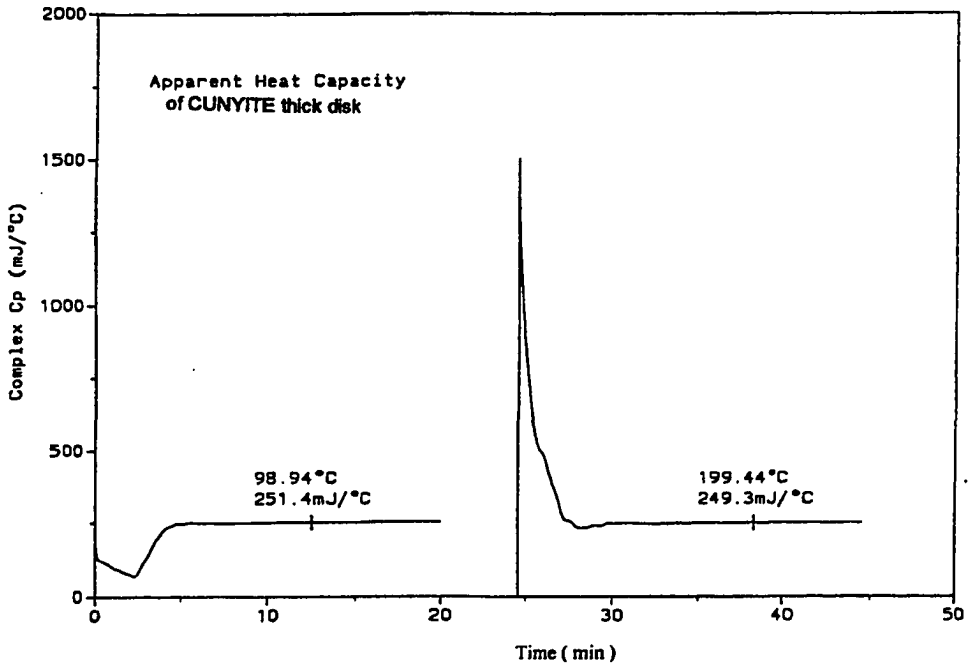

Fig. 6.3.6 Apparent heat capacity of CUNYITE thick disk. Modulation at 100 seconds.

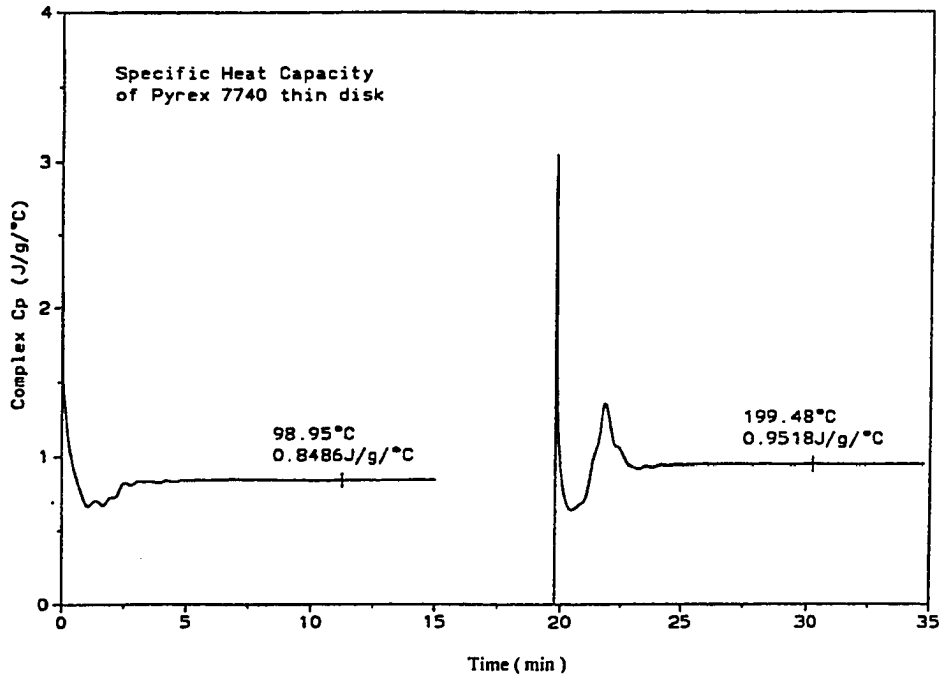

Fig. 6.3.7 Specific heat capacity of Pyrex 7740 thin disk. Modulation at 80 seconds.

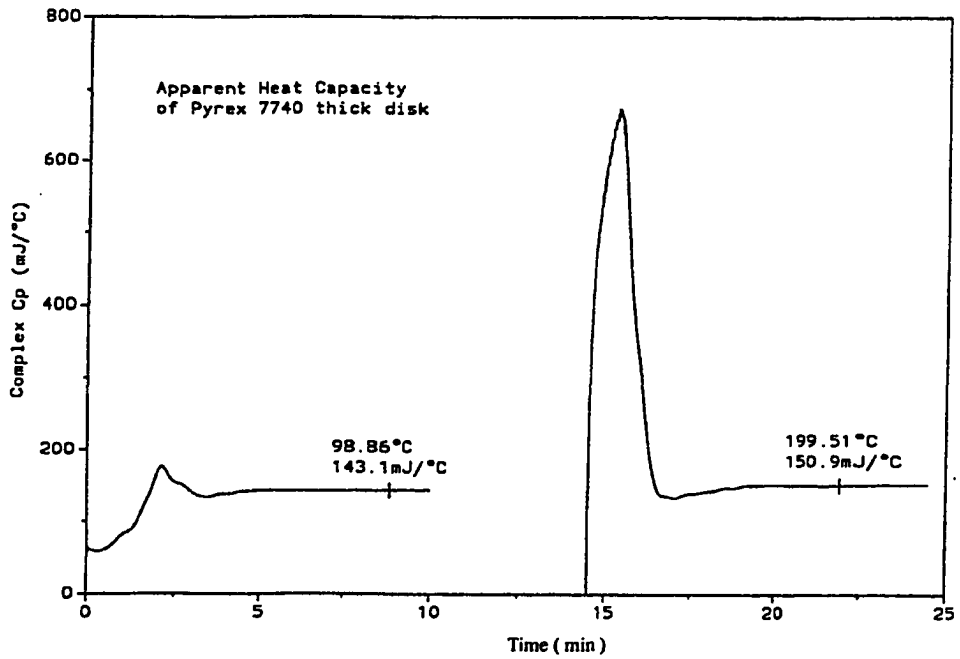

Fig. 6.3.8 Apparent heat capacity of Pyrex 7740 thick disk. Modulation at 80 seconds.

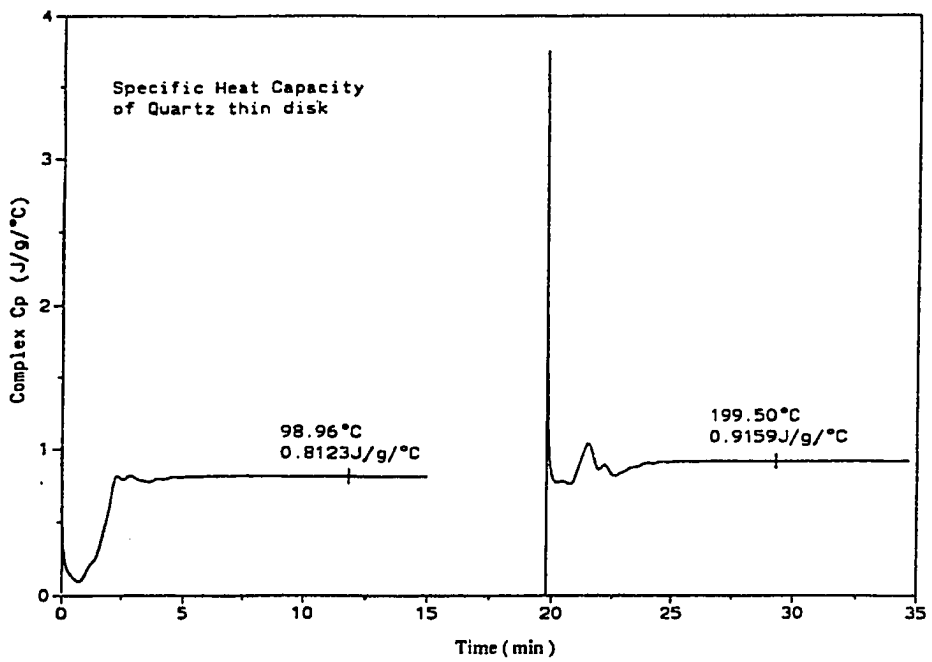

Fig. 6.3.9 Specific heat capacity of Quartz thin disk. Modulation at 80 seconds.

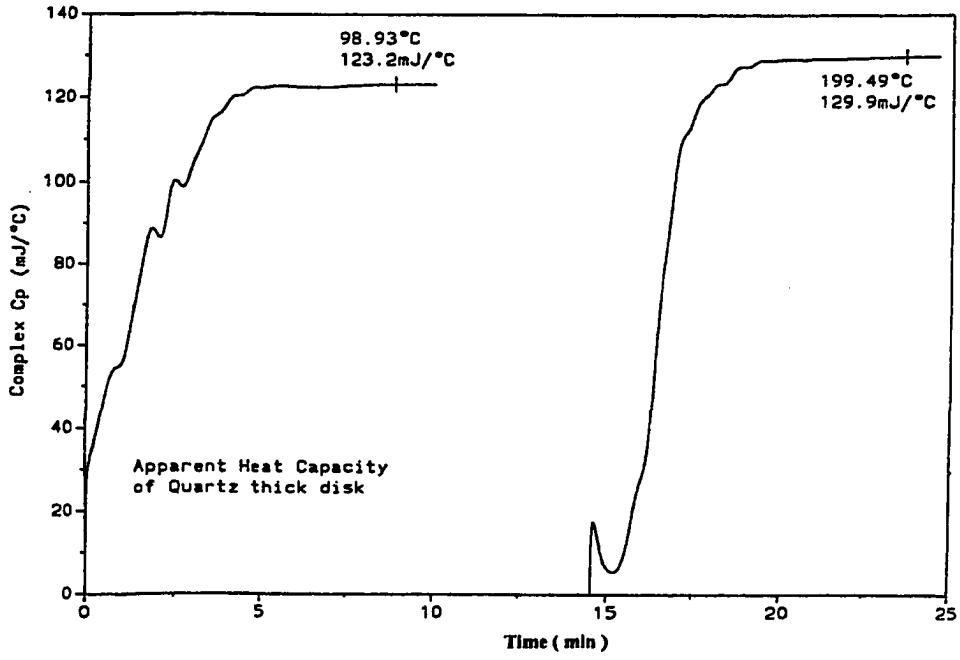

Fig. 6.3.10 Apparent heat capacity of Quartz thick disk. Modulation at 80 seconds.

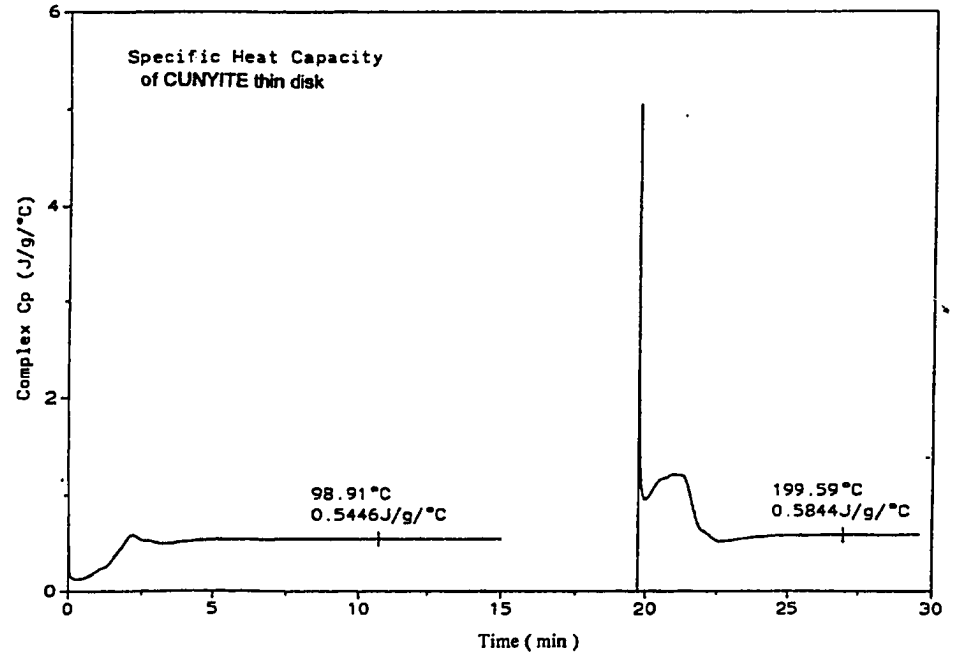

Fig. 6.3.11 Specific heat capacity of CUNYITE thin disk. Modulation at 80 seconds.

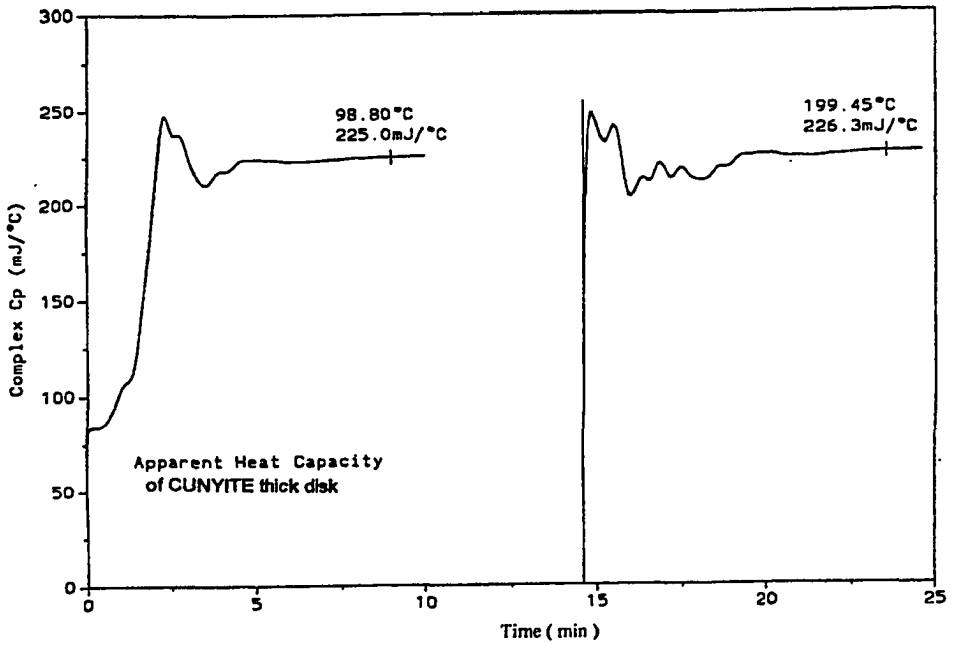

Fig. 6.3.12 Apparent heat capacity of CUNYITE thick disk. Modulation at 80 seconds.

6.3.3 Results and Discussions:

The thermal conductivity data for the quartz and CUNYITE samples are summarized in the table below (in the unit of W/mK):

	±0.5°C, 80 Sec	±0.5°C, 100 Sec
Quartz @ 100°C	1.4	1.4
Quartz @ 200°C	1.5	1.5
CUNYITE @ 100°C	2.2	2.2
CUNYITE @ 200°C	2.1	2.3

The calculated thermal conductivity for the quartz sample is at the upper end of the magnitude range for the thermal conductivity determinations doable by this technique. The values for the CUNYITE sample fall outside the range. However, the results are within the accuracy and precision in the MDSC method.

Compared with other solid-state lasers, the thermal conductivity of CUNYITE is less than that of Forsterite. The thermal conductivities of several solid state materials are as follows:

Ca_2GeO_4:	0.023 (W/cmK@370K)
Mg_2SiO_4:	0.08 (W/cmK@300K)
YAG:	0.13 (W/cmK@300K)
$BeAl_2O_4$:	0.23 (W/cmK@300K)
Al_2O_3:	0.35 (W/cmK@300K)
BeO:	3.7 (W/cmK@300K)

The thermal diffusivity, κ, of Cr:Ca_2GeO_4 can be readily evaluated by means of the defining formula:

$$\kappa = K / (C_p \rho)$$

At 370 K, the heat capacity of Ca_2GeO_4 is 160 (J/mol.K), ρ = 3.2 (kg/cm^3). Therefore, the thermal diffusivity of Ca_2GeO_4 is:

$$\kappa_{Ca2GeO4} = 4.4921875 \times 10^{-5}$$

6.4 Measurement of the thermal expansion coefficient

Knowledge of the thermal expansion coefficient of solid state laser materials is of technical importance when they are used in devices working at temperatures above or below the ambient. The designer of a device must take account of the thermal stress induced. Thermal expansion is an anisotropic property.

TMA was employed to determine the thermal expansion coefficients. A Du Pont 943 thermo-mechanical analyzer was used for these measurements. Aluminum and indium are used as the standard materials for the calibration of the instrument.

6.4.1 Experimental procedure

The samples used for measuring the thermal expansion coefficient are single crystals grown from TSSG technique, and are cut into oriented rectangular parallel of each surface.

Sample information:

Li_2CaSiO_4(single crystal): 2.21x2.37x1.85 mm

$LiScGeO_4$(single crystal): 2.21x2.30x3.05 mm

Ca_2GeO_4(single crystal): 6.50x6.00x5.80 mm

The linear thermal expansion coefficient (α) of Cr-doped Li_2CaSiO_4, Ca_2GeO_4, and $LiScGeO_4$ were measured from room temperature to 800K along the principal crystal axes.

Before the thermal expansion coefficients of the samples could be measured, the calibration of the DuPont 943 thermo-mechanical analyzer must be performed, which include: Baseline Calibration, Temperature Calibration, Y-Axis Static Calibration, and Y-Axis Dynamic Calibration.

Calculation of Y-axis Calibration Coefficient:

The experimental apparatus was calibrated by comparison with known results of the thermal expansion coefficient. Aluminum was used as the calibration sample. To determine the dynamic calibration coefficient K of the experimental instrument, Equation (6.4.1) was used:

$$K = \Delta(\text{lit.}) / \Delta(\text{exp.}) \qquad (6.4.1)$$

where:

K is the dynamic calibration coefficient,

Δ(lit.) is the literature value of thermal expansion coefficient from Table 6.4.1,

Δ(exp.) is the experimental value of thermal expansion coefficient.

The Y-axis dynamic calibration coefficients at different temperature were calculated by Equation (6.4.1). The results were the following (Aluminum initial length $L=7.65\times10^{-3}$m):

Table 6.4.1 Thermal expansion coefficient of Aluminum*

T (°C)	Coefficient of Expansion (μm/m°C)
-73	20.0
-23	21.9
27	23.2
77	24.1
127	24.9
227	26.4
327	28.3
427	30.7
527	33.8

- American Institute of Physics Handbook, [2nd edition], 4-66 [1963])

Table 6.4.2 Y-Axis Calibration Coefficient

Temperature(oC)	Aluminum Δ(lit.) (μm/m°C)	Aluminum Δ(exp.) (μm/m°C)	Y-Axis Calibration Coefficient K
77	24.1	20.24	1.1909
127	24.9	24.17	1.0301
227	26.4	29.4	0.8981
327	28.3	28.9	0.9793
427	30.7	32.47	0.9456
527	33.8	37.52	0.9009

6.4.2 Results and Discussion

The thermal expansion coefficients α of the samples can be determined by Equation (6.4.2):

$$\alpha = K * (\Delta L / \Delta T) * (1/L) \qquad (6.4.2)$$

where:

α - the measured thermal expansion coefficient in ($\mu m/m°C$)

L - sample initial length in (m)

ΔL - change in sample length in (μm)

ΔT - change in temperature (°C)

K - Y-Axis Calibration Coefficient.

Samples of Chromium doped Ca_2GeO_4, Li_2CaSiO_4 and $LiScGeO_4$ were used and the experimental results are shown in Fig. 6.4.1 through Fig. 6.4.4. a-axis, b-axis and c-axis are the crystallographic orientations.

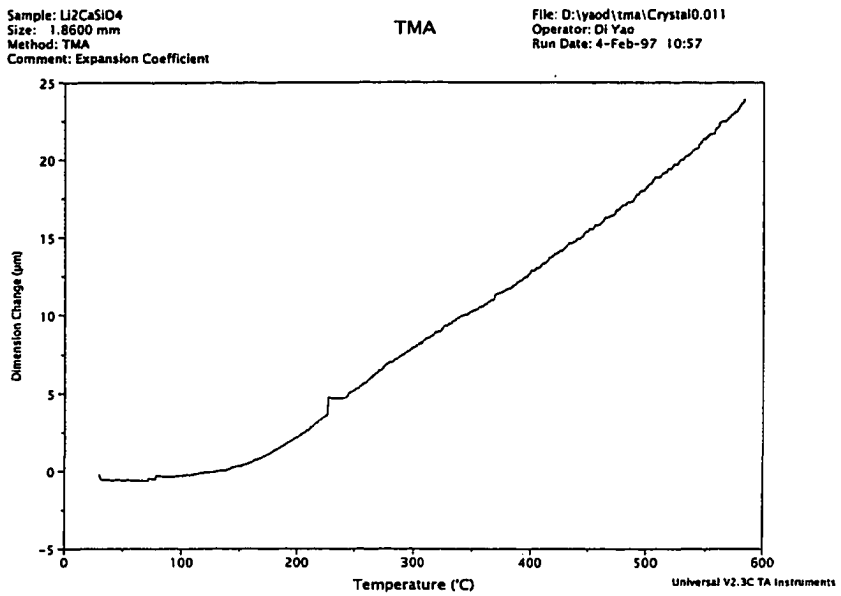

Fig. 6.4.1 Experimental result of thermal expansion coefficient for Li_2CaSiO_4 (a-axis)

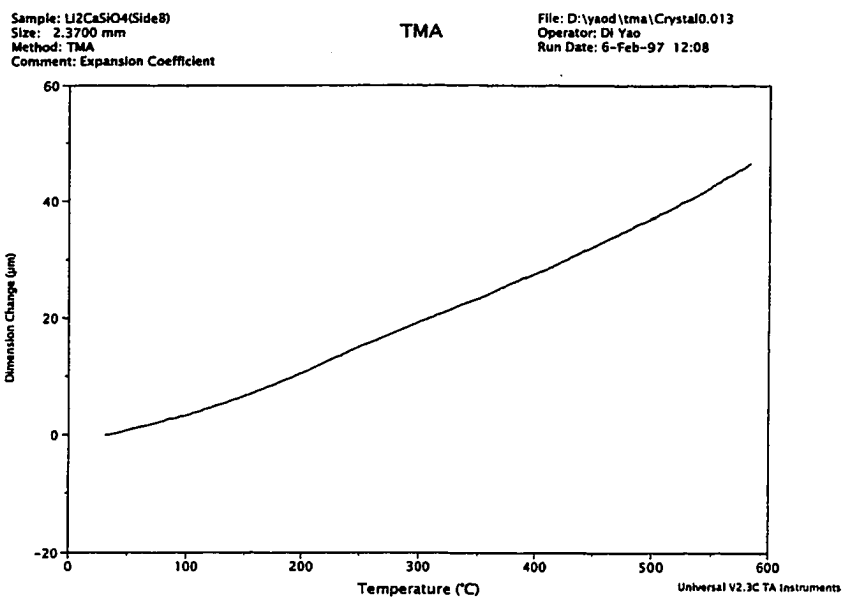

Fig. 6.4.2 Experimental result of thermal expansion coefficient for Li_2CaSiO_4 (c-axis)

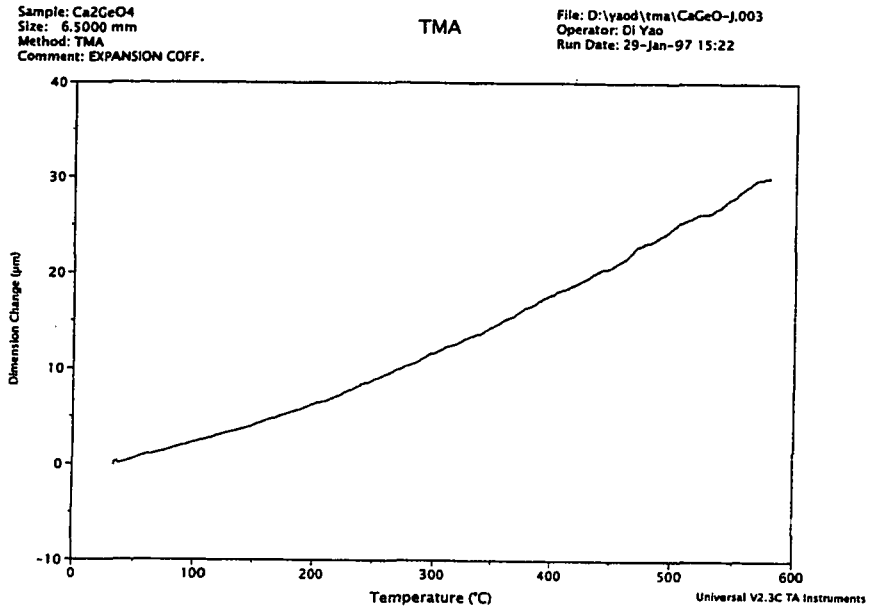

Fig. 6.4.3 Experimental result of thermal expansion coefficient for Ca_2GeO_4.

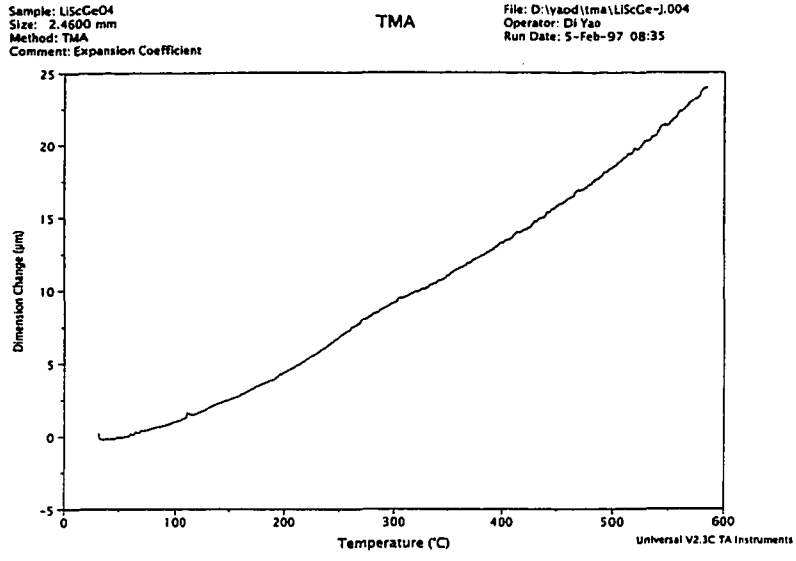

Fig. 6.4.4 Experimental result of thermal expansion coefficient for $LiScGeO_4$.

Expansion Coefficient of Li_2CaSiO_4

Li_2CaSiO_4 (a-axis) initial length L= $2.21x10^{-3}$m

Temperature	Calibration Coefficient	Expansion Coefficient (μm/m.°C)				
T(^{0}C)	K	1	2	3	4	Average
77	1.1909	9.16	7.84	8.44	8.29	8.43
127	1.0301	8.66	9.42	8.86	10.76	9.42
227	0.8981	17.04	14.52	14.38	18.71	16.16
327	0.9793	24.10	17.12	17.56	17.19	18.99
427	0.9456	21.28	20.98	18.38	19.43	20.02
527	0.9009	27.27	21.48	21.70	18.61	22.26

We have the relationship between Temperature and Expansion Coefficient, after linear regression (see Fig. 6.4.5):

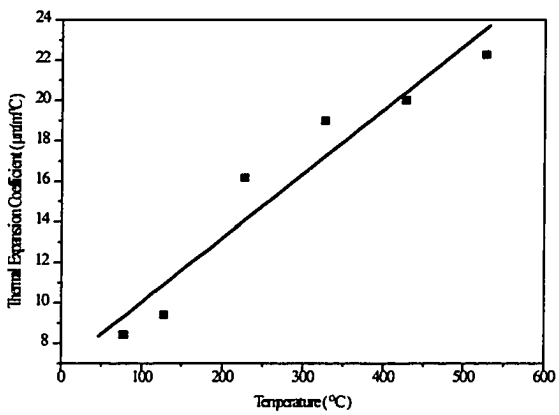

Fig. 6.4.5 Li_2CaSiO_4 (a-axis) Expansion Coefficient vs. Temperature and linear fitted.

Linear Regression for Li_2CaSiO_4: $Y = A + B * X$

Param	Value	sd
A	6.84345	1.4686
B	0.03167	0.00449

R = 0.962
SD = 1.75281, N = 6
P = 0.00214

α = 6.84345+0.03167 T (Temperature T range: 77 to 527 °C)

Li_2CaSiO_4 (c-axis) initial length L= $2.37x10^{-3}m$

Temperature	Calibration Coeff.	Expansion Coefficient (μm/m.°C)			
T(^{0}C)	K	1	2	3	Average
77	1.1909	26.84	26.17	27.85	26.95
127	1.0301	26.10	28.96	23.94	26.34
227	0.8981	27.74	33.82	30.63	30.73
327	0.9793	31.21	34.15	33.42	32.93
427	0.9456	31.35	36.73	32.59	33.56
527	0.9009	35.58	41.01	36.69	37.76

We have the relationship between Temperature and Expansion Coefficient, after line regression (see Fig. 6.4.6):

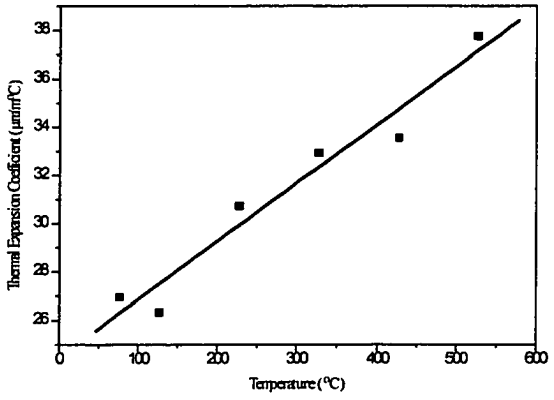

Fig. 6.4.6 Li_2CaSiO_4 (c-axis) Expansion Coefficient vs. Temperature and linear fitted.

Linear Regression for Li_2CaSiO_4: $Y = A + B * X$

Param Value sd

A 24.48515 0.89345

B 0.02416 0.00273

$R = 0.97532$

$SD = 1.06636, N = 6$

$P = 0.00091$

$\alpha = 24.48515+0.02416\ T$ (Temperature T range: 77 to 527 °C)

Expansion Coefficient of $LiScGeO_4$

$LiScGeO_4$ initial length $L=2.45x10^{-3}m$

Temperature	Calibration Coeff.	Expansion Coefficient (μm/m.°C)					
T(^{0}C)	K	1	2	3	4	5	Average
77	1.1909	10.30	7.22	10.63	8.86	12.43	9.89
127	1.0301	9.78	7.09	12.91	8.71	10.63	9.82
227	0.8981	15.86	18.77	17.84	14.72	17.64	16.97
327	0.9793	19.53	21.71	15.56	17.16	19.65	18.72
427	0.9456	21.55	22.65	19.51	19.55	19.74	20.60
527	0.9009	24.69	26.10	22.85	25.34	24.87	24.77

We have the relationship between Temperature and Expansion Coefficient, after linear regression (see Fig. 6.4.7):

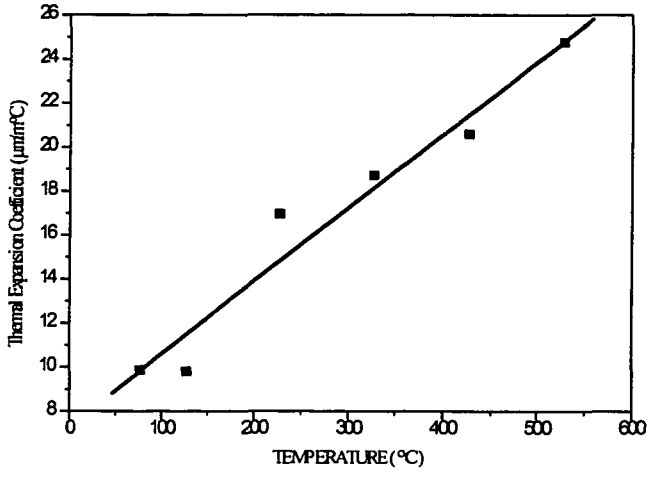

Fig. 6.4.7 $LiScGeO_4$ Expansion Coefficient vs. Temperature and linear fitted.

Linear Regression for $LiScGeO_4$: $Y = A + B * X$

Param	Value	sd
A	7.26549	1.222
B	0.0334	0.00374

$R = 0.97583$

$SD = 1.45849, N = 6$

$P = 0.00087$

$\alpha = 7.26549+0.0334\ T$ (Temperature T range: 77 to 527 °C)

Expansion Coefficient of Ca_2GeO_4

Ca_2GeO_4 initial length L=6.49x10^{-3}m

Temperature	Calibration Coeff.	Expansion Coefficient (μm/m.°C)				
T(^{0}C)	K	1	2	3	4	Average
77	1.1909	6.71	6.20	6.89	5.41	6.30
127	1.0301	5.13	5.52	6.70	6.68	6.01
227	0.8981	7.63	7.17	7.82	8.58	7.80
327	0.9793	10.94	8.84	8.42	8.80	9.25
427	0.9456	12.00	9.54	9.58	9.94	10.26
527	0.9009	11.25	9.83	11.21	10.98	10.82

We have the relationship between Temperature and Expansion Coefficient, after line regression (see Fig.6.4.8):

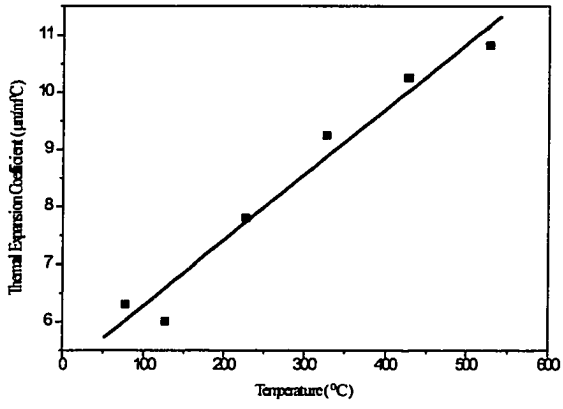

Fig. 6.4.8 Ca_2GeO_4 Expansion Coefficient vs. Temperature and linear fitted.

Linear Regression for Ca_2GeO4: $Y = A + B * X$

Param	Value	sd
A	5.15215	0.35908
B	0.01141	0.0011

R = 0.98194
SD = 0.42857, N = 6
P = 0.00049

α = 5.15215+0.01141 T (Temperature T range: 77 to 527 °C)

Samples of Chromium doped Ca_2GeO_4 single crystals were used and the experimental results are shown in Fig. 6.4.9.

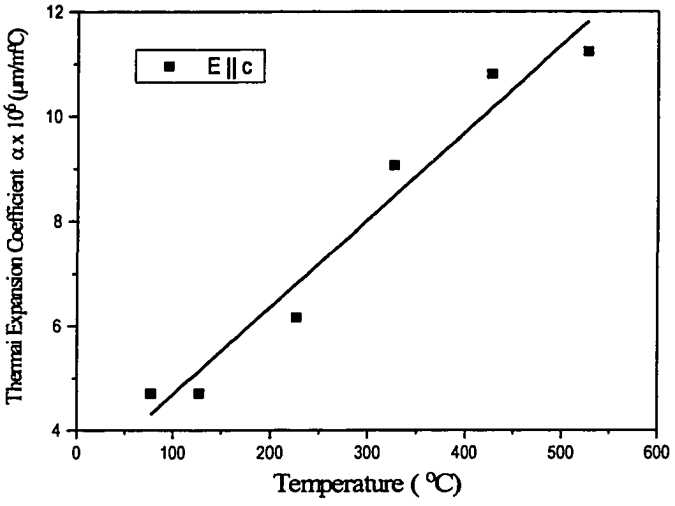

Fig. 6.4.9 (a)

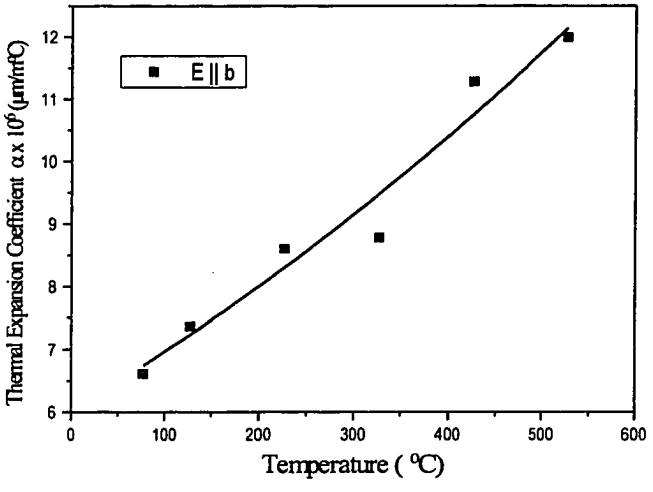

Fig. 6.4.9 (b)

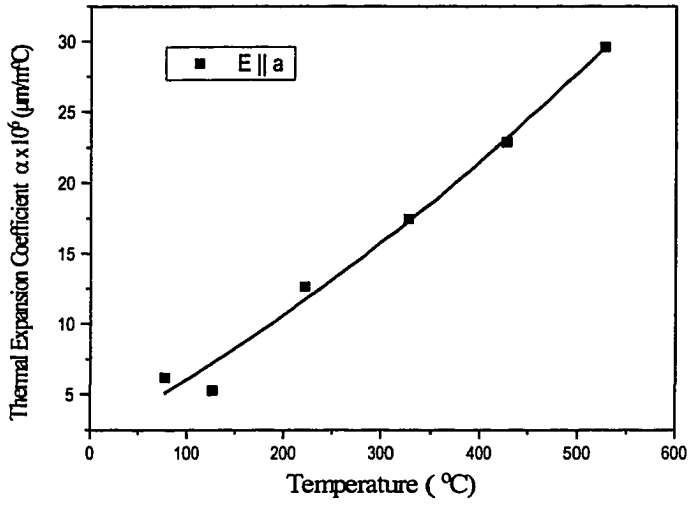

Fig. 6.4.9 (c)

Fig.6.4.9 Thermal expansion coefficient data for Chromium doped Ca_2GeO_4. (a)c-axis, (b)b-axis, (c)a-axis.

The coefficients needed to describe the expansion of crystals with different symmetries are shown in Table 6.4.3. The principal coefficients (α_1, α_2 and α_3) describe the volume change of the crystal with

$$\beta = \alpha_1 + \alpha_2 + \alpha_3$$

These coefficients apply to orthogonal directions, but not necessarily those of the crystallographic translation vectors. The remaining coefficients (α_4, α_5 and α_6) describe the change in shape (but not the symmetry) of the crystal.

Table 6.4.3 Thermal Expansion Coefficients for Various Crystal Symmetries

Cubic	α_1	α_1	α_1	0	0	0
Hexagonal	α_1	α_1	α_3	0	0	0
Tetragonal	α_1	α_1	α_3	0	0	0
Trigonal	α_1	α_1	α_3	0	0	0
Orthorhombic	α_1	α_2	α_3	0	0	0
Monoclinic	α_1	α_2	α_3	0	α_5	0
Triclinic	α_1	α_2	α_3	α_4	α_5	α_6

For Li_2CaSiO_4, $\alpha_1 = 6.84345+0.03167\ T$

$\alpha_3 = 24.48515+0.02416\ T$

Therefore, $\beta = \alpha_1 + \alpha_1 + \alpha_3 = 38.17205 + 0.0875\ T$ (x 10^6 μm/m°C)

For Ca_2GeO_4, $\alpha_1 = 2.0465144 + 0.037585137\ T + 2.7826324\ 10^{-5}\ T^2$

$\alpha_2 = 6.0369392 + 0.0087695246\ T + 5.342955\ 10^{-6}\ T^2$

$\alpha_3 = 2.2973155 + 0.018466029\ T + 3.0448358\ 10^{-6}\ T^2$

Therefore, $\beta(T) = 10.38077 + 0.064821\ T + 3.62\ 10^{-5}\ T^2$ (x 10^6 μm/m°C)

The density of the crystals can be calculated from the following equation:

$$\beta = \frac{1}{\rho}\left(\frac{\partial \rho}{\partial T}\right)_P$$

For Li_2CaSiO_4, by substituting the β into the above equation, we have:

$$(1/\rho)(d\rho/dT) = (38.17205 + 0.0875\ T)\ 10^{-6}$$

$$d(\ln\rho) = (\ 38.17205 + 0.0875\ \ T\ )\ 10^{-6}dT$$

Integrating the above equation, we get:

$$(\rho/\rho_{298}) = \exp[38.17205\ (T\text{-}298) + 0.04375\ (\ T\text{-}298)^2\ ]10^{-6}$$

With the Taylor expansion, we can expand the above expression into a simple expression as follows:

$$\frac{\rho}{\rho_{298}} = \sum_{n=0}^{n} a_i (T - 298)^i$$

where: $a_0 = 1$

$a_1 = 3.817205*10^{-5}$

$a_2 = 7.28978*10^{-4}$

$a_3 = 9.27179*10^{-3}$

here we neglect the high order terms.

Chapter Seven

Conclusions and Future Work

7.1 Research Summary

7.1.1 Development of Novel Solid State Laser Materials

Chemical compounds with formula Cr^{4+}:$A^{+}_{4}(Si, Ge)O_4$, and $A^{+}_{2}M^{2+}(Si, Ge)O_4$, where A = Na, K, Li and M = Ca, Mg, Zn, Cd, were investigated in searching for crystalline hosts for potential Cr^{4+} doped tunable solid state lasers. Basic spectroscopic properties of the potential laser hosts(Cr^{4+}:$Li_2M^{2+}X^{4+}O_4$) were measured. Strong Cr^{4+} emission in near-infrared (1.1--1.6 μm) region has been observed in Cr-doped $Li_2M^{2+}X^{4+}O_4$(X=Si, Ge) crystalline media. In all the Cr^{4+}-doped $Li_2Ca(Mg, Cd, Zn)Ge(Si)O_4$ laser hosts, Cr^{4+} had been identified as the only optically active center responsible for the near infrared emission in the 1100 - 1600 mm spectral range. Based on the fluorescence spectra of the synthesized compounds, the group of materials with the chemical formulas Cr^{4+}: $Li_2Ca(Mg, Cd, Zu)Ge(Si)O_4$ have good emission properties. We propose these materials as the potential crystalline hosts for the Cr^{4+} doped lasers.

Novel solid-state laser materials were developed using flux method and top seeding solution growth method with pulling technique. Initial work was on the crystal growth of CUNYITE, then we focused on the crystal growth of Cr^{4+} -doped Li_2CaSiO_4 and Li_2CaGeO_4.

In Li_2CaSiO_4 and Li_2CaGeO_4, two phases (high and low temperature) were identified by DTA. The phase transition point is 960°C and 950°C for Li_2CaGeO_4 and Li_2CaSiO_4 respectively, and the melting point is 1150 °C and 1060 °C for Li_2CaGeO_4 and Li_2CaSiO_4 respectively. Pseudo-binary systems of Li_2CaSiO_4 - LiF and Li_2CaGeO_4 - LiF/LiCl were investigated, and the solubility curve of Li_2CaSiO_4 - LiF was obtained. The phase diagram of the pseudo-binary system of Li_2CaSiO_4 - LiF provided the necessary data for designing a crystal growth procedure.

High quality (purity) single crystals of Cr^{4+}:Ca_2GeO_4 and Cr^{4+}:Li_2CaSiO_4 (low temperature phase) have been successfully grown from the Cr^{4+}:Ca_2GeO_4-CaF_2 and Cr^{4+}:Li_2CaSiO_4-LiF solution with the top seeding technique under nitrogen atmosphere and air atmosphere.

The pulling rate we used to grow good quality single crystals was between 0.1 ~ 0.5 mm/hr, and the rotation speed was 15 ~ 40 rpm. The growth direction was perpendicular to "c" axis for Cr^{4+}:Li_2CaSiO_4 and parallel to "b" axis for Cr^{4+}:Ca_2GeO_4.

The grown crystal was confirmed to be that of the low temperature phase of Li_2CaSiO_4 by X-ray powder diffraction.

Absorption and emission spectra of the crystals Li_2CaSiO_4 and Ca_2GeO_4 were measured. Fluorescence spectra of room temperature and liquid nitrogen temperature were also

measured. In all the Cr^{4+}doped laser hosts, Cr^{4+} has been identified as the optically active center responsible for the near-informed emission in the 1100-1600 μm spectral range. The room-temperature lifetime of the Cr^{4+}- emission in Li_2MgGeO_4 is ~ 90 μs, the longest lifetime observed up to now for Cr^{4+}-doped laser systems.

In conclusion, Cr-doped Li_2CaSiO_4-type materials represent new promising groups of tunable solid-state laser crystals based on the Cr^{4+} ion for the 1.1--1.6 μm near-infrared spectral region.

7.1.2 Physical and optical properties of the novel solid state laser materials

The measurements of the optical, thermo-physical and mechanical properties of the new developed laser materials provide very useful information for the application of the materials and the design of laser devices. In this thesis, we used the experimental techniques to investigate the physical properties of the novel laser and the potential laser hosts. The DSC method was dedicated for measuring the heat capacity; the MDSC technique was used in studying the thermal conductivity; and the TMA techniques was for investigating the thermal expansion coefficient. The refractive indices of materials were measured with the Brewster's angle method by using Cary500 spectrophotometer. Table 7.1.1 and Table 7.1.2 gave the research results.

Table 7.1.1 Material parameters of CUNYITE(Cr^{4+}:Ca_2GeO_4)

Laser wavelength (nm)	1350 – 1400
Spontaneous lifetime (μs)	15 (at room temperature)
Index of refraction (1400 nm)	E || a 1.663131
(at room temperature)	E || b 1.615952
	E || c 1.65328
Thermal Expansion: (μm/m. °C)	E || a $2.0465144 + 0.037585137\ T + 2.7826324\ 10^{-5}\ T^2$
(Temperature range: 77-527 °C)	E || b $6.0369392 + 0.0087695246\ T + 5.342955\ 10^{-6}\ T^2$
	E || c $2.2973155 + 0.018466029\ T + 3.0448358\ 10^{-6}\ T^2$
Thermal Conductivity:	0.023 (W/cmK @370K)
Melting Point:	1900 °C
Heat Capacity:	155 (J/mol.K) at T= 300 K

Table 7.1.2 Material parameters of Cr^{4+}:Li_2CaSiO_4.

Spontaneous lifetime (μs)	30 (μs)
Index of refraction (1400 nm)	E || a 1.56923
	E || c 1.60378
Thermal Expansion:	E || a 6.84345+0.03167*T (μm/m. °C)
Temperature range: 77 - 527 °C	E || c 24.48515 + 0.02416*T (μm/m. °C)
Melting Point:	1061 °C
Heat Capacity:	160 (J/mol.K) at T= 300 K

7.2 Future Work

In this research, high temperature solution growth method was successfully employed in single crystal growth. And large single crystals of Cr^{4+}:Ca_2GeO_4 and Cr^{4+}:Li_2CaSiO_4 were grown from TSSG with pulling technique. Although this method is successful in making these single crystals, it is very limited and can not easily be generalized to synthesize other materials, and the process is very expensive. To obtain the single crystals, it is based on the solid state reactions which usually involve very high temperatures due to the high melting point of the materials. Complete component mixing is difficult to achieve at the molecular level, this can cause inhomogeneity, which degrades the quality of the materials.

Because of the difficulty in growing single crystals, the route of preparing and using nano-scale optical materials gained more attention recently. Nano-scale materials are the materials with at least one dimension in the range of nano-meters. The nano-structures can be one-dimensional (fibrous), two-dimensional (layered) or three-dimensional (crystallites). The advantages of these materials are that they combine the processability of the host (usually commercially available products) with the special features (electrical, mechanical, optical etc.) of the nano-scale particles. The nano-scale optical materials are not only just a substitute for the single crystal laser materials, but also open up new ways for the synthesis of laser materials. It provides us the ability to manipulate the material's property on the nano-range, or even on the molecular level. This nano-technology has been described as the manufacturing technology of the 21st century.

Biboliography:

- Atanasov, M. "On the nature of the lowest excited state of Cr^{4+} doped olivines" Chemical Physics Letters, **234** (1995) 313-318
- Baur, W. H. and T. Ohta, Journal of Solid State Chemistry **44**, 50-59, 1982.
- Baxter, R.A., in "Thermal Analysis" (Schwenker, R.F., Jr. and Garn, P.D., Editors). Vol. 1, Academic Press, New York, NY, 1969.
- Belruss, V. (1971) *Mat. Res. Bull.* **6**, p899
- Bond, Journal of Applied Physics, Volume 36, Number 5, p112,1961.
- Bruce, P. G. and A. R. West, Journal of Solid State Chemistry 44, 354-365, 1982.
- Burshtein, Y. Shimony, I. Levy, A. M. Lejus, J. M. Benitez, and F. Mougel, J. Opt. Soc. Am. B, Vol. 13, No. 9, p68, 1996.
- Cassel, B., "New Techniques in DSC: Differential Heat Capacity Determinations for Maximum Accuracy." Pressented at the Pittsburgh Conference on Analytical Chemistry, Cleveland, OH, 1974.
- Chiu, J. and P.G. Fair, "Thermochim. Acta". **34**, 267-273 (1979).
- Cotton, F. A. *Chemical Application of Group Theory*, Wiley, New York(1990)
- Dmitriev, V. G. *et al Handbook of Nonlinear Optical Crystals*, Springer-Verlag 1991
- Duswalt, A. A., 48th Calorimeter Conference, Durham NC, (1993)
- Eimerl, L. Davis, S. Velsko, E. K. Graham, and A. Zalkin, J. Appl. Phys. **62** (5), p17 September 1987.
- Elwell, D. and H. J. Scheel, *Crystal Growth from High-Temperature Solutions*, Academic Press (1975)

- Fiquet, G., Philippe Gillet, and Pascal Richet, "Anharmonicity and High-Temperature Heat Capacity of Crystals: the Examples of Ca_2GeO_4, Mg_2SiO_4, and $CaMgGeO_4$ Olivines", Phys Chem Minerals (1992) **18**: 469-479
- Gard, J. A. and A. R. West, "Prepareation and Crystal Structure of Li_2CaSiO_4 and Isostructural Li_2CaGeO_4" J. Solid State Chemistry, **7**, 422-427 (1973)
- Gary, A.P., in "Analytical Calorimetry" (Porter, R.S. and Johnson, J.F., Editors), Plenum Press, New York, NY, 1968.
- Harrick, N. J. *Applied Spectroscopy*, Volume 31. Number 6, p548, 1977.
- Hazenkamp, H., U. Gudel, M. Atanasov, U. Kesper and D. Reinen, Phys. Rev. B53, 2367 (1996).
- Hazenkamp, M. F. *et al* "Absorption and luminescence spectroscopy of Cr^{4+} -doped Ca_2GeO_4. A potential near infrared laser material" Chemical Physics Letters, **233** (1995) 466-470
- Ito, Jun "Crystal synthesis of a new olivine, $LiScSiO_4$", American Mineralogist, **62**, 356-361 (1977)
- Johnson, L. F. Phys. Rev. Lett. **11**, 318-320 (1963)
- Keating, M.Y. and C.S. McLaren, "Thermochim. Acta." 166, 69-76 (1990).
- Kenyon, Peter T., L. Andrews, B. McCollum, and A. Lempicki, IEEE Journal of Quantum Electronics, Vol. QE-18, No. 8, p122, 1982.
- Koechner, Walter "*Solid-State Laser Engineering*", 2nd ed., New York, 1988.
- Koetke, S. Kuck, K. Petermann, G. Huber, G. Cerullo, M. Danailov, V. Magni, L. F. Qian, and O. Svelto, "Quasi-continuous wave laser operation of Cr^{4+} -doped Y_2SiO_5 at room temperature." Opt. Commun. 101, 195 (1993).

- Kokta, Milan R. "Growth of Crystals for Solid State Lasers", Tunable Solid State Lasers, Editors: P. Hammerling, A. B. Budgor, and A. Pinto, 1984
- Kuck, S. *et al* "Near-infrared emission of Cr^{4+} -doped garnets: Lifetimes, quantum efficiencies, and emission cross sections" Physical Review B 51, 1995, p17323
- Kuck, S., Hartung, K. Petermann, and G. Huber, "New Cr^{4+}-doped Oxide Crystals as Sources for Tunable Solid State Lasers at room Temperature" , Appl. Phys. B 58, p153 (1994).
- Kuck, S., K. Petermann, U. Pohlmann, U. Schonhoff, and G. HuberLaudise, R. A. *The Growth of Single Crystals*, Prentice-Hall, New Jersey (1970)
- Lever, A. B. P. *Inorganic Electronic Spectroscopy*, Elsevier Publishing Company (1968)
- Li, H. H. Journal of Physical and Chemical Reference Data, Volume 5, No. 2, p329-528, 1976.
- Li, Y., V. Petricevic and R. R. Alfano, "Advances in Cr^{4+}-Doped Tunable Solid-State Lasers" in Novel Laser Sources and Applications, J. F. Becker *et al* Eds. (SPIE Optical Engineering Press, Bellingham, Washington DC, 1994), p103-115
- Linz, A., (1965) *Electrochem. Soc.* Spring Meeting, San Francisco, Extended Abstract **2**, p87
- Malacara, Daniel (ed.), "*Physical Optics and Light Measure*ments", Academic Press Inc., 1988.
- Marcus, S.M. and R.L. Blaine *TA Instruments Publication: Thermal Analysis & Rheology*

- McClure, D. S. in *Solid State Physics*, Vol 9, F. Seitz and D. Turnbull, eds., (Acdemic, New york, 1959) p408
- Medenbach, and R. D. Shannon, J. Opt. Soc. Am. B, Vol. 14, No. 12, p211, December 1997.
- Moller, "Optics", University Science Books, 1988.
- Moncorge, R., G.Cormier, D. J. Simkin, and J. A. Capobianco, IEEE Journal of Quantum Electronics, Vol. 27, No. 1, 21, 1991.
- Moulton, P. F. IEEE J. QE-**18** 1185-1188 (1982)
- Moulton, P. F. "Tunable Paramagnetic-Ion Lasers" in *Laser Handbook*, Vol 5, M. Bass and M.L. Stitch ed. pp203-288 (1986)
- Murthy, Krishna and F. A. Hummel, "Phase Equilibria in the System Lithium Metasilicate-Forsterite-Silica", J. American Ceramic Society, Vol 38, **2**, pp55 (1955)
- Nikogosyan and G. G. Gurzadyan, Sov. J. Quantum Electron. 17 (8), p98, 1987.
- O'Neill, M.J., Anal. Chem., 36, 1238-45, 1964.
- Oetliker, Ueli, Markus Herren, Hans U. Gudel, Ute Kesper, Christa Albrecht, and Dirk Reinen, J. Chem. Phys 100 (12), 15 June 1994.
- Petricevic, V. *Ph. D. Thesis*, New York, 1990
- Petricevic, V., S. K. Gayen, and R. R. Alfano, Appl. Phys. Lett. 53, 2590 (1988).
- Petricevic, V., S. K. Gayen, R. R. Alfano, Kiyoshi Yamagishi, H. Anzai, and Y. Yamaguchi, Appl. Phys. Lett. 52 (13), 28 March 1988.
- Petricevic, V., A. B. Bykov, J. M. Evans, and R. R. Alfano, "Room temperature near-infrared tunable laser operations of Cr^{4+}:Ca_2GeO_4", Optics Letters, Vol 21, No. 21, 1996 pp 1~4

- Rams, A. Tejeda, and J. M. Cabrera, J. Appl. Phys. 82 (3), 1 August 1997.
- Reinen, D. *et al* "Cr^{4+} in Tetrehedral Coordination of Oxidic Solids: A Spectroscopic and Structural Investigation" Inorg. Chem. 1995, 34, 184-192
- Scheel, H. J. and Elwell, D. J. J. Electrochem. Soc. **120**, 818 (1973)
- Shannon, R. D. "Revised Effective Ionic Radii and Systematic Studies of Interatomic Distance in halides and Chalcogenides", Acta Cryst. A32, 751-767 (1976)
- Shannon, R. D. and C. Calvo, Journal of Solid State Chemistry 6, 538-549, 1973.
- Shirvinskaya, A. K. Izv.Akad. Nauk SSSR, Negor. Mater. **2**, 332 (1966)
- Shkadrevich, OSA Proceedings on tunable solid State Lasers, edited by M. L. Shand and H. P.Jenssen (Optical society of America, washington, D. C., 1989), Vol. 5, pp. 60-65.
- Sircar, A.K. and J.L. Wells, "Rubb. Chem. Tech." 54, 191-207 (1982).
- Smith, J. M. and H. C. Van Ness *Introduction to Chemical Engineering Thermodynamics*, 4th Ed., McGraw-Hill Book Company (1987)
- TA Instruments Publication MDSC 1-3.
- Tanabe, Yukito and Satori Sugano, *Multiplets of transition-metal ions in crystals.* New York, 1970
- Tanaka, K., Tsuyoshi Ohgoh, Kazuya Kimura, Hajime Yamamoto, Kiminari Shinagawa and Katsuaki Sato, Jpn. J. Appl. Phys. Vol. 34 (1995) pp. 1651-1654, Part 2, No. 12B, 15 December 1995.
- Verdun, L., M. Thomas, D. M. Andrauskas, T. McCollum, and A.Pinto, appl. Phys. Lett. 53, 2593 (1988).
- Walling, J. C., Opt. Lett. **4**, 182 (1979)

- Wendlaudt, Wesley Wm. " *Thermal Analysis*" 3rd Ed. John Wiley and Sons, New York, 1986.
- West, A. R. and F. P. Glasser, Journal of Materials Science 5, 557-565, 1970.
- West, A. R. and F.P. Glasser, "Crystallisation of Lithium Zinc Silicates", J. Materials Science **5** (1970) 557-565
- West, A. R. and F.P. Glasser, "Preparation and Crystal Chemistry of Some Tetrahedral Li_3PO_4-Type Compunds" , J. Solid State Chemistry, **4**, 20-28 (1972)
- Whitmore, Michael H., Ann Sacra, and David J. Singel, J. Chem. Phys **5**, 98 March 1, 1993.
- Wilcox, W. R., J. Crystal Growth **7**, 203 (1970)
- Yamaguchi, Yasuhide, Kiyoshi Yamagishi and Yukio Nobe, Journal of Crystal Growth **128** (1993) 996-1000, North-Holland.
- Zverev and A. V. Shestakov, OSA Proceedings on Tunable Solid State Lasers 1989, pp. 66-70.